

An Abstract of the Thesis of

Martin B. Fuchs for the degree of Master of Science in Physics presented on December 4, 1991.

Title: Brueckner Theory of Nuclear Matter

Redacted for Privacy

Abstract approved: _____

Philip J. Siemens

The Bethe-Goldstone equation was solved numerically for uniform nuclear matter with local two-nucleon interactions. The reference spectrum method was combined with a rapidly converging polynomial representation to obtain the full nuclear matter reaction matrix. A self-consistent mean field for states below the Fermi level was deduced from the effective interaction. Calculations at various densities were performed and yielded the expected binding and saturation properties for nuclear matter. Saturation was reached at a Fermi momentum of $k_{fm} = 1.48 \text{ fm}^{-1}$ and an average energy of $\bar{\epsilon} = -12.52 \text{ MeV/nucleon}$ using Reid's soft-core potentials. Good agreement with prior calculations confirmed the feasibility of the computational methods employed. The mean field calculation could not be extended successfully to particle states because the present formalism can not properly treat singularities which arise for those states.

Brueckner Theory of Nuclear Matter

by

Martin B. Fuchs

A Thesis
submitted to
Oregon State University

in partial fulfillment of
the requirements for the
degree of

Master of Science

Completed December 4, 1991

Commencement June 1992

Approved:

Redacted for Privacy

Philip J. Siemens, Professor of Physics in charge of major

Redacted for Privacy

Kenneth S. Krane, Chairman, Department of Physics

Redacted for Privacy

Dean of Graduate School

Date thesis is presented December 4, 1991

Typed by Martin B. Fuchs for Martin B. Fuchs

Acknowledgements

*Why is there something,
rather than nothing ?*

(Memories of philosophy)

While the above quote usually provokes profound discussions, at least among physicists, it ought to be interpreted quite narrowly concerning the topic of the thesis: How come that nucleons stick together? But to the thesis and its 'author', the quote applies as well. And there the answer is clear: Many people contributed and this is the opportunity to thank them.

Why is there something? I thank my parents for nurturing my interest in nature and for their encouraging and steadfast support during my studies at the University of Stuttgart and at Oregon State.

...rather than nothing? On the academic side many thanks are due to Prof. Phil Siemens. His insights and his advice at every stage, from the initial phase of the project to the very end have been a true enrichment to my understanding.

Major and minor obstacles with computations and equipment were overcome with readily available help from Mark Gummin, Bianca Hermann, Martin Rosenbauer and Linhua Xia. For bearing the permanent background noise of a rattling keyboard, my officemates Axel Vischer and Neil Roberts deserve special thanks. The number of misprints and other errors in the final copy of the thesis was greatly reduced thanks to the careful review by Mark Gummin and Axel Vischer.

Table of Contents

	<u>Page</u>
1. The Nuclear Matter Problem	1
1.1 <u>Introduction and Survey</u>	1
1.2 <u>Scope of the Present Work</u>	3
2. Brueckner Theory	4
2.1 <u>Independent Pair Approximation and Bethe-Goldstone Equation</u>	5
2.2 <u>Perturbation Expansion for the Nuclear Groundstate</u>	7
2.3 <u>Nuclear Matter</u>	14
3. Solution of the Bethe-Goldstone Equation	17
3.1 <u>The Reference Spectrum Method</u>	17
3.2 <u>Calculating the Reference Reaction Matrix</u>	18
3.3 <u>Legindgaard's Method and Full Nuclear Matter Reaction Matrix</u>	21
3.4 <u>The Pauli Exclusion Operator</u>	23
4. Brueckner-Hartree-Fock Theory	29
4.1 <u>Single-Particle Spectrum - Method</u>	29
5. Numerical Solution of the Bethe-Goldstone Equation	34
5.1 <u>Reference Reaction Matrix</u>	34
<u>Solution of the Reference Wave Equation - Conventions</u>	34

	<u>Page</u>
<u>Reference Wave Equation - Numerical Method</u>	35
<u>Matrix Elements</u>	37
<u>Miscellanea and Critique</u>	37
5.2 <u>Legindgaard's Method for the Full Nuclear Matter Reaction Matrix</u>	38
<u>Polynomial Transforms of the Reaction Matrix</u>	38
<u>Angle Averaged Propagator Correction</u>	39
<u>Matrix Inversion - Miscellanea</u>	39
5.3 <u>Considerations for the Self-Consistent Calculation of the Spectrum</u>	39
 6. Examples and Discussion	 41
6.1 <u>Nuclear Matter Reaction Matrix</u>	41
6.2 <u>Self-Consistent Calculation of the Hole Spectrum</u>	49
6.3 <u>Extension to Particle States</u>	53
 Bibliography	 54
 Appendix A Partial Wave Basis	 56
Appendix B Hartree-Fock Approximation	58
Appendix C Converting to the Reaction Matrix	61
Appendix D Numerical Data - Samples	63

List of Figures

<u>Figure</u>		<u>Page</u>
1	Construction of Goldstone Diagrams	9
2	Geometry of the Pauli Operator and the Legindgaard Subspace	27
3	Angle Averaged Pauli Operator	28
4	Integration over Occupied States	30
5	Coupled Channel Potentials	42
6	Potential and Reference Wave Function in Channel 1S_0	43
7	Integrand for Reference Reaction Matrix in 1S_0	44
8	Nuclear Matter Reaction Matrix for 1S_0	45
9	Nuclear Matter Reaction Matrix for 3S_1	46
10	Nuclear Matter Reaction Matrix for 3S_1 – 3D_1	47
11	Nuclear Matter Reaction Matrix for 3D_1	48
12	Self-Consistent Hole Spectrum	50
13	Single-Particle Potential: Partial Wave Decomposition	51
14	Saturation Plot for Nuclear Matter	52

Brueckner Theory of Nuclear Matter

1. The Nuclear Matter Problem

1.1 Introduction and Survey

Ideally it should be possible to relate the observed properties of nuclei to the interactions among the constituent nucleons, qualitatively and ultimately quantitatively. Empirically, the nucleus is described well by a phenomenological mean field theory, the shell model. In it, the constituent nucleons behave essentially as if they were independent. Given that nuclei are many-fermion systems one might hope, guided by atomic physics, that the nuclear mean field can be derived as a Hartree-Fock potential *ab initio* from the forces between the nucleons. In striking contrast to the existence of nuclei, this is not possible for realistic nuclear forces. Their key feature, strong repulsion at short distances, is incompatible with the independent particle motion implied by the Hartree-Fock approximation. To overcome this difficulty Brueckner and Goldstone [1,2] developed a perturbative many-body approach based on multiple scattering theory which replaces the bare nuclear interaction in favor of an effective interaction which is well behaved and which yields a modified independent particle model, the independent particle approximation. It amounts to introducing pair correlations in the nucleons' motion in addition to the apparently insufficient Pauli principle, so that the repulsion is de-emphasized by shifting the independent particles' wave function more to the attractive regions of the potential. Obviously this must be done in a way which leads to binding and saturation, and a simple test for the theory is provided by comparing the bulk properties like density and binding energy to the empirical values. In principle one can construct the single-particle Hamiltonian from the effective interaction and solve the corresponding Schrödinger equation for the single-particle eigenstates and energies. The problem can be attacked using a discrete basis of states from which one has to determine the eigenstates and the mean field potential self-consistently. Considering the number of nucleons involved this is a sizeable task even today and has defeated numerical attempts in the past. The local density approximation instead uses a density dependent interaction, with non-locality limited to spin and angular momentum dependence. The advocating argument is that the nucleus is a low-density system where short range correlations are dominant so that a test nucleon is mainly influenced by the other nucleons in the vicinity. The approximate interaction may be constructed [3,4] from the effective interaction in an

infinite model system of uniform density, nuclear matter. The translational invariance tremendously simplifies the problem because the wave functions are known *a priori*, they are plane waves, and the remaining question is how to find a reasonable mean field. Clearly, nuclear matter is a purely hypothetical system and probes only the nuclear bulk properties, for any surface is absent and one can not account for any effects due to the finiteness of real nuclei with this model. Furthermore the Coulomb interaction must be "switched off". Actual calculations first of all test whether a *given* nucleon-nucleon potential leads to reasonable properties. The foremost criterion is that the system can reach a stable groundstate, i.e. that it is bound and that it saturates. As a uniform Fermi gas it is characterized by the Fermi momentum k_{fm} which relates to the density ρ as

$$\rho = g \frac{1}{6\pi^2} k_{fm}^3 \quad (1.1)$$

where the degeneracy factor $g = 4$ indicates that each momentum state can be occupied with 4 nucleons of different spin and isospin. Related is the mean distance r_0 between nucleons

$$\rho^{-1} = \frac{4\pi}{3} r_0^3 \quad (1.2)$$

and the equilibrium values are given by [5]

$$\rho = 0.17 \text{ fm}^{-3} \quad \Leftrightarrow \quad k_{fm} = 1.36 \text{ fm}^{-1} \quad (1.3)$$

The average binding energy $\bar{\epsilon}$ should be compared to the value of the volume term in the mass formula of the liquid drop model [4], in the limit of an infinite nucleus

$$\bar{\epsilon} = -15.68 \text{ MeV/nucleon}. \quad (1.4)$$

It should be remarked that the nuclear matter problem is a well plowed field. Reviews are given in [6,7]. The idea of using multiple scattering theory to describe the motion of the nucleons reaches back into the 1950s and it is fair to say that by the beginning of the 1970s the field reached a stationary state. A major revision after the mid-1970s is due to the authors of [7], who showed that the previously used prescription to set the potential energies for states above the Fermi momentum equal to zero should be abandoned in favor of treating them self-consistently like the occupied states. However it is still a worthwhile system to study: It is a many-fermion system par excellence with a relatively complicated spin and angular momentum dependent interaction [8]. But foremost, it provides access to finite problems via the density dependent interaction mentioned above.

1.2 Scope of the Present Work

The scope of this work encompassed two major tasks. The central part of the thesis project was the design of two Fortran subroutines [9] to calculate the nuclear matter reaction matrix with an angle averaged Pauli operator. The code TREF calculates the partial wave projections of the reference reaction matrix [10]. Its input consists only of the partial wave projections of a local potential and the reference spectrum parameters. The code TNM obtains the full nuclear matter reaction matrix in a rapidly converging polynomial expansion [11] and requires as input the user-provided nuclear matter spectrum, the parameters of the preceding calculation of the reference reaction matrix. The numerical feasibility of the codes was confirmed by comparing their results with previous calculations [3,12]. After the successful completion of this first part, the codes were employed to obtain the single-particle spectrum and the average binding energy as a function of k_{fm} . The reported calculations are based on Reid's soft core potentials [13]. These are scalar two-body interactions, which are local in the separation, but depend on the relative angular momentum and the total spin of the interacting pair.

Chapter 2 gives a review of Brueckner theory. Two viewpoints are explored, a short approach which appeals to the idea of the multiple scattering of the two nucleons and a rather formal approach based mostly on a diagrammatic representation of many-body perturbation theory. This chapter provides the theoretical background for the application-oriented formalism in chapter 3. Chapter 3 establishes the analytical framework as implemented in the numerical calculations. Bethe's reference spectrum method is presented in some detail followed by an outline of Legindgaard's method for the full reaction matrix and a discussion of the angle averaged Pauli exclusion operator. Chapter 4 describes the Brueckner-Hartree-Fock approximation to the mean field building on the formal development in the previous chapters. At this stage, the treatment is applicable to particle and hole states. Chapter 5 presents some methods, the Numerov algorithm, integration procedures etc., used in the numerical computations and discusses them. It reflects the algorithm implemented in the developed programs. Chapter 6 is devoted to some numerical results to illustrate the methods of chapter 3 and the self-consistent calculations following chapter 5. An argument is presented why the self-consistency condition can not be imposed on the particle states with the present method along with some preliminary thoughts how the theory needs to be extended. Appendix A is concerned with some technicalities and conventions about partial wave expansions. Appendix B supplements chapter 2 with a discussion of the usual Hartree-Fock method. Appendix C further illustrates the use of diagrams in Brueckner theory. Appendix D contains reference results of numerical calculations.

2. Brueckner Theory

Brueckner theory provides a means to calculate groundstate properties in finite as well as in infinite nuclear systems. In the first two subsections no specialization towards infinite nuclear matter is implied. It is presented with the understanding that the nuclear forces are purely two-body interactions and that it ultimately treats the problem non-relativistically.

The motivation for Brueckner's theory originated in the puzzle that the shell model [4] as a phenomenological mean field theory is successful in describing many properties of nuclei but that conventional many-body approximations like the Hartree-Fock method for the mean field, see Appendix B, fail if realistic nucleon-nucleon potentials are considered. For the model case of nuclear matter two problems prevail in the independent fermion model, saturation and binding. In an atomic system the Coulomb repulsion between the electrons is balanced by the attractive background potential of the nuclei and it is not a surprise that the system has a bound groundstate. In the case of nuclear matter there is no stabilizing background and consequently any *ab initio* theory which starts only from the form of the two-body interactions must also provide for the saturation property. Because in the independent particle model the ratio of potential and kinetic energy per particle is not bound as a function of the density, no saturation is possible, and the system is unbound or collapses, depending on whether the average potential energy is positive or negative. For the nucleon-nucleon interaction the strong repulsion at short interparticle separations causes the potential energy to be positive and nuclear matter would be unbound. Considering the part of the repulsion, the reason for the failure is clear. In the independent particle model the nucleons can approach too closely and experience predominantly the repulsive part of the interaction, despite the Pauli principle which usually keeps identical particles apart. Apparently the motion of the interacting particles should be correlated beyond mere antisymmetrization to prevent close approach. Of course, the attraction gained thereby must also exhibit the correct density dependence to achieve saturation.

As a first step one can introduce just pair-correlations, and Brueckner's theory provides the framework for doing this. It can be understood in the context of multiple scattering of the interacting pair in the presence of the nuclear medium, with the principal question of how to treat the strong short-range repulsion. Brueckner theory is restricted to groundstate properties since it is inherently a zero-temperature theory rather than the thermodynamic limit of a finite temperature theory for an infinite system. A thorough account of the interchangeability of both limits may be found in [14]. In the case of nuclear matter, both methods are equivalent [10]. Section 2.1 presents an abbreviated, more intuitive version of Brueckner theory [4]. Section 2.2 outlines a more formal

justification based on many-body perturbation theory, supplemented by diagrammatic methods, the Goldstone diagrams. For notational simplicity, the theory is displayed for finite systems. Section 2.3 focuses on infinite nuclear matter and establishes notational conventions for the subsequent calculations.

2.1 Independent Pair Approximation and Bethe-Goldstone Equation

The formalism for scattering of two particles in free space via a two-body interaction V can be utilized as a guideline to describe the motion of an interacting pair in the presence of the other nucleons which act as passive spectators. The starting point is the Lippmann-Schwinger equation for the T -matrix T_E

$$T_E = V + VG_ET_E, \quad (2.1)$$

where all operators are two-body operators. The subscript E indicates the dependence on the energies of the scattering particles. If the scattering takes place within the many-nucleon system, the two-body operators act on the two-particle projections of the complete many-body wave function. Without the effects of scattering, a single nucleon moves in the mean field produced by all the other nucleons, which one actually wants to extract from this development. Hence the homogeneous part of the scattering two-particle wave function is a product of two bound eigenstates of some single-particle Hamiltonian corresponding to the mean field and the single-particle energies must reflect the binding. In addition, the spectator fermions prevent the interacting pair from scattering into already occupied intermediate states by the Pauli principle, so that only scattering states above the Fermi level are permissible. Thus the propagator G_E in (2.1) needs to be modified regarding two aspects: (1) It has to account for the influence of the surrounding medium on the interaction by correcting the single-particle spectrum. (2) The propagator must project the intermediate states on the unoccupied states above the Fermi level. Explicitly, eq. (2.1) becomes

$$T_E = V + V \frac{Q}{E - H_0} T_E, \quad (2.2)$$

referred to as Bethe-Goldstone equation. The Pauli exclusion operator Q projects onto the unoccupied states and is given by

$$Q = \sum_{ij} (1 - n_i)(1 - n_j) |ij\rangle\langle ij|, \quad (2.3)$$

with $n_{i,j}$ as occupation numbers of the single-particle levels. In the groundstate $n_i = 1$ if the state i is occupied and $n_i = 0$ if it is unoccupied. With the single-particle energies ϵ_i

corresponding to the mean field Hamiltonian H_0 the Bethe-Goldstone equation for the groundstate of nuclear matter follows from (2.2)

$$\langle ij|T_E|kl\rangle = \langle ij|V|kl\rangle + \sum_{mn} \langle ij|V|mn\rangle \frac{\langle mn|Q|mn\rangle}{E - \epsilon_m - \epsilon_n} \langle mn|T_E|kl\rangle. \quad (2.4)$$

E is usually called the starting energy and enters as a parameter. While eq. (2.4) is a two-body equation which applies to the interacting pair the other nucleons do not enter explicitly, but they serve to modify the propagator. This passive role is condensed in the name *independent pair approximation* for the above treatment. There are no singularities in the propagator for occupied states by virtue of the exclusion principle. For states above the Fermi level a choice exists, either one uses a principal value integral for the scattering term or one evaluates it always off-shell. Both should correspond to bound states, and in the following treatment the latter is adopted. The T -matrix obtained by (2.4) might be considered as an effective interaction which includes pair correlations induced by potential scattering to all orders in V . According to its definition

$$T_E|\Phi_0\rangle = V|\psi_0\rangle = V\Omega_E|\Phi_0\rangle \quad (2.5)$$

T_E acts upon the uncorrelated state $|\Phi_0\rangle$ to reproduce the action of V on the correlated state $|\psi_0\rangle$ after the Møller operator Ω_E distorts the uncorrelated state. Eventually, it is then possible to regain the independent particle description by constructing the Hartree-Fock Hamiltonian from the effective interaction rather than from the bare V . The Hartree-Fock groundstate energy (B.12) is then given in terms of the single particle energies ϵ_i and the effective interaction

$$\langle \phi_0|H_{HF}|\phi_0\rangle = \sum_i \epsilon_i(E) - \frac{1}{2} \sum_{ij} (\langle ij|T_E|ij\rangle - \langle ij|T_E|ji\rangle), \quad (2.6)$$

with $|\phi_0\rangle$ denoting the many-nucleon groundstate and the sums covering the occupied states. This is not really a Hamiltonian, after all the interaction depends on the energy and there is the question of how to select E . One might select it on-shell from the single-particle spectrum, $E = \epsilon_i + \epsilon_j$ for the hole states in (2.6) in the spirit of a self-consistency problem, see App. B. However the particle states also enter the potential in the single-particle Schrödinger equation which ultimately determines the spectrum, and the question of how to choose E for them arises again. The answer emerges in section 2.1. Essentially the single-particle spectrum should be calculated self-consistently regardless of whether the state corresponds to a hole or a particle.

In analogy to the free-space scattering, eq. (1) relates the correlated, "distorted" and the uncorrelated two-particle state (2.5) via the defect wave function

$$|\Phi_0\rangle - |\psi_0\rangle = -\frac{Q}{E-H_0}V|\psi_0\rangle. \quad (2.7)$$

With the bound state boundary condition the scattered wave must vanish for large separations of the scattering nucleons. This is depicted by the concept of healing. The interaction inflicts a "wound" on the wave function which heals with a characteristic constant γ and the defect wave function vanishes asymptotically. The goodness of the independent pair approximation is then assessed by comparing the healing distance γ with the average spacing r_0 of the nucleons. If $\gamma \ll r_0$, the wave function at r_0 is the independent particle wave function in the mean field and for the purpose of scattering it is justified to look upon the other nucleons just as spectators, since they are remote from the scattering region. Another viewpoint is, that the probability to find three nucleons within a sphere of the order of γ is much smaller than for only two, consequently three-particle correlations are expected to be less important than pair correlations. Typically one has $\gamma/r_0 \approx 0.5$. The concept of healing will be revisited under a different aspect in ch. 4.

2.2 Perturbation Expansion for the Nuclear Groundstate

A more formal approach to the effective interaction compared to the intuitive arguments in sec. 2.1 is based on many-body perturbation theory. The idea is to view the two-body interaction as a perturbation of an assumed, unperturbed mean field Hamiltonian. One obtains the ground state energy by means of a linked cluster expansion in powers of the interaction. By rearranging the series and summing over a certain type of terms one can overcome the difficulty with the strength of the nucleonic interaction and arrive at an expansion in powers of the nuclear reaction matrix. The lowest order terms correspond to the effective interaction from which in turn defines a modified mean field. The traditional approach employs time-dependent perturbation theory and yields the perturbed state via a Dyson expansion of the time-development operator in the adiabatic limit for the time dependence. The topic is usually referred to as Goldstone-Hugenholtz method; it can be found elsewhere [5,15] along with the auxiliary theorems due to Wick needed in the evaluation of time-ordered products. Some basic equations are presented in this section and a diagrammatic representation of the terms in the perturbation series is given which facilitates the interpretation of the various terms in the perturbation series. The use of operators in second quantization is not mandatory but allows for ready interpretation.

The starting point is the definition of an auxiliary, yet unknown mean field Hamiltonian, which is constructed from Hamiltonians H_{ij}^s of the n individual nucleons

$$H_{ij}^s = [\langle i|T|j\rangle + \langle i|U|j\rangle] a_i^\dagger a_j \quad (2.11)$$

with eigenstates $|\phi_i\rangle$ the mean field many-body Hamiltonian is given by

$$H_o = \sum_{ij} [\langle i|T|j\rangle + \langle i|U|j\rangle] a_i^\dagger a_j. \quad (2.12)$$

T stands for the kinetic energy here and U denotes the single-particle potential. The basis for the perturbation theory is the many-body eigenstates $|\phi\rangle$ of (2.12) which are the antisymmetrized products of the single-particle eigenstates of (2.11)

$$|\phi(E)\rangle = A \prod_{i=1}^n |\phi_i(E)\rangle \quad (2.13)$$

with the energy eigenvalue E as the sum of the eigenvalues corresponding to the $|\phi_i(E)\rangle$. The energy of the unperturbed groundstate $|\phi_o\rangle$ is then given as a sum over the lowest single-particle eigenvalues. The perturbation proper is the nucleon-nucleon interaction V but one has to subtract also the spurious auxiliary potential, thus the definition of the perturbation

$$H_p = \sum_{ijkl} \langle ij|V|lk\rangle a_i^\dagger a_j^\dagger a_k a_l - \sum_{ij} \langle i|U|j\rangle a_i^\dagger a_j. \quad (2.14)$$

In essence the Hamiltonian H for the interacting system has been separated in a mean field part (2.12) and a perturbing part (2.14)

$$H = H_o + H_p, \quad (2.15)$$

where H should not depend on the auxiliary potential U . The choice of U provides some freedom to influence the convergence properties of the perturbation expansion, which is given for the groundstate energy by

$$\begin{aligned} \langle \psi_o | H | \psi_o \rangle &= \frac{\langle \phi | H | \phi_o \rangle}{\langle \phi | \phi_o \rangle} \\ &= \langle \phi_o | H_o | \phi_o \rangle + \sum_m \langle \phi_o | H_p \left[H_p \frac{1 - |\phi_o\rangle\langle\phi_o|}{E_o - H_o} H_p \right]^{m-1} | \phi_o \rangle, \end{aligned} \quad (2.16)$$

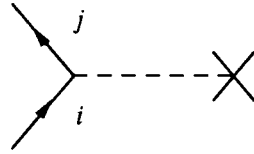
under the normalization $\langle \phi | \phi_o \rangle = 1$ and the condition that $|\phi_o\rangle$ is non-degenerate. The second term in (2.16) represents the corrections to the unperturbed groundstate, and as in ordinary perturbation theory the intermediate states are projected off the unperturbed state. The operators in (2.16) are sums of one- and two-body operators by eqs. (2.14, 2.12) which single out the particular one- and two-particle projections of the many-

nucleon states. Inserting them explicitly yields terms like e.g. first order in V

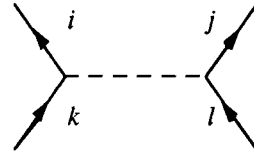
$$\langle \phi_0 | H_p | \phi_0 \rangle = \sum_{ijkl} \langle ij | V | lk \rangle \langle \phi_0 | a_i^\dagger a_j^\dagger a_k a_l | \phi_0 \rangle - \sum_{ij} \langle i | U | j \rangle \langle \phi_0 | a_i^\dagger a_j | \phi_0 \rangle, \quad (2.17)$$

where the sums sample *all* possible single-particle states. It is understood that only distinct terms are retained, for example $\langle ij | V | lk \rangle = \langle lk | V | ij \rangle$ is counted only once. The expansion (2.17) can be cast into a diagrammatic representation, due to Goldstone [2]. Each term is represented by a diagram. They are constructed from basic elements and their contributions to the perturbation series are evaluated according to the following rules [2,5].

Rule I Fermion lines. Particles are represented by a line pointing upwards, holes by lines pointing downwards. The time is directed upwards.



(a) $\langle i | U | j \rangle$



(b) $\langle ij | V | lk \rangle$

Rule II Interactions. For each interaction $\langle i | U | j \rangle$ draw a basic one-body vertex (a). Interactions $\langle ij | V | lk \rangle$ are represented by a two-body vertex (b).

The creation and annihilation operators in (2.6) act between the unperturbed groundstate. Consequently no external lines can enter or leave a vertex, all fermion lines are paired up, contracted, and all possible combinations contribute.

Rule III Contractions. Connect all the fermion lines in all possible ways with all possible orderings of the vertices. Lines entering a vertex from below denote fermion destruction, lines leaving a vertex represent fermion creation.

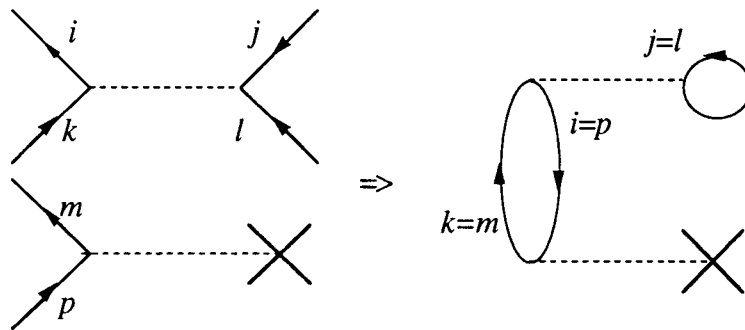


Figure 1 Construction of Goldstone Diagrams. Example of a 2nd order contribution to the perturbation series (2.16) according to rule III. At the lower

vertex a nucleon is excited out of state i into a state k . Two nucleons, in a hole state i and in a particle state k propagate as particle-hole excitation. At the upper vertex the excitation is destroyed by an interaction with a passive unexcited nucleon in the occupied state j . Note that this diagram does not obey momentum conservation and will not contribute to the groundstate energy of nuclear matter.

Starting with order $m=2$ the propagators contribute energy denominators which represent the excitation energy

$$(E-H_0)^{-1} = e^{-1} = \left(\sum_{\text{holes}} \epsilon_h - \sum_{\text{particles}} \epsilon_p \right)^{-1} \quad (2.18)$$

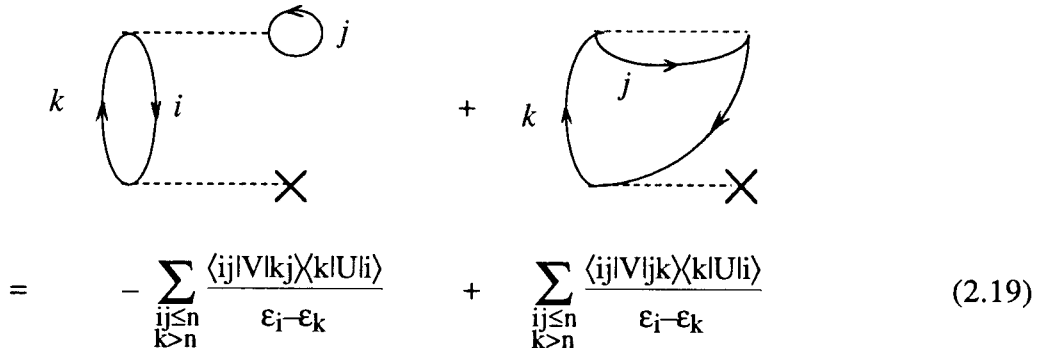
where the sums include all particle and hole lines at a given instance (horizontal section) in a diagram. Note that e as defined in (2.18) is a negative quantity.

Rule IV Energy Denominators. Include $m-1$ factors $1/e$ with the denominator being the excitation energies defined in eq. (2.18).

Rule V Sign Rule. Each hole line, each closed fermion loop and each one-body vertex contribute a factor of -1 . Bubbles as in fig. 1 count as hole lines.

Rule VI Intermediate States. Sum over all lines without observing the Pauli principle in intermediate (particle) states. All intermediate states are taken as simple product states. Include a factor of $1/2$ for each pair of equivalent lines. Two lines are equivalent if they point in the same direction and if they start at the same vertex and terminate at the same vertex.

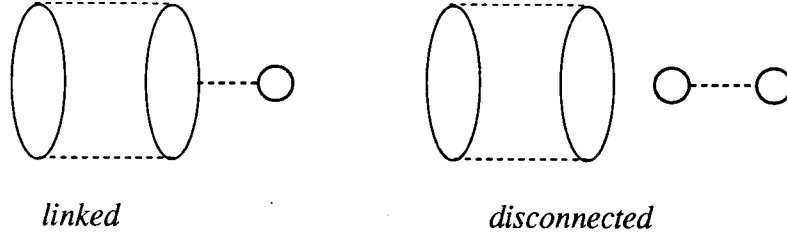
As an example, the diagram in fig. 1 is second order, so one has $m-1=1$ energy denominator with $e = \epsilon_k - \epsilon_i$. There are 2 intermediate hole lines, labeled i and j . There are 2 fermion loops, including the bubble, they contribute a factor $(-1)^2$. From the one-body vertex one gets an additional factor -1 . This leads to the equation



$$= - \sum_{\substack{ij \leq n \\ k > n}} \frac{\langle ij | V | kj \rangle \langle k | U | i \rangle}{\epsilon_i - \epsilon_k} + \sum_{\substack{ij \leq n \\ k > n}} \frac{\langle ij | V | jk \rangle \langle k | U | i \rangle}{\epsilon_i - \epsilon_k} \quad (2.19)$$

where the right graph is the exchange term associated with the left one, since it has one fermion loop less, it has the opposite sign. Beginning with third order in the

perturbation, also disconnected diagrams occur, for example



It can be shown that only linked graphs contribute to the perturbation series (2.16). This is expressed by the Linked Cluster Theorem [15], due to Goldstone

$$\langle \psi_0 | H | \psi_0 \rangle = \langle \phi_0 | H_0 | \phi_0 \rangle + \sum_m \langle \phi_0 | H_p \left[H_p \frac{1 - |\phi_0\rangle\langle\phi_0|}{E_0 - H_0} H_p \right]^{m-1} | \phi_0 \rangle_{\text{Linked}} . \quad (2.20)$$

Besides the significant reduction of the number of terms one has to evaluate, each term alone in eq. (2.20) exhibits the correct volume dependence, a feature not shared by the conventional Schrödinger perturbation series. At fixed density ρ , each linked diagram is proportional to the total number n of particles in the system and a graph with h independent hole lines is proportional to $n\rho^{h-1}$ [16]. Thus one has explicitly physical behavior in all orders, and the perturbation series can be terminated at a particular order without having to worry about spurious unphysical contributions which might eventually cancel out in higher orders. In lowest order the Hartree-Fock potential can be recovered from eq. (2.20). The groundstate energy is given in diagram notation by

$$\langle \psi_0 | H | \psi_0 \rangle = \langle \phi_0 | H_0 | \phi_0 \rangle + \text{diagram 1} + \text{diagram 2} + \text{diagram 3}$$

where the diagrams contribute nothing if evaluated according to

$$\frac{1}{2} \sum_{ij < n} (\langle ij | V | ij \rangle - \langle ij | V | ji \rangle) = \sum_{i < n} \langle i | U | i \rangle \quad (2.21)$$

which one recognizes as the Hartree-Fock potential. If the auxiliary potential is defined in this way, the mean field Hamiltonian (2.12) is correct to lowest order perturbation theory and incorporates the Pauli principle. Actually the definition (2.21) does more, it cancels all bubble insertions and the corresponding exchange graphs in all orders [2], this is illustrated below for the T -matrix. Correlations beyond mere antisymmetrization are then studied by examining the remaining diagrams, with the order of the correlation given by the number of hole lines, which represents the number of nucleons involved.

As it stands (2.20) can not be used for the nucleonic interaction because the strong short range repulsion renders all matrix elements V or V/e so large that the series can not

converge in powers of V . However the perturbation series can be rearranged in partial sums to account for the most important terms. Guidance is provided by the fact that nuclear matter behaves like a low-density Fermi gas, where the average spacing of the nucleons r_0 is much larger than the range a of the short-range repulsion. Each summation over a hole line roughly scales like $\rho \approx k_{fm}^3 \approx r_0^{-3}$ and it turns out that $(\rho a^3) \ll 1$ is a sensible parameter to classify the terms, dependent on their number of independent (not constrained by momentum conservation) hole lines [5]. The idea, due to Brueckner [1], is now to sum up all terms which are equivalent by this argument in the hope that the emerging series will converge. The prime candidates are those with repeated interactions between fermion lines, the so called ladder diagrams. Consider the two-hole line graphs

$$\langle ij|T_E|ij\rangle = t^{(1)} + t^{(2)} + t^{(3)} + \dots \quad (2.22)$$

with the ladder contributions

$$t^{(1)} = \langle ij|V|ij\rangle \quad t^{(2)} = \frac{1}{2} \sum_{lm>n} \frac{\langle ij|V|lm\rangle \langle lm|V|ij\rangle}{E - \epsilon_l - \epsilon_m}$$

$$t^{(3)} = \frac{1}{4} \sum_{\substack{lm>n \\ pq>n}} \frac{\langle ij|V|lm\rangle \langle lm|V|pq\rangle \langle pq|V|ij\rangle}{(E - \epsilon_l - \epsilon_m)(E - \epsilon_p - \epsilon_q)} \quad \text{etc.} \quad (2.23)$$

where E is the starting energy. Generally E depends on the entire diagram, see Appendix C. By defining the Pauli operator Q and the propagator Q/e from eq. (2.18) together with the operator $(1 - \phi_0)\langle\phi_0\rangle H_p$ in (2.16) one gets

$$Q = \sum_{lm>n} |lm\rangle \langle lm| \quad \frac{Q}{e_E} = \sum_{lm>n} |lm\rangle \langle lm| \frac{1}{E - \epsilon_l - \epsilon_m}, \quad (2.24)$$

which agrees with (2.3) in projecting off the states below the Fermi level. In its generalized form, eq. (2.22) defines the reaction matrix T_E via the series

$$T_E = V + V \frac{Q}{e_E} V + V \frac{Q}{e_E} V \frac{Q}{e_E} V + V \frac{Q}{e_E} V \frac{Q}{e_E} V \frac{Q}{e_E} V \dots \quad (2.25)$$

which is quite like the Born series in scattering theory. In the limit of an infinite system, it is equivalent to the integral equation for the T -Matrix

$$T_E = V + V \frac{Q}{e_E} T_E. \quad (2.26)$$

For a given starting energy, T_E is a well behaved hermitian operator. Remarkably, its matrix elements are finite despite the behavior of the bare nucleon-nucleon interaction. If one replaces the V -vertices by the corresponding T -vertices (wiggly lines) following the scheme of (2.23) the groundstate energy can be written as

$$\begin{aligned} \langle \Psi_0 / H / \Psi_0 \rangle = & \langle \phi_0 / H_0 / \phi_0 \rangle + \text{diagram 1} + \text{diagram 2} + \text{diagram 3} \\ & + \text{diagram 4} + \text{diagram 5} + \text{diagram 6} + \dots \\ & + \text{diagram 7} + \text{diagram 8} + \dots \end{aligned} \quad (2.27)$$

No second order graphs appear here because they are already absorbed in the first order diagrams for T_E . Some care needs to be exercised to avoid double counting of diagrams, the ultimate check for correctness of the rearranged expansion being comparison with the original one. The exposition here remains of course incomplete. For a detailed discussion the reader is referred to [5]. Convergence problems persist also for the revised series, and essentially it needs to be rearranged again with the number of independent hole lines as a "parameter". The most important diagrams are then the 2-hole line bubble and the exchange bubble in (2.27). In practice one can consider only those, having again the independent pair approximation, while the contributions of higher graphs can eventually be simulated by an appropriate choice of the auxiliary potential [9]. If one chooses the auxiliary potential as in the Hartree-Fock approximation one arrives at a new mean field Hamiltonian (2.12) which now includes the most important correlation effects arising from the short-range repulsion. Consider

$$\frac{1}{2} \sum_{ij} (\langle ij / T_E / ij \rangle - \langle ij / T_E / ji \rangle) = \sum_i \langle i / U / i \rangle, \quad E = \epsilon_i + \epsilon_j. \quad (2.28)$$

as definition for the mean field. The T -matrix is evaluated under the proviso that the

starting energy should be evaluated on-shell, so $E = \epsilon_i + \epsilon_j$, regardless of the rest of the diagram. This is necessary to achieve uniqueness for the single-particle potential. As before for the bare V , all bubble-insertions and associated exchange terms cancel in all orders

$$(2.29)$$

and apparently it those terms which modify the spectrum. The procedure of selectively cancelling terms at a given order in general has loopholes, because it is not clear *a priori* that the remaining fragments are less important. It is demonstrated in [5] that the on-shell prescription as a bonus also treats equal terms consistently. A self-consistency problem, see App. B, arises from the on-shell condition since U determines the ϵ_i and the eigenstates $|i\rangle$ in (2.18). The choice whether to demand self-consistency for intermediate particle as well as for hole states had a controversial history, but the established prescription today is to satisfy it for all states [7]. There is some freedom in determining the single-particle spectrum, due to the fact that the Hamiltonian (2.12) need not agree for occupied and unoccupied states, see App. B. The prior choice, due to Bethe, was to obtain the hole spectrum self-consistently and to set $U = 0$ for particle states. This appeals to the argument that for high momentum states the kinetic energy should prevail over the potential energy and moreover that the contributions of 3-body correlations are suppressed by this choice. While according to [7] the latter remains true also if all states are treated self-consistently, one obtains a better estimate of the binding energy. A sketchy reason is that the former method implies a big gap at the Fermi surface which suppresses low-momentum excitations which pertain to long-range correlations, see fig. 12 in ch. 6. If those increase the two-particle wave function in the attractive region of the potential, one would gain additional binding energy as opposed to the case where they are excluded.

2.3 Nuclear Matter

The preceding sections provided the theoretical background for the treatment of many-nucleon systems. This one establishes some conventions needed before one can proceed with actual calculations. The major advantage of considering nuclear bulk properties via nuclear matter is the conservation of momentum associated with the translational invariance. Thus the single-particle states can be chosen as eigenstates $|k_i\rangle$ of the single-nucleon momentum operator. Also for the one-body vertex, momentum

conservation requires $k_i=k_j$. For the two-body vertex $k_i+k_j=k_k+k_l$, and, among many others, diagrams like fig. 1 are excluded because they would simultaneously have a particle and a hole in the same state. The fixed set of momentum basis states further obliterates any self-consistency condition for the single-particle states. The wave function at position \mathbf{r}_i for a nucleon with momentum \mathbf{k}_i is the plane wave

$$\langle \mathbf{r}_i | \mathbf{k}_i \rangle = \frac{1}{(2\pi)^{3/2}} e^{i\mathbf{k}_i \mathbf{r}_i}, \quad (2.30)$$

normalized to the 3-dimensional δ -function. Summations over discrete levels in a finite system of volume V are replaced by integrations in the usual way

$$\lim_{V \rightarrow \infty} \frac{1}{V} \sum_m^{n, \infty} F((\mathbf{k}_i)_m) \quad \rightarrow \quad \frac{1}{(2\pi)^3} \int_0^{k_{fm}, \infty} d^3 k_i F(\mathbf{k}_i). \quad (2.31)$$

The two-body scattering problem is separable into the center-of-mass and the relative motion of the two particles 1 and 2 with momenta \mathbf{k}_1 and \mathbf{k}_2 . The underlying transformation to the center-of-momentum *cms*-frame is defined by

$$\text{relative momentum} \quad \mathbf{k} = \frac{1}{2} (\mathbf{k}_1 - \mathbf{k}_2) \quad (2.32)$$

$$\text{average momentum} \quad \mathbf{K} = \frac{1}{2} (\mathbf{k}_1 + \mathbf{k}_2)$$

Corresponding in position space are the transformations

$$\text{relative separation} \quad \mathbf{r} = (\mathbf{r}_1 - \mathbf{r}_2) \quad (2.33)$$

$$\text{cms-position} \quad \mathbf{R} = (\mathbf{r}_1 + \mathbf{r}_2)$$

noting that this deviates from the usual definition for \mathbf{K} and \mathbf{R} . A two-particle product wave function expressed in the *cms*-quantities becomes

$$\langle \mathbf{R} \mathbf{r} | \mathbf{K} \mathbf{k} \rangle = \langle \mathbf{r}_1 \mathbf{r}_2 | \frac{(\mathbf{k}_1 + \mathbf{k}_2)}{2} \frac{(\mathbf{k}_1 - \mathbf{k}_2)}{2} \rangle = \frac{1}{(2\pi)^3} e^{i\mathbf{K} \mathbf{R}} e^{i\mathbf{k} \mathbf{r}}, \quad (2.34)$$

where the separation of the relative and *cms*-motion is manifest by the product. Neutrons and protons are treated as an isospin doublet and are distinguished only by their isospin projection. Conventional spins and isospins of the scattering particles are coupled and yield the total spin S and total isospin I . The related eigenstates are already antisymmetrized and incorporated into the two-particle states by direct multiplication

$$|KkSM_SIM_I\rangle = |Kk\rangle \otimes |SM_S\rangle \otimes |IM_I\rangle \quad (2.35)$$

Unless otherwise specified the spatial part will not be antisymmetrized. Of course one has triplets $S, I=1$ as well as singlets $S, I=0$.

In the notation throughout the rest of the thesis, the spin or isospin dependence will be implied but not be written out if unambiguous, e.g. the integration in (2.8) also implies the summation over the spin variables. The isospin quantum numbers will be suppressed as they are determined once parity and spin are specified later on. Although not inherently limited by the theory, the subsequent development will be restricted to symmetric nuclear matter.

Unless stated otherwise, all energy-like quantities, e, V, T_E etc. are given in units fm^{-2} , i.e. they are scaled with

$$\frac{\hbar^2}{M} = 41.47 \text{ MeV } fm^2 \quad (2.36)$$

where M is the nucleon mass. For example the energy of a free nucleon becomes $1/2k^2$ in these units.

3. Solution of the Bethe-Goldstone Equation

3.1 The Reference Spectrum Method

Apart from the question of how to choose the single-particle spectrum of the intermediate states, conflicting computational demands arise from the Pauli operator and the short-range repulsion of the interaction. The short-range correlations induced by the interaction require many high momentum components to describe them adequately. In position space those correlations are readily treated. For example in the case of an infinite hard core potential the main correlation effect consists of the vanishing wave function inside the core, which is equivalent to the boundary condition that the wave function, see (3.14), vanishes at the core edge. By contrast, the Pauli operator Q is diagonal in the relative momentum and is represented by a Heavyside function, see eq. (3.32). In position space this implies on the other hand that Q is a long-ranged, non-local operator. Thus neither the position nor the momentum space representation offer any particular computational incentive if one solves the integral equation (2.4) directly [1]. Alternatively the calculation can be attempted in two stages by obtaining an approximate solution in position space and by then improving it in momentum space. This is done in the reference spectrum method [5,10]. It is based on two observations. First, those intermediate states which are most important in building up the short-range correlations lie well above the Fermi momentum up to $k \approx 3...5 \text{ fm}^{-1}$ [5]. The single particle spectrum in this region can be approximated sufficiently well by a modified free particle spectrum of the form

$$E^R(k) = \frac{1}{2m^*} k^2 + A, \quad (3.1)$$

where the effective mass m^* and the constant single-particle potential A reflect the influence of the surrounding medium on the scattering particles. Typical values are $m^* = 0.65$ and $A \geq 0$, see fig. 12 in chapter 6. Second, since those intermediate states are at momenta above the Fermi momentum, they are not affected by the Pauli operator. For intermediate states below the Fermi momentum the Pauli operator may be neglected as well, because they contribute a much smaller fraction to the two-particle phase space than those above the Fermi level and moreover the scattering into them is suppressed by the large values of the excitation energies ($> 50 \text{ MeV}$) [2]. This provides the motivation for setting Q equal to unity for all states. The reference T -matrix T^R is then defined from (2.27) by

$$T^R = V + \frac{1}{e^R} V T^R, \quad (3.2)$$

where the propagator is now given in terms of the reference spectrum E^R as

$$e^R = E - \frac{1}{m^*} (K^2 + k^2) - 2A, \quad (3.3)$$

with the *cms* choice (2.32). The starting energy E corresponds to a set of momenta below the Fermi momentum. Since the energies of the intermediate states for hole momenta are taken from the reference spectrum and since particle states enter eq. (3.3) always off-shell, no singularities are introduced into (3.2) and the healing property of the correlated pair wave function is preserved. The reference spectrum is thus concerned with the short-range effects of the potential only and the quadratic form of (3.3) permits one to transform the integral equation (3.2) into an ordinary differential equation in position space, from which the correlated reference wave functions readily derive. Once T^R has been obtained the actual reaction matrix T follows formally as [10]

$$T = T^R + T^R \left[\frac{1}{e^R} - \frac{Q}{e} \right] T. \quad (3.4)$$

The propagator difference accounts for the corrections to T^R due to the initial neglect of the Pauli principle and the shift of the single particle spectrum in the reference spectrum method. With the Pauli operator present, eq. (3.4) can be treated appropriately in momentum space and it is also the starting point for Legindgaard's method

3.2 Calculating the Reference Reaction Matrix

According to the previous section the intermediate aim is now to obtain a momentum space representation of T^R with the actual calculation carried out in position space. Starting from the differential equation equivalent to (3.2) one arrives at correlated reference wave functions $\psi^R(k,r)$ which yield T^R as an integral in position space. With the help of the reference Møller operator Ω^R one can express T^R as

$$T^R = V \Omega^R. \quad (3.5)$$

Using eq.(3.3) this can be manipulated in eq. (3.2) and one has

$$e^R (1 - \Omega^R) = -V \Omega^R. \quad (3.7)$$

The momentum operators in e^R become differential operators in position space and (3.7) constitutes a differential equation for the defect wave function $\zeta^R(k,r) = \Phi(k,r) - \psi^R(k,r)$ which measures the defect inflicted by the pair interaction upon the uncorrelated wave function $\Phi(k,r)$. With the spin variables written out

$$(\nabla^2 - \gamma^2 E, K)) \zeta_{SM_s}(kr) = -m^* V(r, S) \psi_{SM_s}(kr), \quad (3.8)$$

where the healing parameter γ essentially describes how rapidly the defect wave function decays with increasing r so that the motion of the scattering particles becomes independent again. Since the Pauli operator is absent in this approximation, one expects that the healing parameter is quite incorrect [3], especially at low relative momenta. It is defined from (3.1) and (3.2) by

$$\gamma^2 = K^2 + m^*(2A - E). \quad (3.9)$$

Exploiting the isotropy of nuclear matter and given that the interaction V depends on the total spin S and the relative angular momentum l of the interacting pair a partial wave decomposition is introduced. Projecting eq.(3.8) onto the partial wave bases $|KkJISM\rangle$ and $|KrJISM\rangle$ yields

$$\langle KrJISM_s | (\nabla^2 - \gamma^2) (1 - \Omega^R) | kS'M'_s \rangle = -m^* \langle KrJISM_s | V \Omega^R | kS'M'_s \rangle. \quad (3.10)$$

With regard to the spherical symmetry the quantization axis is chosen along the *cms* momentum K . J denotes the total angular momentum in a state with orbital angular momentum l if the pair has total spin S ; M stands for the z -projection of J . More details concerning the partial wave expansion are given in Appendix A. In particular, the basis transformation between radial position and momentum representation of correlated states follows

$$\langle KrJISM | \Omega^R | KkJ'I'S'M' \rangle = \delta_{JJ'} \delta_{SS'} \delta_{MM'} \left(\frac{2}{\pi} \right)^{1/2} i^{l'} \frac{u_{JII'S}(kr)}{kr}. \quad (3.11)$$

Here, the $u_{JII'S}(kr)$ are explicitly independent of M , and l' is commonly called the entrance channel. The scalar interaction potential V is taken to be local and has the components

$$\langle KrJISM | V | Kr'J'I'S'M' \rangle = \delta_{JJ'} \delta_{SS'} \delta_{MM'} \delta(r-r') V_{JII'S}(r). \quad (3.12)$$

Eq. (3.4) implemented in the partial wave basis constitutes now a differential equation for the radial correlated partial waves $u_{JII'S}(kr)$

$$\left[\frac{\partial^2}{\partial r^2} - \frac{l(l+1)}{r^2} - \gamma^2 \right] \left(\delta_{II'} J_l(kr) - u_{JII'S}(kr) \right) = -m^* \sum_{I'} V_{JII'S}(r) u_{JII'S}(kr), \quad (3.13)$$

where regularity at $r=0$ and the healing property impose the boundary conditions

$$u_{Jl'l'S}(0) = 0, \quad \lim_{kr \gg 1} u_{Jl'l'S} = \delta_{ll'} J_{l'}(kr). \quad (3.14)$$

The unperturbed components $J_l(kr)$ are derived from spherical Bessel functions $j_l(kr)$ according to $J_l(kr) = kr j_l(kr)$. The partial wave projections of T^R are obtained from the projections of the correlated and uncorrelated wave functions and lead to the expansion

$$\begin{aligned} & \langle KkSM_s/T^R/Kk'SM'_s \rangle \\ &= \int d^3r \Phi_{SM_s}(\mathbf{kr}) V(r) \Psi^R_{SM'_s}(\mathbf{k'r}) \\ &= \frac{4\pi}{(2\pi)^3} \sum_{JM} i^{l-l'} Y_{lm}(\Omega_k) C_{mM_s M}^{lSJ} Y_{l'm'}^*(\Omega_{k'}) C_{m'M'_s M}^{l'SJ} \langle KkJISM/T^R/KkJ'I'SM \rangle, \\ & \quad \text{with } lml'm' \end{aligned} \quad (3.15)$$

with the spherical harmonics $Y_{lm}(\Omega_k)$ and the Clebsch-Gordan coefficients $C_{mM_s M}^{lSJ}$. The convention for partial wave constituents of T^R takes on the form

$$\langle KkJISM/T^R/KkJ'I'SM \rangle \equiv \frac{4\pi}{kk'} \left[\sum_{l''} \int_0^\infty dr J_{l''}(kr) V_{Jl''S} u_{l''l'JS}(k'r) \right]. \quad (3.16)$$

If the potential contains also a hard core of radius r_c , the product $V\psi$ becomes undetermined inside the core. Via the two potential form of the Lippmann-Schwinger equation one can derive an additive separation of contributions from the core (subscript "<") and the potential $V_>$ in the outer region

$$T^R = \Omega_{<} V_{>} \Omega + T^R_{<}. \quad (3.17)$$

The modified eq.(3.16) includes then the contributions of the hard core and the outer region as two distinct terms

$$\begin{aligned} \langle KkJISM/T^R/KkJ'I'SM \rangle &\equiv \frac{4\pi}{kk'} \left[\sum_{l''} \int_{r_c}^\infty dr (J_{l''}(kr) - H_{l''}(k, \gamma)) V_{Jl''S} u_{l''l'JS}(kr) \right. \\ &\quad \left. + \delta_{ll'} \left\{ (\gamma^2 + k^2) \int_0^\infty dr J_l(kr) J_{l'}(k'r) + J_l(kr_c) \frac{\partial}{\partial r} (J_{l'}(k'r) - H_{l'}(k', \gamma_c)) \right\} \right]. \end{aligned} \quad (3.18)$$

Here the functions $H_l(k, \gamma)$ are the decaying spherical Hankel functions resulting from the core scattering. They are normalized to $J_l(kr_c)$ and

$$H_l(k, \gamma) \equiv H_l^{(-)}(\gamma) \frac{J_l(kr_c)}{H_l^{(-)}(\gamma_c)}, \quad (3.19)$$

with $H_l^{(-)}(x) = i^{l+1} (ix) h_l^{(1)}(ix)$. The form of the differential equations (3.13) remains unaltered by introducing a hard core, $V_{JHS}(r)$ of course being replaced by the finite potentials in the outer region and the lower boundary becoming r_c . Both, core volume and core edge contributions - the second integral and the derivative term in (3.18) - vanish if $r_c \rightarrow 0$ and eq.(3.16) is gained back, e.g. for the RSCP potentials.

3.3 Legindgaard's Method and Full Nuclear Matter Reaction Matrix

Having T^R as first approximation, eq. (3.4) furnishes the prescription how to proceed towards the full reaction matrix. In principle one could discretize it and iterate the solutions in position space [12]. This way the true wave functions, with the low momentum components diminished compared to the reference wave function due to the exclusion principle, emerge naturally during the calculation. But this transparency contrasts the computational effort of the iteration procedure which must be performed for each matrix element separately. The situation is remedied by benevolent convergence [7] and in cases where one does not need to know off-diagonal elements (see ch. 4). Another method is due to Legindgaard [11] and takes advantage of two observations. As explained in section 3.1 the reference spectrum suitably approximates the true nuclear matter spectrum for larger single particle momenta, $k_i \geq 3...5 fm^{-1}$. If one chooses $E^R(k_i)$ to coincide with the true single particle spectrum $E(k_i)$ beyond some cutoff momentum $k_{max} > k_{fm}$ the difference of the propagators in eq. (3.4) vanishes above this cutoff.

Formally, the two-particle states with $k > k_{max}$ lie in the nullspace L of the operator $1/e^R - Q/e$. If one is just interested in solutions up to moderate momenta $k < k_{max}$, e.g. in binding energy calculations, it is sufficient to consider eq. (3.4) only in the complement of L , which includes then only states for which the propagator difference does not vanish identically. An inspection [12] of the functional dependence on magnitude of the relative momentum k revealed that matrix elements $T(K, k)$ depend smoothly on k and can be represented by low-order polynomials. The polynomials are constructed from the requirement that the underlying polynomial basis must span the described subspace of the Hilbert space, i.e. define a complete orthonormal basis for $k \in [0, k_{max}]$. In the Kk -basis the model space can be taken as a sphere in the relative momentum with radius $k_{max} > 2k_{fm}$, see fig. 2. The transformation between the entrance channel basis (3.10) the polynomial basis $|KnJISM\rangle$ obeys the relation

$$\langle KkJISM|KnJISM\rangle = F_n(k), \quad (3.20)$$

where the polynomials $F_n(k)$ form a complete set of orthogonal functions on the interval $[0, k_{max}]$

$$\sum_{n=1}^{\infty} F_n(k) F_n(k') = \frac{\delta(k-k')}{k^2}, \quad (3.21)$$

$$\int_0^{k_{max}} k^2 dk F_n(k) F_{n'}(k) = \delta_{nn'} \quad (3.22)$$

The polynomials $F_n(k)$ are of order $n-1$ and are given by

$$F_n(k) = \left(\frac{2n+1}{k_{max}^3} \right)^{1/2} (-1)^{n-1} \sum_{s=0}^{n-1} \frac{(-1)^s (n+s+1)!}{s! (n-1-s)! (s+2)!} \left(\frac{k}{k_{max}} \right)^s \quad (3.23)$$

Partial wave components of $T(Kk)$ in the polynomial representation are obtained with the unitary transformation (3.20) as

$$\langle K n J l S M / T / K n' J l' S M \rangle = \int_0^{k_{max}} k^2 dk \int_0^{k_{max}} k'^2 dk' F_n(k) F_{n'}(k') \langle K k J l S M / T / K k' J l' S M \rangle. \quad (3.24)$$

The inverse transformation, truncated at order n_{max} is given by

$$\langle K k J l S M / T / K k' J l' S M \rangle_{n_{max}} = \sum_{n, n'=0}^{n_{max}} F_n(k) F_{n'}(k') \langle K n J l S M / T / K n' J l' S M \rangle. \quad (3.25)$$

The convergence in n_{max} is well established for both, T and T^R [11]. In practice $n_{max} = 5$ usually proved to be adequate. The polynomial representation (3.24) applied to eq. (3.4) results now in a low-dimensional matrix equation

$$\begin{aligned} \langle K n J l S M / T / K n' J l' S M \rangle = & \langle K n J l S M / T^R / K n' J l' S M \rangle + \sum_{\substack{n_1, n_2 \\ J_1, J_2 \\ l_1, l}} \langle K n J l M / T^R / K n_1 J_1 l_1 M \rangle \\ & \times \langle K n_1 J_1 l_1 S M / \frac{1}{e^R} - \frac{Q}{e} / K n_2 J_2 l_2 S M \rangle \langle K n_2 J_2 l_2 S M / T / K n' J l' S M \rangle. \end{aligned} \quad (3.28)$$

The apparent simplicity of (3.28) is blurred by the Pauli operator. It breaks rotational invariance and couples states with different l so that J and M are no longer conserved. The rotational symmetry is usually restored with immaterial loss in accuracy [11,18] by considering only an angle averaged version of Q . At first sight however an expansion in any discrete set of functions in k appears unsuitable for Q since it is diagonal in k and it is not analytic as a function of k at the Fermi surface. Fortunately the expansions of T and T^R converge rapidly enough to overcome this difficulty. The angular momentum

sums in eq. (3.28) are modest: For $S=0$ one has $l=J$ while for $S=1$, the tensor interaction allows for $l=J\pm 1$. If one considers J_{max} couplings induced by the Pauli operator, the Bethe-Goldstone equation is realized by a matrix equation of dimension $N_D = n_{max} J_{max}$ or, in the tensor coupled cases, $N_D = 2n_{max} J_{max}$. The polynomials (3.23) can be viewed as best fits in the sense that they minimize the mean square deviation

$$\sigma^2 = \int_0^{k_{max}} k^2 dk \left| {}^{n_{max}}T(k, k') - T(k, k') \right|^2, \quad (3.29)$$

where ${}^{n_{max}}T(k, k')$ is obtained from $T(n, n')$ via the inverse Legendgaard transformation (3.24) with the cutoff $n, n' \leq n_{max}$. Recalling that the reference spectrum method provides by itself a good first approximation the difference $T(k, k') - T^R(k, k')$ should exhibit a smoother dependence on k than either $T(k, k')$ or $T^R(k, k')$. The polynomial expansion of this difference in deed converges faster. The preferred approach is then to calculate only $T - T^R$ in the polynomial basis by means of the rearranged eq. (3.4)

$$T - T^R = \left[I - T^R \left\{ \frac{I}{e^R} - \frac{Q}{e} \right\} \right]^{-1} T^R - T^R \quad (3.30)$$

and to add the difference back to T^R [11] in momentum space representation.

3.4 The Pauli Exclusion Operator

In sec. 2.1 the Pauli operator Q was introduced into the two particle scattering equation to prevent particles from scattering into already occupied intermediate states. This section discusses some properties of Q in uniform matter. It starts with a description of the geometric properties of Q in the cms system of the scattering pair. An explicit expression for Q in the partial wave basis is given and the analytical behavior of Q is addressed with respect to the discrete angular and radial expansions in momentum space. The angle averaged approximation concludes the discussion.

The Pauli operator is diagonal in the single-particle momenta and thus in \mathbf{K} and \mathbf{k} by the transformation (2.32); the cms representation of Q is given by

$$\begin{aligned} \langle \mathbf{Kk} | Q | \mathbf{K'k'} \rangle &= \delta^3(\mathbf{K}-\mathbf{K'}) \delta^3(\mathbf{k}-\mathbf{k'}) (1 - n(\mathbf{K}+\mathbf{k})) (1 - n(\mathbf{K}-\mathbf{k})) \\ &\equiv Q(\mathbf{Kk}), \end{aligned} \quad (3.31)$$

with the occupation densities $n(\mathbf{k})$

$$n(\mathbf{k}) = \theta(|\mathbf{k}| - k_{fm}). \quad (3.32)$$

As a consequence of the isotropy of the medium $Q(Kk)$ can be completely described by the magnitude and the relative orientation of K and k , given by the angle θ_{Kk} . The z -axis was chosen in sec. 3.2 along K to take advantage of the rotational symmetry. The selection rule eq. (3.31) in terms of these variables can be rewritten as

$$\begin{aligned} Q(Kk) &= 1 && \text{for } K^2 + k^2 - 2Kk |\cos\theta_{Kk}| \geq k_{fm}^2, \\ Q(Kk) &= 0 && \text{else} \end{aligned} \quad (3.30)$$

For fixed average and Fermi momenta the two particle phase space separates in three domains shown in fig. 2. If k lies outside a sphere with radius $(K^2 + k_{fm}^2)^{1/2}$, the Pauli principle is never violated and $Q = 1$, whereas for k inside a sphere with radius $k_{fm} - K$, $Q(Kk)$ always vanishes. In the intermediate region $Q(Kk)$ depends also on θ_{Kk} , with a discontinuity at the characteristic cut-off angle $\theta_c(K, k)$ defined by

$$\cos\theta_c(K, k) = \frac{K^2 + k^2 - k_{fm}^2}{2Kk}. \quad (3.31)$$

For the solution of the Bethe-Goldstone equation Q is needed in the partial wave representation of eq. (3.28). The azimuthal symmetry of $Q(Kk)$ suggests a multipole expansion, which can be readily used in the partial wave representation where the angular functions are spherical harmonics and can be regarded as spherical tensor operators. They couple partial waves with different l , parity being conserved for $Q(Kk)$ being an even function of $\cos\theta_{Kk}$ (3.30). Because of the coupling in l the total angular momentum J is no longer conserved, whereas its z -projection M remains unaffected due to the azimuthal symmetry and Q 's independence of the particles' spin. Consider the matrix element in the ppw (polynomial and partial wave) representation

$$\begin{aligned} &\langle KnJISM | Q | Kn'J'I'S'M' \rangle \\ &= \int_0^{k_{max}} k^2 dk F_n(k) F_{n'}(k) \langle KkJISM | Q(K, k) | KkJ'I'S'M' \rangle, \end{aligned} \quad (3.32)$$

where the $F_n(k)$'s are the Legendgaard polynomials. The multipole expansion is defined in terms of the Legendre polynomials $P_L(\cos\theta_{Kk})$ as

$$Q(Kk) = \sum_L q_L(K, k) P_L(\cos\theta_{Kk}),$$

or equivalently in terms of the associated spherical harmonics $Y_{L0}(\Omega_k)$

$$Q(Kk) = \sum_L \left(\frac{4\pi}{2L+1} \right)^{1/2} Y_{L0}(\theta_{Kk}, \phi) \quad (3.33)$$

with the multipoles $q_L(K, k)$ given by

$$q_L(K, k) = \frac{2L+1}{2} \int_{-1}^1 dx Q(Kk) P_L(x) , \quad x = \cos \theta_{Kk} . \quad (3.34)$$

After decoupling the total angular momentum J in (3.32) into l and spin S and projecting the partial waves $|klm\rangle$ onto the basis states $|k\rangle$, see App. A., one arrives at

$$\begin{aligned} & \langle KkJISM | Q | KkJ'I'S'M' \rangle \\ &= \delta_{SS'} \sum_{mm'S_s} C_{mM_sM}^{ISJ} C_{m'M_sM}^{I'SJ'} \langle KklmSM_s | Q | Kkl'm'SM_s \rangle \\ &= \delta_{SS'} \sum_{mm'S_s} C_{mM_sM}^{ISJ} C_{m'M_sM}^{I'SJ'} \sum_L q_L(K, k) \frac{(4\pi)^{\frac{1}{2}}}{\hat{L}} \int d\Omega_k Y_{lm}^*(\Omega_k) Y_{L0}(\Omega_k) Y_{l'm'}(\Omega_k) . \end{aligned} \quad (3.35)$$

Here and in the following $\hat{L} = (2L+1)^{1/2}$. The integral over solid angle clearly manifests the tensor character of Q , it may be evaluated using the Wigner-Eckart theorem [15],

$$\begin{aligned} \int d\Omega_k Y_{lm}^*(\Omega_k) Y_{l'm'}(\Omega_k) Y_{L0}(\Omega_k) &= \langle lm | Y_{L0} | l'm' \rangle \\ &= C_{m0m'}^{lLl'} \frac{\langle l || \tilde{Y}_L || l' \rangle}{\hat{L}} \end{aligned} \quad (3.36)$$

The Clebsch-Gordan coupling coefficient reflects the selection rule $m = m'$, which results in $M = M'$. Finally a matrix element of Q in the polynomial representation reads

$$\begin{aligned} & \langle KnJISM | Q | KnJ'I'S'M' \rangle \\ &= \delta_{SS'} \delta_{MM'} \sum_{mM_s} C_{mM_sM}^{ISJ} C_{m'M_sM}^{I'SJ'} \sum_L \frac{\hat{L}}{\hat{L}^2} (-1)^m C_{m-m0}^{lLl'} C_{000}^{l'L} \int_0^{k_{max}} k^2 dk F_n(k) F_{n'}(k) q_L(K, k), \end{aligned} \quad (3.37)$$

where the sum over m collapses because of the restriction $m = M - M_s$. Similar to the poor convergence of this expansion in the order n of the polynomials $F_n(k)$ the lack of analyticity of Q viewed as a function of θ_{Kk} requires many multipoles to accurately model the angular dependence, see fig. 3. This flaw is overcome by the fact that in eq. (3.28) Q appears only integrated over intermediate states. There the partial wave projections of T decline rapidly with increasing l as a consequence of the weakening interaction V for those channels and thus the couplings to states with higher l are irrelevant. This at least applies to the case of the Reid potentials, which account for $J \leq 2$ only, and furthermore already the angle averaged prescription where one limits oneself

to the monopole term in (3.37) yields results accurate to within a few percent [18] even for higher partial waves. In principle no difficulties arise from the couplings of different l , but apart from breaking the spherical symmetry they enlarge the matrices in eq.(3.28) and complicate the evaluation of the partial wave expansion for T , which is similar to eq. (3.15) and enters the calculation of the single particle spectrum, see ch.4 . Thus it is also convenient to resort to the angle averaging procedure which is pictured in fig. 4. Formally, the coupling coefficients in (3.37) satisfy

$$C_{m-m0}^{ll'L} C_{000}^{ll'L} \stackrel{L=0}{=} \delta_{ll'} \frac{(-1)^m}{\hat{l}^2}. \quad (3.38)$$

After inserting eq. (3.38) in (3.37) the unitarity of the Clebsch -Gordan coefficients can be used to give the angle averaged Pauli operator Q_{av} defined by

$$\langle KnJlSM | Q | Kn'J'l'S'M' \rangle_{av} = \delta_{JJ'} \delta_{ll'} \delta_{SS'} \delta_{MM'} \int_0^{k_{max}} k^2 dk F_n(k) F_{n'}(k) q_0(K, k), \quad (3.39)$$

confirming the restored diagonality in all angular momentum quantum numbers. Q_{av} is thus a scalar operator, given by the Legendgaard transform of the monopole of $Q(Kk)$ obtained from eq. (3.33). In this connection the Bethe prescription for the full nuclear matter spectrum from sec. 3.3. provides a useful means to check the numerical methods used to calculate the propagator difference in (3.30). Then

$$\frac{1}{e^R(Kk)} - \frac{Q(Kk)}{e(Kk)} = \frac{1 - Q(Kk)}{e^R(Kk)}, \quad (3.40)$$

where $e^R(Kk)$ is independent of θ_{Kk} , and a matrix element of the averaged operator reads

$$\langle KkJlSM | \frac{1 - Q}{e^R} | KkJlSM \rangle_{av} = \begin{cases} 0 & \text{if } (k - K)^2 \geq k_f^2 \\ \frac{1}{e^R(Kk)} & \text{if } (k^2 + K^2) \leq k_f^2 \\ \frac{1 - \cos \theta_c(Kk)}{e^R(Kk)} & \text{else.} \end{cases} \quad (3.41)$$

The cutoff angle $\theta_c(Kk)$ is the same as in eq.(3.31).

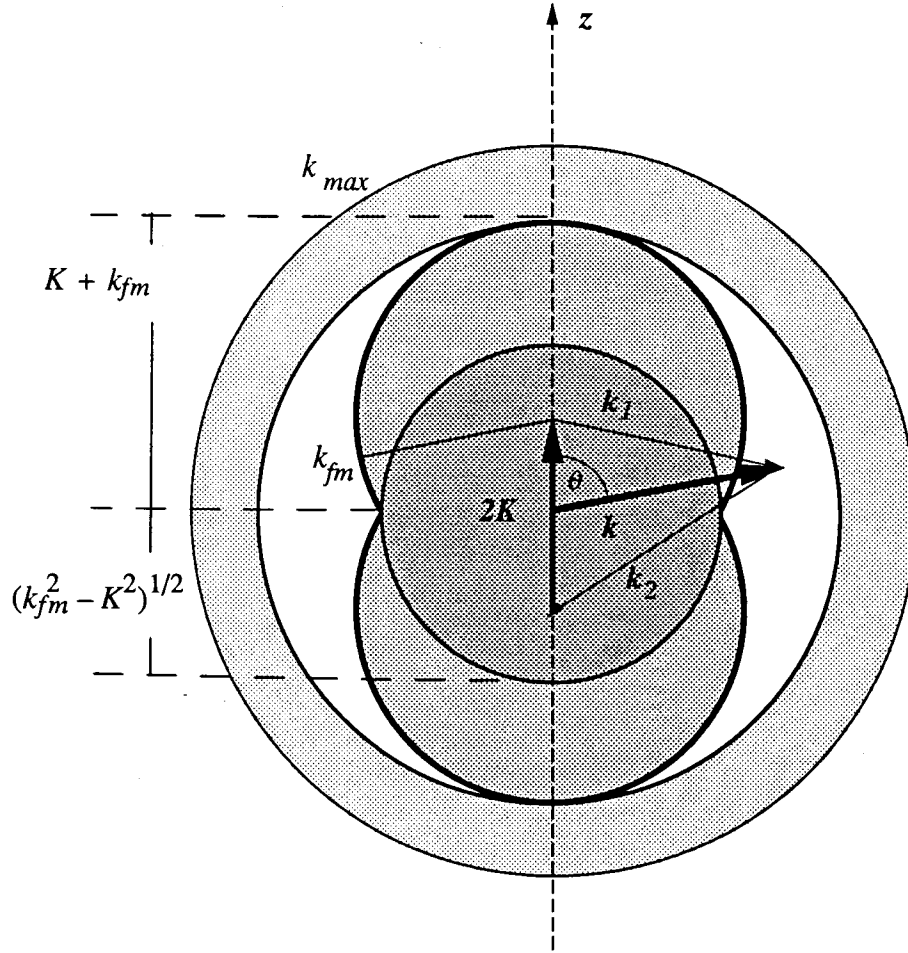


Figure 2 Geometry of the Pauli Operator and the Legendgaard Subspace. Inside the darkly shaded sphere the Pauli operator always vanishes for all angles θ . If k lies inside the two single-particle Fermi spheres (lightly dotted), separated by the true *cms* momentum $2K$, it vanishes beyond some cutoff angle. For the propagator correction the coarsely grained region up to the cutoff of the Legendgaard subspace at k_{max} is important, if reference and true nuclear matter spectrum differ.

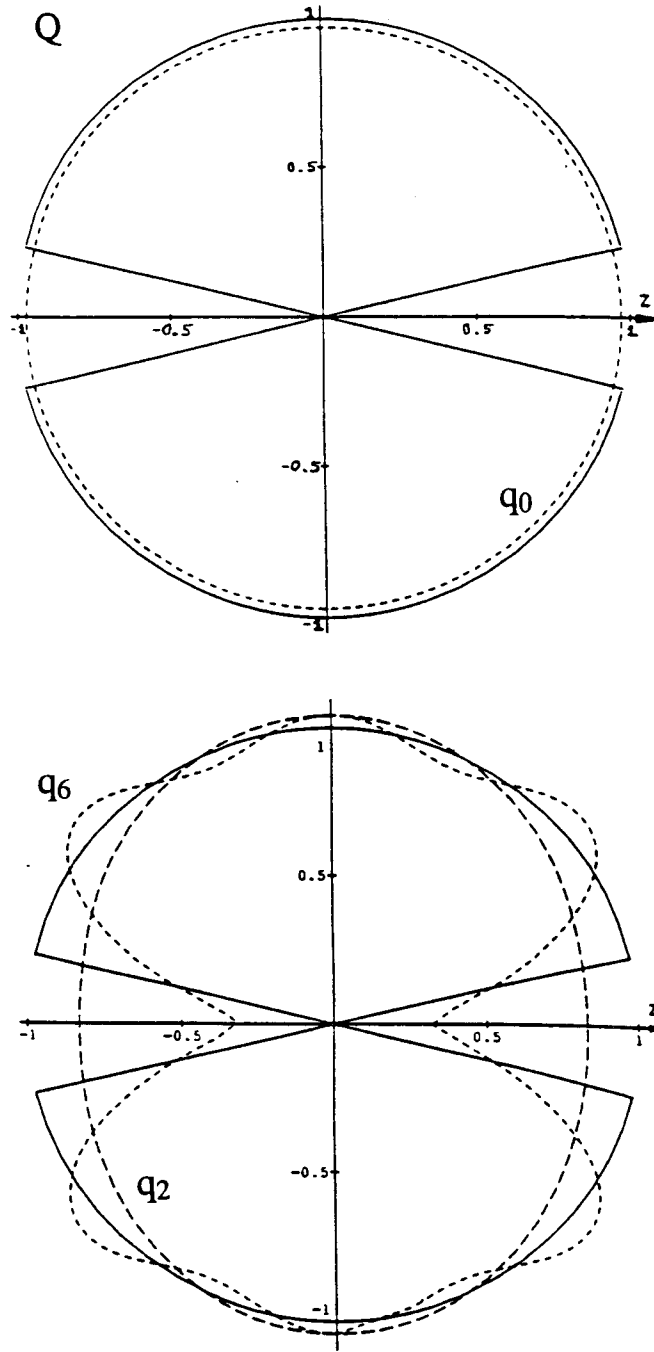


Figure 3 Angle Averaged Pauli Operator. The upper polar plot shows the angle averaged operator Q for $k = 1.88 fm^{-1}$. Parameters are $k_{fm} = 1.4 fm^{-1}$ and $K = 0.5 fm^{-1}$. The resulting cutoff angle is $\theta = 14^\circ$, causing the discontinuity from $Q = 1$ to $Q = 0$. The angle averaged operator is represented by the dashed line. The lower plot shows the approximation by a 2nd order (long dashes) and a 6th order (short dashes) multipole expansion.

4. Brueckner-Hartree-Fock Theory

An application of Brueckner theory is to calculate the single-nucleon spectrum and related quantities like the Fermi energy and the average binding energy. In Section 2.2 it was argued that the Hartree-Fock choice (2.29) of the auxiliary potential accounts for the most important contributions to the groundstate energy of nuclear matter. This is called the *Brueckner-Hartree-Fock approximation*. With the starting energy calculated on-shell many terms in the perturbation series are cancelled consistently. One can therefore expect that (2.29) defines a mean field which reasonably approximates the correlation corrections represented by the terms in the series (2.21). The aim is now to obtain the spectrum in a self-consistent way. Contrary to finite nuclei, in the case of infinite nuclear matter just the spectrum is subject to this requirement. Section 4.1 presents the methods needed to perform calculations using the development for the reaction matrix from chapter 3. It is not specific with respect to whether the self-consistency shall be applied to hole states only or to particle states as well. Section 4.2 displays and discusses results of numerical computations for various nuclear densities. Some questions concerning numerics are deferred to section 5.3.

4.1 Single-Particle Spectrum - Method

Momentum conservation implies that the average potential U is diagonal in momentum space. Further, the nucleons carry spin and isospin which is conserved by the scalar interaction. Their z -projections $\{m_s, m_i\} = \eta$ are averaged for the purpose of calculating the potential U . Overall there are $g=4$ spin-isospin states associated with each value of the relative momentum k , so an average matrix element of U is given by

$$\langle k_1 | U | k_1 \rangle = \frac{1}{g} \sum_{\eta_1} \langle k_1 \eta_1 | U | k_1 \eta_1 \rangle, \quad (4.1)$$

where the summation (2.28) over the hole states enters according to

$$\langle k_1 \eta_1 | U | k_1 \eta_1 \rangle = \int_{k_2 \leq k_{fm}} d^3 k_2 \sum_{\eta_2} \left(\langle k_1 \eta_1 k_2 \eta_2 | T | k_1 \eta_1 k_2 \eta_2 \rangle - \langle k_1 \eta_1 k_2 \eta_2 | T | k_2 \eta_2 k_1 \eta_1 \rangle \right). \quad (4.2)$$

To actually evaluate (4.2) one has to obtain the averaged antisymmetrized matrix elements from the partial wave constituents (3.16) and the integration has to be expressed in terms of the relative momentum k .

First to the transformation in (4.2) from k_2 to the relative momentum k , ignoring

spatial antisymmetrization. The matrix $\langle k_1 k_2 S M_s T T_3 / T / k_1 k_2 S M_s T T_3 \rangle$ is transformed into the Kk -basis by (2.32), where it remains diagonal in k . With the z -axis chosen along k_1 , the integral (4.2) is conveniently expressed in spherical coordinates; a factor of 2^3 attached to the $3d$ -volume element in the Kk -basis comes from the Jacobian. Fig.(4) illustrates the restrictions on k and the polar angle Θ arising from the condition that k_2 always denotes occupied levels below the Fermi level. For the polar integration this leads to a cut-off similar to the case of the Pauli operator.

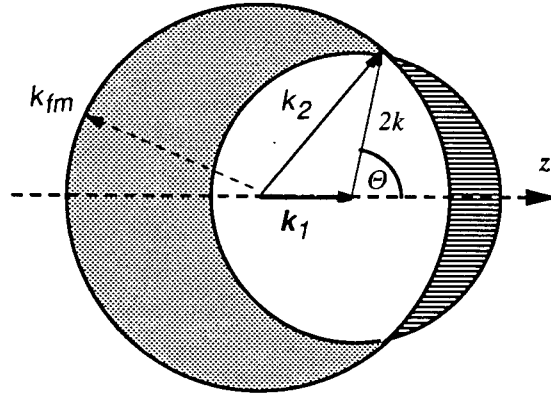


Figure 4 Integration over occupied states. At a given single-particle momentum k_1 the integration in k samples only the blank area. Only momenta k_2 within the Fermi sphere (dotted) are allowed, and values k_2 falling into the shaded area outside the Fermi sphere do not contribute. This puts a restriction on the polar angle Θ , its maximum value is defined by the intersection of the Fermi sphere and the sampling sphere of radius $2k$ (shaded). Note the rotational symmetry around k_1 .

The magnitude of the average momentum at which the T -matrix is evaluated is derived from k_1 and k by means of (2.32). Rewritten in the cms -system, (4.2) reads

$$\langle k_1 / U / k_1 \rangle = \frac{2^3}{g} \int_{k_<}^{k_>} dk k^2 \int_{-1}^{\cos \Theta} d \cos \Theta \sum_{\eta_1 \eta_2} \left(\langle K k \eta_1 \eta_2 / T / K k \eta_1 \eta_2 \rangle - \langle K k \eta_1 \eta_2 / T / K - k \eta_2 \eta_1 \rangle \right) \quad (4.3)$$

where the limits of integration and the parameters are given by

$$\begin{aligned}
k_{<} &= \max\left(0, \frac{k_I - k_{fm}}{2}\right) & k_{>} &= \frac{k_I + k_{fm}}{2} \\
\cos\Theta_{>} &= \min\left(1, \frac{4k^2 + k_I^2 - 4k_{fm}^2}{4k_I k}\right) & K &= k^2 + k_I^2 - 2k_I K \cos\Theta.
\end{aligned} \tag{4.4}$$

Now to the average over the internal degrees of freedom. First, single-particle spin and isospin are coupled to the total spin and isospin of the interacting pair. Second, the matrix elements are expressed in terms of the expansion of eq. (3.15), whose constituents $\langle KkJISM/T/KkJl'M \rangle$ are invariant under rotations and independent of M in the case of the angle averaged Pauli operator. Thus they may be evaluated with $\mathbf{k} \parallel \mathbf{e}_z$. As a result one obtains

$$\begin{aligned}
&\sum_{\eta_1 \eta_2} \left(\langle Kk\eta_1\eta_2/T/Kk\eta_1\eta_2 \rangle - \langle Kk\eta_1\eta_2/T/K-k\eta_2\eta_1 \rangle \right) \\
&= 2 \frac{1}{(2\pi)^3} \sum_{SI} (2I+1) \left(\sum_{Jl} (2J+1) \langle KkJISM/T/KkJlM \rangle \right).
\end{aligned} \tag{4.5}$$

Eq. (4.2) can then be written as

$$\langle k_I/U/k_I \rangle = \frac{1}{\pi^2} \int_{k_{<}}^{k_{>}} dk k^2 \int_{-1}^{\cos\Theta_{>}} d\cos\Theta \sum_{SI} (2I+1) \left(\sum_{Jl} (2J+1) \langle KkJISM/T/KkJlM \rangle \right) \tag{4.6}$$

For definite parity, the summation over l naturally splits into partial sums with odd and even parity, which can be further classified into single and coupled channels. Respectively the sum over spin-isospin becomes

$$\begin{aligned}
&\sum_{SI} (2I+1) \left(\sum_{Jl} (2J+1) \langle KkJISM/T/KkJlM \rangle \right) \\
&= \sum_{\text{odd } l} (2l+1) \langle KkJISM/T/KkJlSM \rangle_{S,I=0} + 3 \sum_{\text{even } l} (2l+1) \langle KkJISM/T/KkJlM \rangle_{S=0,I=1} \\
&+ \sum_{\text{even } l} (2J+1) \langle KkJISM/T/KkJlM \rangle_{S=1,I=0} + 3 \sum_{\text{odd } l} (2J+1) \langle KkJISM/T/KkJlM \rangle_{S,I=1}.
\end{aligned} \tag{4.7}$$

The treatment in this section applies to potentials with and without a core, not however if higher Pauli couplings break the spherical symmetry. Then the parts in (3.15) can not be simplified in the manner leading to (4.7). Finally the single-particle spectrum is obtained by adding the kinetic and potential energies

$$\varepsilon(k_I) = \frac{1}{2} k_I^2 + U(k_I). \quad (4.8)$$

An effective mass m^* and the Fermi energy ε_{fm} are defined by

$$m^* = \left(1 + \frac{\partial U}{\partial \varepsilon}\right)^{-1}, \quad \varepsilon = \varepsilon(k_{fm}). \quad (4.9)$$

At a given Fermi momentum k_{fm} the density ρ follows from eq. (1.1) and with (4.8) and (B.10) the average energy $\bar{\varepsilon}$ of a nucleon in the Fermi sea is given by

$$\bar{\varepsilon} = \frac{1}{2} \times \frac{g}{\rho} \frac{4\pi}{(2\pi)^3} \int_0^{k_{fm}} k_I^2 dk_I U(k_I) + \frac{3}{5} k_{fm}^2. \quad (4.10)$$

where g is the degeneracy factor from above. The T -matrix in (4.7) must be calculated on-shell with the starting energy E evaluated according to

$$E(k_I, k_2) = \frac{1}{2} k_I^2 + \frac{1}{2} k_2^2 + U(k_I) + U(k_2), \quad (4.11)$$

where k_2 , given by (2.32), depends on the variables k_I , k and $\cos\Theta$. The starting energy determines together with k and K the healing parameter γ in the reference spectrum method. For the self-consistent calculation of the hole states Bethe's prescription was used in the intermediate states above the Fermi level, so that $U(k_i > k_{fm}) = 0$. The effective mass for those states was set to $m^* = 1$. Since then both reference and the full spectrum above k_{fm} are parabolas in k , the condition that both coincide outside the modelspace is naturally fulfilled if one chooses them to be the same. If one attempts the particle states self-consistently, more rigorous requirements must be imposed on the reference spectrum. Ideally, one has to determine m^* and the offset A from the magnitude and the slope of the true nuclear matter spectrum at the cut-off of the Legindgaard subspace. This is hardly feasible from the outset, but from [18] it is known that m^* should be close to its free space value in this momentum region. The offset was judiciously set to a value which would presumably ensure positiveness of γ in (3.9). The idea was that the value of A could be checked once the self-consistent iterations have converged. The procedure failed to produce a stable spectrum, most certainly because of a fundamental inadequacy of the purely real treatment of the propagators. This is discussed below.

To avoid the laborious evaluation for many different sets of parameters, two observations are helpful. While increasing K enhances the defect wave function for small relative momenta, it also enlarges the phase space region excluded by the Pauli operator,

diminishing the contributions of low lying momenta. Hence both effects tend to compensate, so that $T_E(Kk)$ depends only weakly on K . In practice the polar integration was done as a 2-point Gauss-Legendre integral. After each self-consistent iteration the spectra were obtained by fitting an even forth order polynomial in k_I to the calculated points. The fitted curves were then used for (4.8) during the next iteration. This fit is physically more reasonable than an unrestricted interpolation with odd powers of k_I present, since viewed as a power series in k , it incorporates explicitly inversion symmetry.

5. Numerical Solution of the Bethe-Goldstone Equation

The numerical work to solve the Bethe-Goldstone equation encompasses three major tasks. In the first step the reference reaction matrix is calculated in terms of its partial wave projections (3.16), this is realized by the code TREF. Secondly, the Legindgaard representation of (3.30) must be realized by transforming the reference reaction matrix and the propagators into the polynomial representation. In the last step, the matrix inversion in (3.30) is carried out and the resulting solution is transformed back into momentum space via (3.25). The code TNM executes this Legindgaard method. The Sections 3.2 - 3.4 provide the corresponding analytical framework around these steps and the related computer codes are essentially a straightforward implementation of the theory. The central numerical methods are discussed in the subsequent sections. The given descriptions represent the actual conventions used in the codes. A short critique of the choice of the various algorithms concludes the discussion.

5.1 Reference Reaction Matrix

The matrix elements are calculated from the radial distorted waves (3.11) as the position space integrals (3.16). Although it appears to have a rather auxiliary purpose, the repeated solution of the reference wave equation (3.13) is actually the numerically most demanding and also the most time-consuming part in the entire calculation. Hence, it deserves the emphasis awarded by the somewhat detailed description to follow.

Solution of the Reference Wave Equation - Conventions

The radial reference wave functions $u_{Jl'l's}(kr)$ are the solutions to the second order ordinary differential equations (3.13). In the case of the tensor interaction one has two coupled equations

$$\left[I \frac{\partial^2}{\partial r^2} + V(r) \right] \mathbf{u}(r) = \mathbf{w}(r), \quad r \geq r_c. \quad (5.1)$$

where the wave functions \mathbf{u} and the driving terms \mathbf{w} are given in terms of the $u_{Jl'l's}(kr)$ and the Bessel functions $J_{J+1}(kr)$ as

$$\mathbf{u}(r) = \begin{pmatrix} u_1(r) \\ u_2(r) \end{pmatrix} \quad \text{entrance channel} \quad l'=J-1 : u_1 \equiv u_{J(J+1)(J-1)1}, \quad u_2 \equiv u_{J(J-1)(J-1)1},$$

$$l'=J+1 : u_1 \equiv u_{J(J+1)(J+1)1}, \quad u_2 \equiv u_{J(J-1)(J+1)1},$$

$$w(r) = -(k^2 + \gamma^2) \begin{pmatrix} 0 \\ J_{J-1}(kr) \end{pmatrix} \text{ if } l'=J-1, \quad w(r) = -(k^2 + \gamma^2) \begin{pmatrix} J_{J+1}(kr) \\ 0 \end{pmatrix} \text{ if } l'=J+1. \quad (5.2)$$

The matrix $V(r)$ contains the orbital angular momentum potential and the interaction potential. Here V^D is the direct and V^T the tensor coupled part of the particular Reid interaction potential $V_{Jl'S}$, the eigenvalues of the LS and the S_{12} operators are absorbed into $V_{Jl'S}$.

$$V(r) = \begin{pmatrix} -\frac{J(J+1)}{r^2} - \gamma^2 & 0 \\ 0 & -\frac{(J+1)(J+2)}{r^2} - \gamma^2 \end{pmatrix} - m^* \begin{pmatrix} V_{J-1}^D(r) & V^T(r) \\ V^T(r) & V_{J+1}^D(r) \end{pmatrix} \quad (5.3)$$

The expressions for single channels are the analogs in one dimension.

Reference Wave Equation – Numerical Method

The solutions $u(r)$ to eq. (5.1) with (5.2) and (5.3) are subject to the boundary conditions (3.14) and are obtained with a Newton iteration [21]. It treats the problem like an initial value problem and improves linearly on solutions computed from trial initial conditions at the lower boundary r_c to meet the conditions at the upper boundary where $kr \gg 1$. Its discussion is followed by an outline of the Numerov algorithm [19], which was used to tackle the differential equation.

The present 2-point boundary value problem has the size $n=1$ in the single channel cases and $n=2$ in the coupled cases and the ordinary second order equation (5.1) requires n adjustable parameters, which are defined to be the undetermined initial conditions v_k at the core radius

$$v_k = u_k(r=r_c + \delta r). \quad (5.4)$$

The boundary value problem expressed in functions $f_i(u_j, v_k)$ of the $j=1..n$ solutions u_j obtained from the trial v_k are, e.g. for $l'=J-1$

$$kr \gg 1 : \quad f(u_j, v_k) \equiv \begin{pmatrix} u_1(kr) \\ u_2(kr) \end{pmatrix}_{v_k} - \begin{pmatrix} J_{J-1}(kr) \\ 0 \end{pmatrix}. \quad (5.5)$$

The boundary conditions are satisfied by $v_k = \tilde{v}_k$ taken to yield

$$kr \gg 1 : \quad f(u_j, \tilde{v}_k) = 0. \quad (5.6)$$

Assuming that the solutions $u_i(r)$ depend smoothly on the v_k , $f(u_j, v_k)$ may be approximated by its Taylor expansion in v_k around \tilde{v}_k ,

$$f_i(u_l, v_m) = 0 + \left(\frac{\partial f_i}{\partial v_j} \right)_{v_j=\tilde{v}_j} (v_j - \tilde{v}_j) + O((v_j - \tilde{v}_j)^2). \quad (5.7)$$

To fulfill (5.6) one has to find improvements δv_j such that

$$(v_j + \delta v_j - \tilde{v}_j) \equiv 0. \quad (5.8)$$

Substituting this into (5.7) and solving for δv_j yields

$$\delta v_i = (\partial f^{-1})_{ij} f_j(u_l, v_m), \quad \text{with} \quad (\partial f)_{ij} = \left(\frac{\partial f_i}{\partial v_j} \right)_{v_j=\tilde{v}_j}. \quad (5.9)$$

The improvements δv_i were derived from the gradient matrix ∂f calculated in subsequent trials with slightly different v_k , whose starting values were estimated from the slopes of the Bessel functions at the origin and which were held fixed for all values of the relative momentum. For the linear equations (5.1) the gradient matrix is constant and a single iteration should lead to the correct \tilde{v}_k , however a second iteration was performed if (5.6) was not satisfied to within a specified margin. The matrix inversion was done straightforwardly with Cramer's rule.

The Numerov algorithm used to integrate the eq. (5.1) exploits the fact that only second order derivatives appear in them. The solutions $\mathbf{u}_{n+1} \equiv \mathbf{u}(r=r_{n+1})$ are found explicitly from \mathbf{u}_{n-1} and \mathbf{u}_n according to

$$\begin{aligned} \mathbf{u}_{n+1} = & \left[\mathbf{I} + \frac{h^2}{12} \mathbf{V}_{n+1}(r) \right]^{-1} \left\{ 2 \left[\mathbf{I} - \frac{5h^2}{12} \mathbf{V}_n \right] \mathbf{u}_n - \left[\mathbf{I} + \frac{h^2}{12} \mathbf{V}_{n-1} \right] \mathbf{u}_{n-1} \right. \\ & \left. + \frac{h^2}{12} \left[\mathbf{w}_{n+1} + 10\mathbf{w}_n + \mathbf{w}_{n-1} \right] \right\}, \quad (5.10) \end{aligned}$$

where h is the stepsize between r_n and r_{n+1} . The local truncation error ε is given in leading order by

$$\varepsilon_i \approx \frac{h^6}{144} (w_i - V_{ij} u_j)^{(4)} \quad (5.11)$$

so that the method is of 5th order. To initialize the algorithm the values \mathbf{u}_{n_0} and \mathbf{u}_{n_0+1} must be specified, \mathbf{u}_{n_0+1} being the free parameters of eq. (5.4). In the coupled channel cases the strongly singular behavior of the tensor potential at $r=0$ was ameliorated by introducing an artificial small hard core of radius $0.06 \text{ fm} \geq r_c \geq 0.03 \text{ fm}$. Its smallness ensures compatibility with Reid's soft-core potentials, which were determined also with an auxiliary core [13]. The matrix inversion involved for the coupled channel cases was done troublefree again with Cramer's rule. Numerov's method uses a fixed stepsize h . Whenever different stepsizes were employed the algorithm was initialized anew at the breakpoints where h changed by a 6th order polynomial extrapolation [20].

Matrix Elements

The integral (3.16) was evaluated by the trapezoidal rule on the same position space mesh on which the reference wave function was calculated. It allows for variable stepsizes and it safeguards against subtle weighting effects where the integrand changes rapidly within a few steps. This flexibility stands in contrast to its slow quadratic convergence, which dominates the rapid convergence of the wave functions with finer meshes. While the calculation of the reaction matrix $T^R(k,k')$ is not symmetric with respect to the bra- and ket-states, hermiticity implies that the real matrix $T^R(k,k')$ be symmetric. As a means to check the reliability of the computations the quantity

$$\Sigma_{JlIS}^2 = \frac{\int_0^{k_{max}} k^2 dk \int_0^{k_{max}} k'^2 dk' [\langle KkJlSM/T^R/KkJl'SM \rangle - \langle Kk'Jl'SM/T^R/KkJISM \rangle]^2}{\int_0^{k_{max}} k^2 dk \int_0^{k_{max}} k'^2 dk' [\langle KkJlSM/T^R/KkJl'SM \rangle + \langle Kk'Jl'SM/T^R/KkJISM \rangle]^2} \quad (5.12)$$

was introduced as measure for the hermiticity. It has the desirable property to weigh lower momenta with a small phasespace factor apt to the Legindgaard transforms and the single-particle potential. The expression in the denominator of (5.12) is essentially the symmetrized norm of the T -matrix and can be used to judge the overall accuracy.

Miscellanea and Critique

The Bessel and Hankel functions appearing as the inhomogeneous terms of the differential equations and in the matrix elements are calculated from their analytical forms in $\sin(x)$, $\cos(x)$ and $e^{(-x)}$ for $l \leq 3$ and for higher values recursion schemes are invoked [21].

At first, the single channel equations were attempted as standard initial value problems where the constants of integration are found analytically, e.g. from the matching condition at the upper boundary. For $r \rightarrow 0$ the angular momentum barrier dominates and the initialization can be done in closed form as $u_l(kr) = \alpha(kr)^{l+1}$. However the solutions were then linear combinations of the inhomogeneous and the regular fundamental solutions which had to be subtracted off. This problem was absent when Newton's method was used.

A discretization mesh in r with different step sizes, was chosen to account adequately for the rapidly changing potential at small r , see fig. (5). The Numerov

algorithm has a difficulty with this because it has to be initialized anew if the stepsize changes. This was done somewhat arbitrarily but sufficiently successfully by a 6th order polynomial extrapolation at the breakpoints. The matrix elements of usually T^R deviated less than 1% compared to the case of a uniform mesh, dependent of the choice of the mesh; the check (5.12) however turned out to be quite sensitive upon the number of cuts. As expected it attains a minimum for uniform stepsizes. Still, a non uniform mesh may be useful in a quick first calculation which can then be refined and it is clear that the extrapolation is a rather crude approach. One could do better with interpolation or a Runge-Kutta style reinitialization. It did not seem worthwhile to pursue this, given the option to take a uniform stepsize. Runge-Kutta would of course avoid the problem at all since it advances without explicit information from past points and the most appealing conventional approach might be to combine a variable transformation like $r \rightarrow (\alpha + \beta r)^{-1}$ with Runge-Kutta, possibly with adaptive stepsize control. While the variable transformation emphasizes short distances, it introduces first order derivatives and thus precludes the use of Numerov's method. The major practical advantage of Numerov's method is on the other hand that it needs only 1 evaluation of the right hand side in (5.1) per step, compared to 4 in the 4th order Runge-Kutta scheme. Moreover there is no unused overhead from the expensive evaluations of the potential and especially the Bessel functions whose values need to be known in the intermediate steps of Runge-Kutta. Although the matrix elements are obtained only with the trapezoidal rule a high order method for the differential equations is appropriate due to the unscaled integration range and the pronounced sensitivity of the solutions to the initial conditions.

5.2 Legindgaard's Method for the full Nuclear Matter Reaction Matrix

Polynomial Transforms of the Reaction Matrix

At the beginning of the numerical realization of Legindgaard's method one needs to choose an integration algorithm for the Legindgaard transforms (3.24). A Gauss-Legendre procedure seems attractive, especially as the integrand is a well behaved smooth function of the relative momentum k . If the task is to evaluate the Legindgaard transforms $T^R(n, n')$ up to order n_{max} , a formula with a minimum of $n_{max} + 2$ supports are needed. The transforms converge rapidly with n_{max} and economic meshes of less than 16×16 points proved sufficient. Many more points are undesirable because then very small values of k occur in the reference wave equation (3.13). There the outer boundary condition is reliably enforced only if $kr \gg 1$ and the maximal cut-off radius is limited by the noise-induced growing exponential $e^{\gamma r}$. This is mostly uncritical except in self-consistent calculations where one might reach $\gamma r > 20$ so that the solution becomes

contaminated even under Fortran double precision. Fortunately the phasespace factor k^2 de-emphasizes critically small k and in practice this difficulty needed no further attention. Gauss-Legendre integration was used to reduce the number of intermediate calculations of $T^R(k, k')$. The other suitable method is Simpson's rule, corrected for the excluded value $k=0$. It is much preferred over the slowly converging trapezoidal rule in this case, although it precludes non-uniform meshes. Optimum accuracy was attained roughly for meshes with 50×50 points, dependent on the range of the model space. This was verified by investigating the dependence on the mesh size of the discrepancy between original and the inverted representations of T^R .

Angle Averaged Propagator Correction

For the angle averaged propagator correction (3.40), just 1-dimensional integrals need to be evaluated for both angular and radial momentum space integration. The angle averaging was checked by means of the Bethe prescription (3.41). After splitting the model space into up to three subintervals depending on the discontinuities caused by the cut-offs in the Pauli operator, the radial integral was obtained in each subinterval by a 10-point Gaussian formula. This ensured a precise representation, which is important since the propagator difference is the central quantity in Legindgaard's method.

Matrix Inversion - Miscellanea

The matrices involved are small, usually less than 20×20 , see sec. 3.3, symmetric and well behaved. The matrix inversion was based on LU -decomposition with backsubstitution, according to the version given in [20]. There are actually four distinct classes of partial wave projections, classified by their spin S and their parity Π (equivalently the isospin): $(S, \Pi) = (0, -1), (0, 1), (1, -1)$ and $(1, 1)$. Neither of them is linked by the parity conserving spin-independent Pauli operator. All matrices $\langle KnJISM/T/knJl'SM \rangle$ belonging to a particular class (S, Π) were gathered as blocks in single matrix to prepare for the possibility of using a non-angle averaged propagator difference, where channels with different J can be coupled by the Pauli operator. For the present angle averaged procedure this has no further significance besides enlarging somewhat the dimension of eq. (3.28).

5.3 Considerations for the Self-Consistent Calculation of the Spectrum

In the self-consistent calculation TREF and TNM appear as subroutines and, if the integral (4.6) is evaluated with n_θ angular and n_k radial supports, both are invoked $n_\theta \times n_k$ times. The k -integral was done again via the Gauss-Legendre method with $n_k \geq 10$ supports and $n_\theta = 2$. The spectrum was obtained either as a fit or local

interpolation $n_s \geq 5$ points. So one has roughly 100 subroutine calls per iterated spectrum and to achieve accuracy better than 0.01 MeV/nucleon at least 5 iterations were necessary. In short, if proceeding without further approximations, it will pay in calculation time to reduce the sizes of the meshes in the subroutines. The size of the reference reaction matrix relates to the method in the numerical integration used to obtain the Legendgaard transforms. In order to accelerate the repeated consuming execution of TREF the Gauss-Legendre type integration of sec. 5.2 was employed for the Legendgaard transforms on a 16×16 mesh. As an alternative one might try a Gauss-Jacobi method [22], appealing to the Jacobi-form of the polynomials (3.23). It was not examined whether this would permit an even sparser mesh. The full T -matrix in momentum space was obtained directly from its polynomial representation rather than via eq.(3.30), which would have been more accurate, especially for low values of k , but also somewhat cumbersome in this context.

6. Examples and Discussion

6.1 Nuclear Matter Reaction Matrix

The reaction matrix was calculated for each of the 12 Reid potentials up to $J=3$. The highest angular momentum appears just in the coupling of the states 3P_2 and 3F_2 . No higher partial waves were considered. After studying the convergence of single matrix elements dependent on the stepsize in the solution of the wave equation the calculations were done with an artificial core of 0.05 fm and a uniform mesh with 400 steps between core and a cutoff radius $r_{\text{max}} = 10\text{ fm}$. The relative accuracy of the matrix elements is then better than 10^{-4} . At this point no use was made of the hermiticity of T^R . Output of a sample calculation may be found in Appendix D. The values agree to within 1% with previous calculations of [3,11], based on a different numerical methods. The calculations were performed on a Sun 3/60 workstation with a MC68881 coprocessor and took about 0.25 sec. per matrix element. Fig. 5 illustrates the behavior of the potentials in the 3S_1 channel. Fig. 6 demonstrates the correlation effects induced by the 1S_0 potential. The potential is shown in the top graph, note the shallow attractive region. The middle graph shows the integrand in the matrix element eq. (3.16) and the evolution of the radial integral. The bottom graph illustrates how the unperturbed function $J_0(kr)$ is distorted into the correlated function $u_0(kr)$, basically its maximum is shifted towards the attractive region of the potential. $\zeta(kr)$ illustrates the rapidly healing defect function. The graph is for $k_{\text{fm}} = 1.4\text{ fm}^{-1}$ and $k = 0.91\text{ fm}^{-1}$ and represents a state in the Fermi sea. This shift is somewhat reduced, if the Pauli principle is taken into account [3], which is not shown here because the full wave function does not explicitly appear in the development in ch. 3. The effects of the Pauli operator are introduced via the operator equation (3.4) rather than directly via the wave functions. The polynomial representation of the Bethe-Goldstone equation was usually solved with $n_{\text{max}}=5$ basis polynomials for 40×40 points using Simpson's rule for the transformations. Higher order in the polynomials did not lead to any gain in the accuracy, if one uses Gaussian integration one has to use at least 32×32 points to achieve good convergence for low-lying momenta. The sample output in Appendix D was obtained with the indirect method eq. (3.30). Comparison of output from direct and indirect methods with [12] showed agreement of better than 0.5% for each method. As mentioned previously the indirect method should be preferred over the direct method at small momenta, typically less than 0.5 fm^{-1} . The actual calculations were performed with the full nuclear matter spectrum as input. An example of how the reference reaction matrix is corrected for the spectral and Pauli approximation is shown figs. (7-9). The upper graphs always show the full reaction matrix, while the lower ones illustrate the difference between T and T^R . For the 1S_0 channel the Pauli principle de-

emphasizes the contributions at low momenta by about 10%. It is even more effective in the tensor coupled channel 3S_1 . There the reduction reaches 30%. The execution of the subroutine TNM required in this case about 0.05 sec. per matrix element.

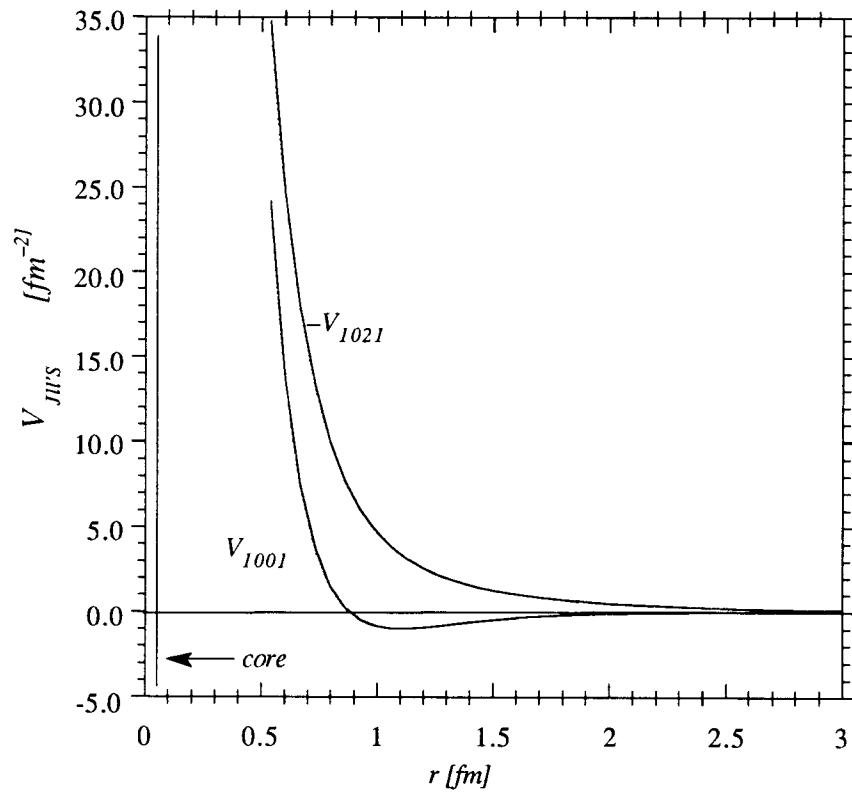


Figure 5 Coupled Channel Potentials. The potential V_{1001} for the direct channel 3S_1 and the tensor potential V_{1021} for the coupling of 3S_1 and 3D_1 are shown.

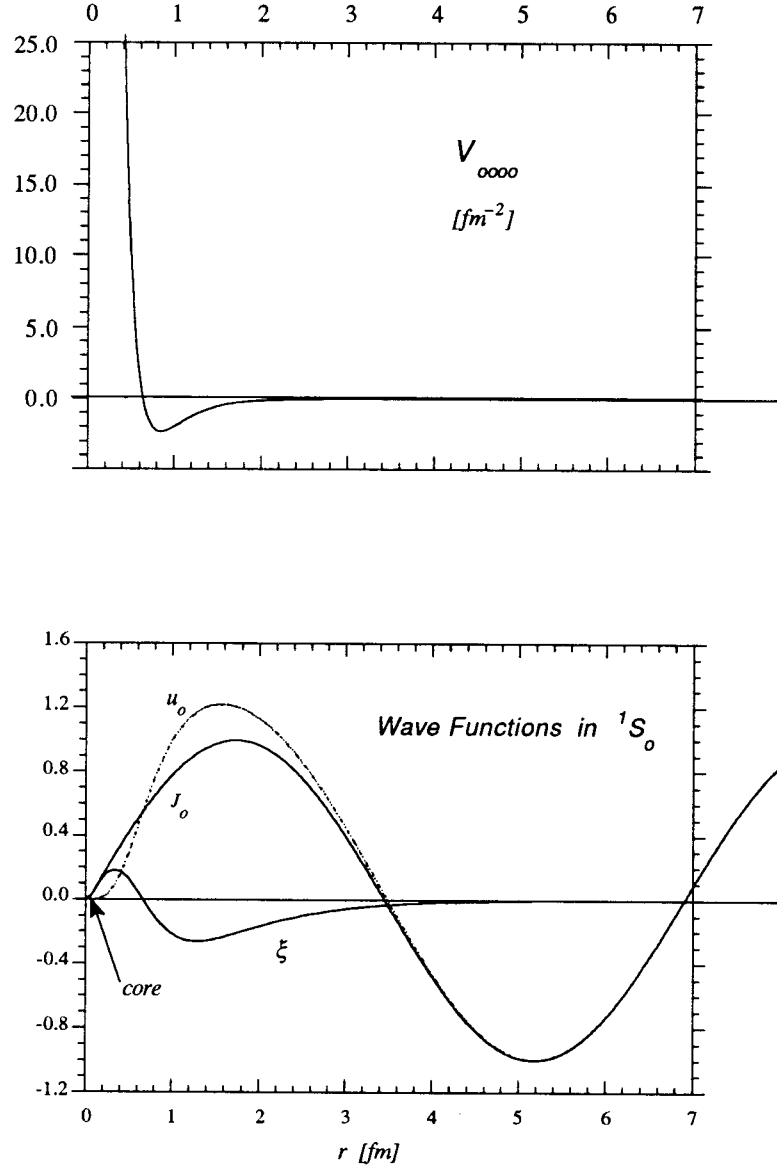


Figure 6 Potential and Reference Wave Function in Channel 1S_0 . The upper graph shows the dependence on the distance r of the two interacting nucleons of the potential $V_{JHS} = V_{0000}$. The lower graph displays the independent particle wave function J_0 , the correlated reference wave function u_0 and the defect wave function ξ versus the radial separation. The relative momentum is $k = 0.91 \text{ fm}^{-1}$ and the healing parameter $\gamma = 1.18 \text{ fm}^{-1}$. The auxiliary core is positioned at $r = 0.05 \text{ fm}$.

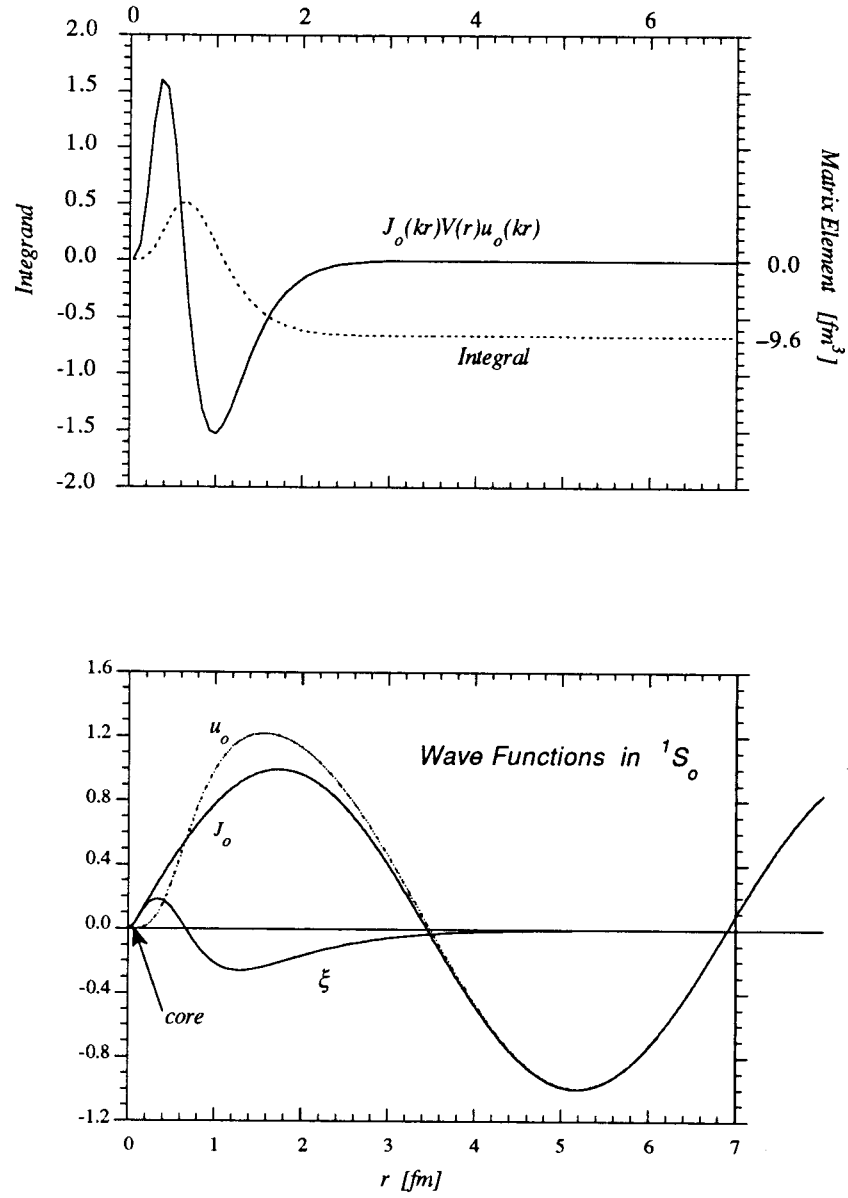


Figure 7 Integrant for Reference Reaction Matrix in 1S_0 . The lower graph and the parameters are as in Fig.(7). The upper graph displays the integrand eq. (3.16) for the diagonal matrix element $\langle KkJlSM|T^R/KkJlSM\rangle$, $JlS = 000$, and shows how the matrix element evolves to its attractive value, cf. Appendix D.

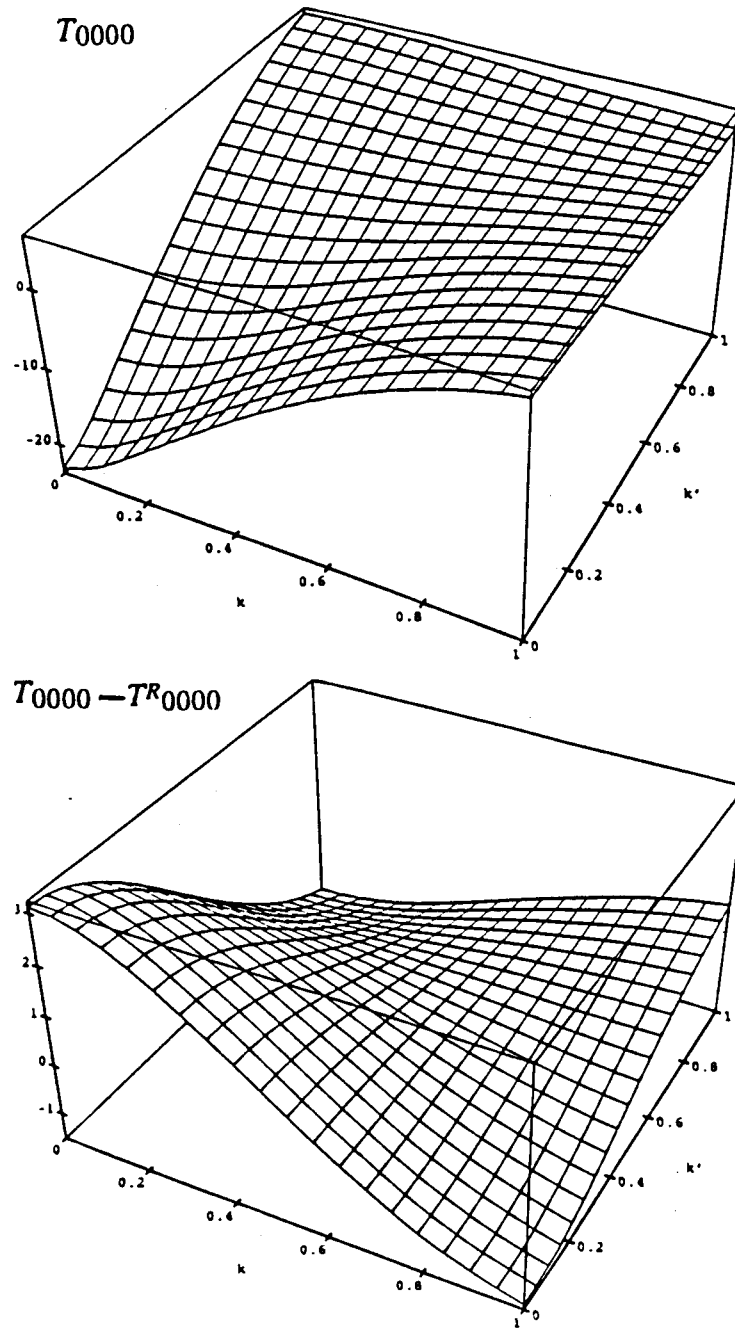


Figure 8 Nuclear Matter Reaction Matrix for 1S_0 . The upper graph shows the full reaction matrix, the lower displays the corrections compared to the reference spectrum calculation. The momentum coordinates are scaled to the subspace cut-off, $k_{\text{max}} = 2.8 \text{ fm}^{-1}$. The ordinate gives the value of the matrix elements in fm^3 . The parameters are as in Appendix D.

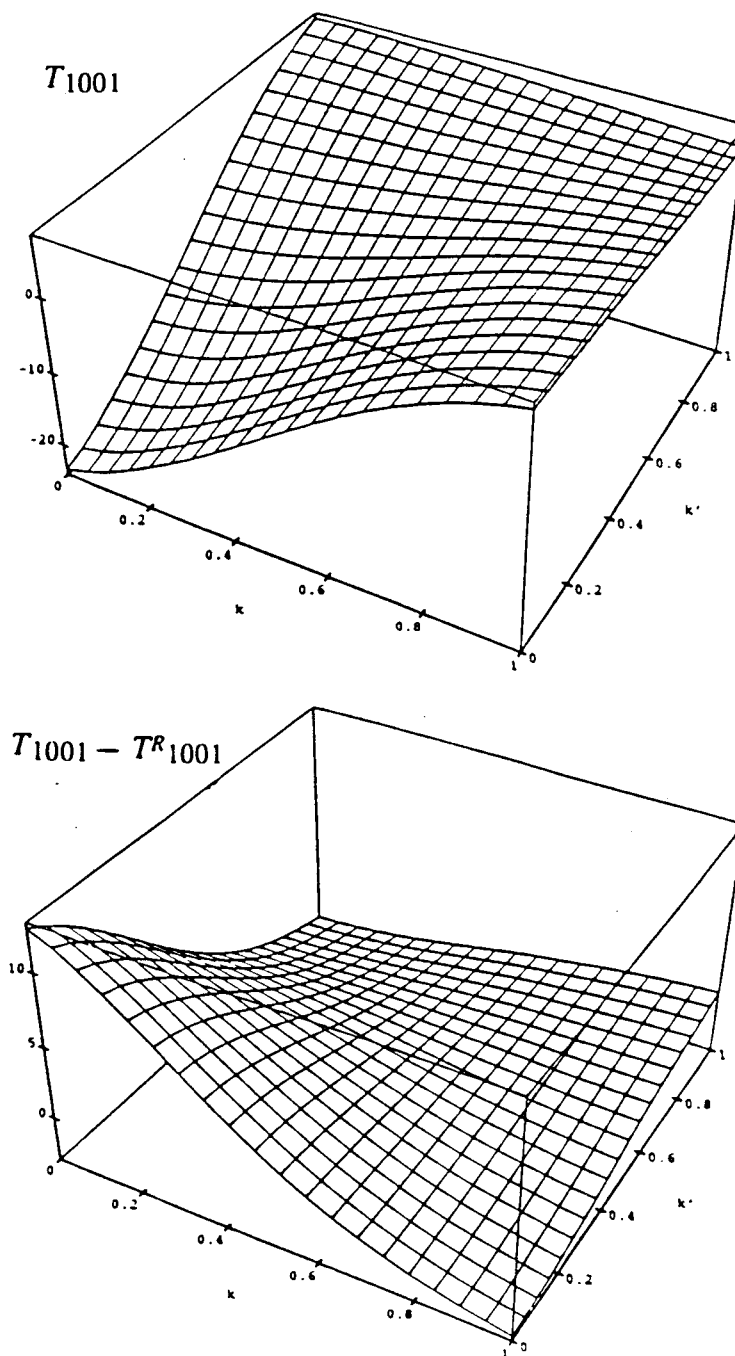


Figure 9 Nuclear Matter Reaction Matrix for 3S_1 . Similar to Fig. 8.

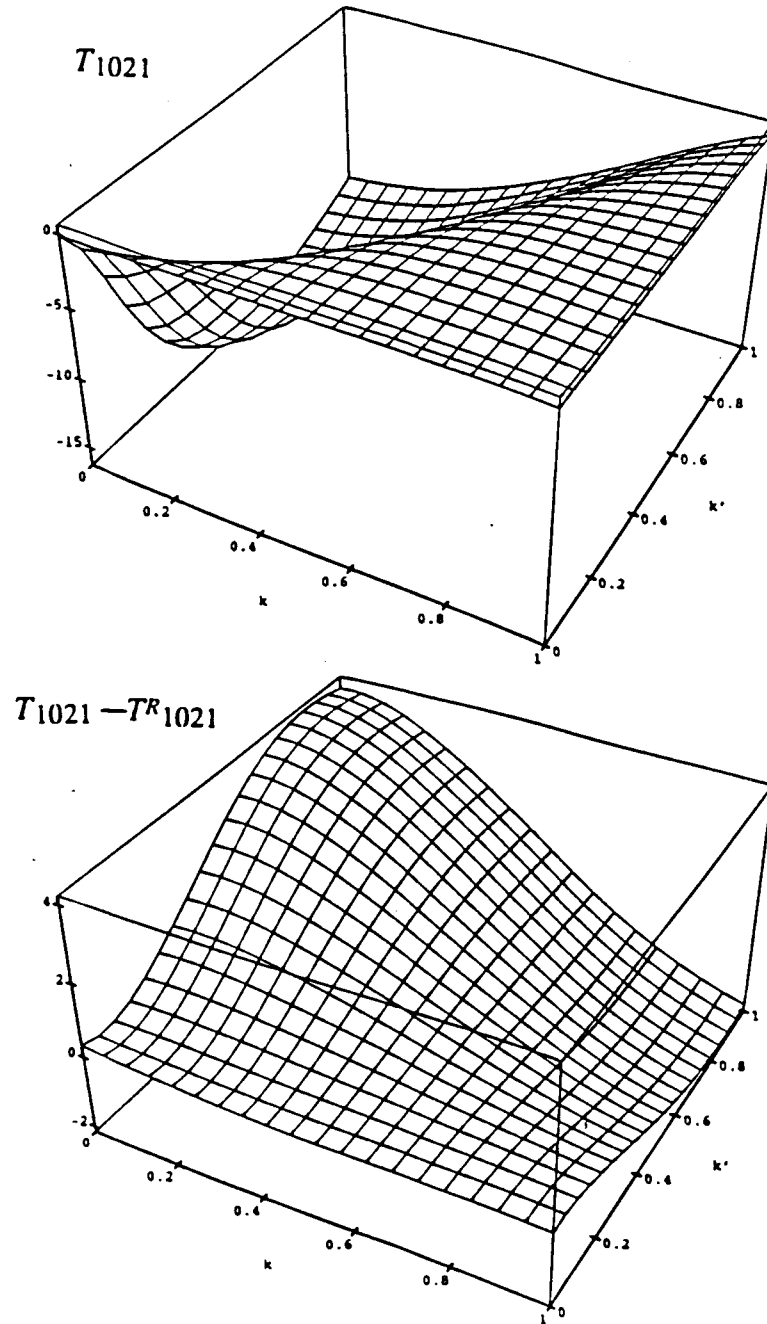


Figure 10 Nuclear Matter Reaction Matrix for 3S_1 – 3D_1 . Similar to Fig. 8. This is the off diagonal matrix $\langle KkJlSM|T|Kk'Jl'SM\rangle$ which is not symmetric just under exchange of k and k' .

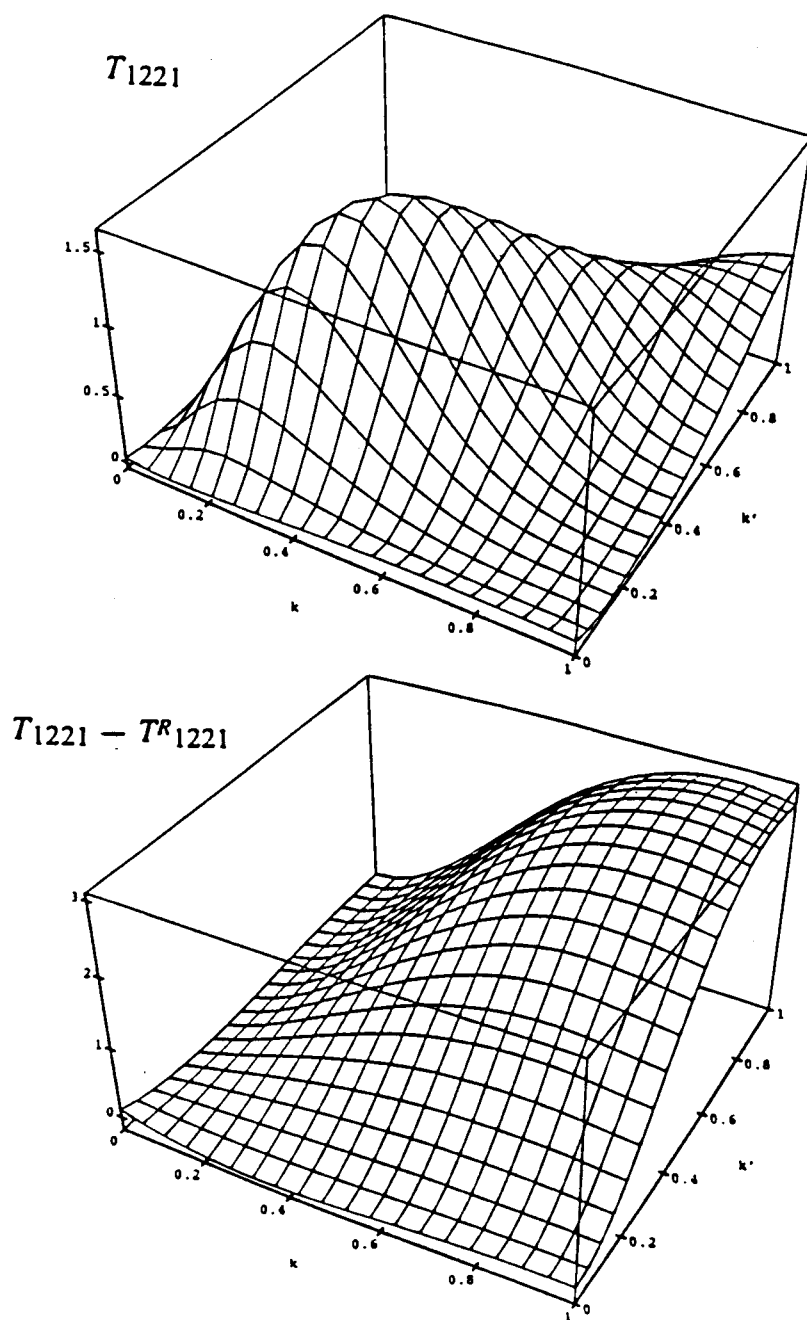


Figure 11 Nuclear Matter Reaction Matrix for 3D_1 . Similar to Fig. 8.

6.2 Self-Consistent Calculation of the Hole Spectrum

As an application of the developed subroutines, the self-consistent spectrum was obtained for hole-states using Bethe's method. This was done with T^R calculated using a reduced mesh of 200 radial points by explicitly exploiting hermiticity, which cuts the calculation time by roughly 40%. The required input size for the transformation was reduced to a 16×16 matrix by using Gaussian quadrature. A reasonable compromise between accuracy and execution time was achieved with a 12 point Gauss quadrature over hole momenta. For the polynomial fit 12 supports were used. The spectra were iterated until a relative accuracy in the coefficients of the polynomials of better than 0.01% was achieved. This required between 5 and 12 iterations dependent on the starting spectrum. The starting spectra were parabolas, derived from [3] for values of $k_{fm} = 1.0, 1.4 fm^{-1}$. Figure 12 shows the self-consistent hole spectrum and the single-particle spectrum for $k_{fm} = 1.4 fm^{-1}$, along with the reference spectrum, which has no potential energy contribution. Figure 13 displays the contributions to the potential for the various partial waves, apparently the binding arises mainly from the S channels, as expected from the binding of the deuteron. Self-consistent iterations were performed for several Fermi momenta in search of the saturation point and the average total energy. Figure 14 shows the dependence on the Fermi momentum of the average energy (4.10). The curve was fitted as a 4th order polynomial. The results are

$$\begin{aligned}
 \text{Saturation Density} \quad k_{fm} &= 1.48 fm^{-1} & \rho &= 0.22 fm^{-3} \\
 \text{Average Energy} \quad \bar{\epsilon} &= -12.52 MeV/nucleon
 \end{aligned} \tag{6.1}$$

These values give a somewhat lower estimate to the average energy than in [3], where $k_{fm} = 1.44 fm^{-1}$ at $\bar{\epsilon} = -11.1 MeV/nucleon$. Although there is a small contribution from the fourth order term, the effective mass changes very little, its value being

$$\text{Effective Mass} \quad m^* \geq 0.68. \tag{6.2}$$

This is larger than the estimate in [5] and the value $m^* = 0.65$ obtained in [7,18]. By comparing with eq.(1.3,1.4) one sees that while including two-particle correlations accounts for the most important effects, saturation and binding at reasonable density, but that one has to resort to more sophisticated approximations to arrive at quantitatively improved results.

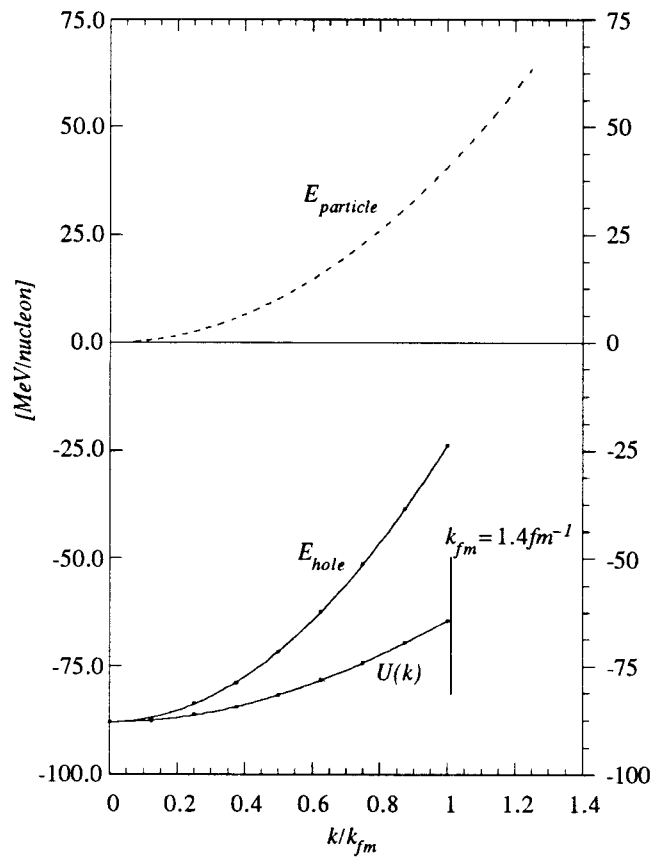


Figure 12 Self-consistent Hole Spectrum. The dashed curve represents the free space dispersion relation and was used as reference and intermediate state spectrum (Bethe's prescription). U denotes the single-particle potential. Note the artificial energy gap at the Fermi momentum in this treatment.

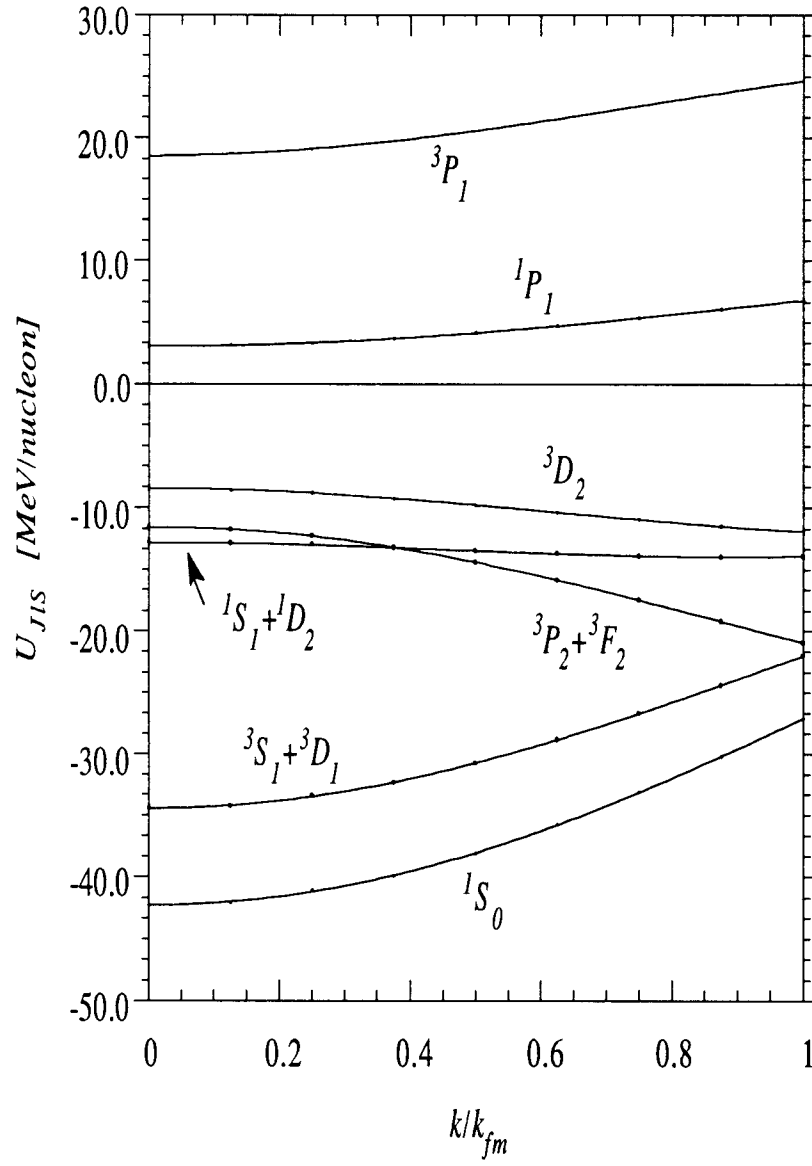


Figure 13 Single-Particle Potential: Partial Wave Decomposition. The graph shows the contributions of the various partial wave projections of the interaction to the hole-potential shown in fig. 12, $k_{fm} = 1.4 fm^{-1}$.

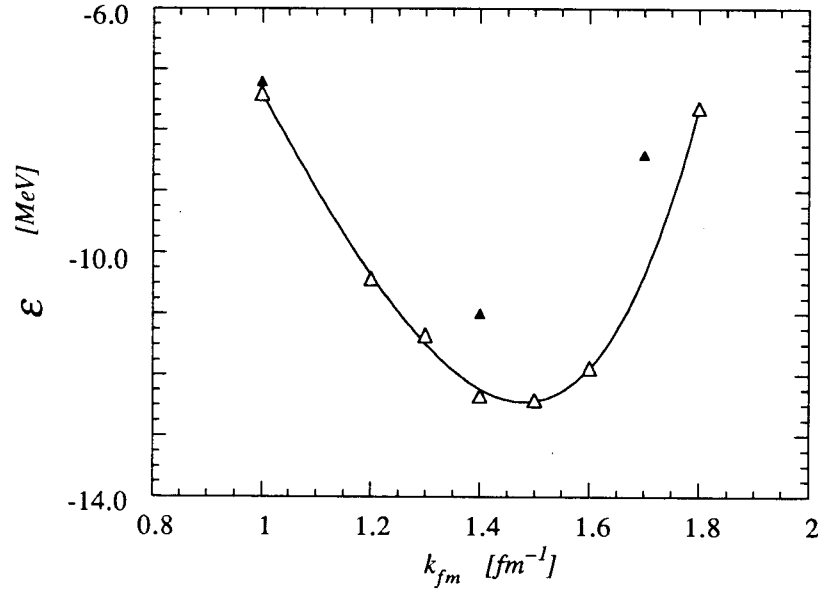


Figure 14 Saturation Plot for Nuclear Matter. Plotted is the average energy per nucleon versus the Fermi momenta, *i.e.* the density. The heavy triangles represent values from ref. [3]. At $k = 1.48 \text{ fm}^{-1}$ and $\bar{\epsilon} = -12.52 \text{ MeV/nucleon}$ the saturation point is reached.

6.3 Extension to Particle States.

All attempts to calculate a self-consistent spectrum including the particle states yielded stable and reasonable solutions for the hole states but became quickly unstable for the particle states and eventually the calculations broke down. The reason why self-consistency cannot be achieved for particle states with the present method might be traced to the properties of the propagators (3.40). For hole states the on-shell starting energy is always less than $2\varepsilon_{fm}$, but the propagators never become singular because the Pauli operator excludes all intermediate states below the Fermi level, so that $\langle E-H_0 \rangle < 0$ holds for all $k_1 \leq k_{fm}$. On the other hand if $E > 2\varepsilon_{fm}$, as possible if a particle state enters, the former condition is violated and $\langle (E-H_0)^{-1} \rangle$ becomes singular at $E = \varepsilon_l + \varepsilon_m$ for states $|lm\rangle$ above the Fermi level since those intermediate states are not blocked by the Pauli principle. This problem has been recognized before in a different approach to the nuclear matter problem [7]. The Legindgaard method as developed in sec. 3.3 and implemented in the computer codes is a real theory which assumes finite integrands (3.4); it can not treat the singularities. To devise a method for handling them so that self-consistency can be imposed on the particle states, one would have to investigate: (1) How to integrate over the poles to obtain the Legindgaard transforms, presumably introducing a complex analog to eq. (3.28) [7,18] and performing the transformations with a principal value prescription. (2) Whether the polynomial expansion is still appropriate, especially for an imaginary part of T_E . The singularity probably arises abruptly for states above a characteristic k . This along with the diagonality of the propagator questions the convergence for the polynomial representation as in the case of the Pauli operator, see sec. 3.4. (3) How suitable the reference spectrum method is, since the singularity implies a phase shift in the correlated wave and consequently the concept of the healing property can not be maintained.

Bibliography

- [1] K. A Brueckner, C. A. Levinson, Phys. Rev. **97**, 1344 (1955)
- [2] J. Goldstone, Proc. Roy. Soc. (London) **A293**, 267 (1957)
- [3] P. J. Siemens, Nucl. Phys. **A141**, 225 (1970)
- [4] P. J. Siemens, A. S. Jensen, *Elements of Nuclei: Many-Body Physics with the Strong Interaction* (Addison-Wesley, Redwood City, 1987)
- [5] B. D. Day, Rev. Mod. Phys. **39**, 719 (1967)
- [6] H. A. Bethe, Ann. Rev. Nucl. Sci. **21**, 93 (1971)
- [7] J.-P. Jeukenne, A. Lejeune, C. Mahaux, Phys. Rep. **25C**, 83 (1976)
- [8] A. L. Fetter, J. D. Walecka, *Quantum Theory of Many-Particle Systems* (McGraw Hill, San Francisco 1971)
- [9] M. Fuchs and P. J. Siemens, *Nuclear Matter Effective Interaction*, in *Computational Nuclear Physics*, S.E. Koonin, K.H. Langanke, J. Maruhn and M. Zirnbaue, eds. (Springer Verlag, Berlin, 1992) in press.
- [10] H. A. Bethe, B. H. Brandow, A. G. Petschek, Phys. Rev. **129**, 225 (1963)
- [11] W. Legindgaard, Nucl. Phys. **A297**, 429 (1978)
- [12] W. Legindgaard, *thesis* (University of Copenhagen, 1977)
- [13] R. V. Reid, Ann. Phys. **50**, 411 (1968)
- [14] J. W. Negele, H. Orland, *Quantum Many-Body Systems* (Addison-Wesley, Redwood City, 1988)
- [15] A. deShalit, H. Feshbach, *Theoretical Nuclear Physics, Volume I: Nuclear Structure* (John Wiley and Sons, New York, 1974)
- [16] B. H. Brandow, Rev. Mod. Phys. **39**, 771 (1967)
- [17] T. Cheon, E. F. Redish, Phys. Rev. C **39**, 331 (1989)
- [18] J.-P. Jeukenne, A. Lejeune, C. Mahaux, Phys. Rev. C **10**, 1391 (1974)

- [19] S. E. Koonin, *Physik auf dem Computer 1* (Oldenbourg Verlag, Munich, 1987)
- [20] W. H. Press, B. P. Flannery, S. A. Teukolsky, W. T. Vetterling, *Numerical Recipes: The Art of Scientific Computing* (Cambridge University Press, Cambridge, 1986)
- [21] H. J. Jansen, *Computational Physics* (Manuscript, Oregon State University, 1990)
- [22] M. Abramowitz, I. A. Stegun, *Handbook of Mathematical Functions...* (National Bureau of Standards, Applied Mathematics Series 55, 1964)
- [23] G. E. Brown, *Many Body Problems* (North-Holland, Amsterdam, 1972)

Appendices

Appendix A Partial Wave Basis

The spatial part of a two-particle product state is represented in the $\mathbf{K}k$ -basis, while the two particle spin space is characterized by the observables for total spin S^2 and its z -projection S_z . In the partial wave projection of the physical states one changes this complete set of commuting observables according to

$$\{ \mathbf{K}, k, S^2, S_z \} \quad \Leftrightarrow \quad \{ \mathbf{K}, k, J^2, L^2, S^2, J_z \},$$

where J^2 denotes the total angular momentum, J_z its z -projection and L^2 the orbital angular momentum. In the first step only the spatial observables are considered. The partial wave basis in relative momentum space is defined by

$$\sum_{lm} \int_0^\infty k^2 dk |\mathbf{K}klm\rangle \langle \mathbf{K}klm| = \mathbf{1}, \quad \{l, m \in \mathbb{Z} \mid l \geq 0, |m| \leq l\},$$

$$\langle \mathbf{K}klm | \mathbf{K}k'l'm' \rangle = \frac{\delta(k-k')}{k^2} \delta_{ll'} \delta_{mm'},$$

and the projection coefficients for the basis transformation

$$\langle \mathbf{K}k | \mathbf{K}klm \rangle = Y_{lm}(\Omega_k), \quad (\text{A.1})$$

with the usual spherical harmonic $Y_{lm}(\Omega_k)$. The quantization is along \mathbf{K} which is an azimuthal symmetry axis. In position space the partial wave basis is completely analogous; the basis transformation between k and the radial coordinate r in relative position space is given by

$$\langle \mathbf{K}rlm | \mathbf{K}kl'm' \rangle = \delta_{ll'} \delta_{mm'} i^l \left(\frac{2}{\pi} \right)^{1/2} j_l(kr), \quad (\text{A.2})$$

where $j_l(kr)$ is the spherical Bessel function of order l . The normalization factor is chosen to give normalization to the 3-dimensional δ -function and the arbitrary phase factor reproduces the expansion of a plane wave, which is just the independent particle wavefunction for the relative motion. Thus

$$\begin{aligned} \langle \mathbf{r} | \mathbf{k} \rangle &= \frac{1}{(2\pi)^{3/2}} e^{i\mathbf{k}\mathbf{r}} \\ &= \frac{1}{(2\pi)^{3/2}} 4\pi \sum_{lm} i^l j_l(kr) Y_{lm}^*(\Omega_k) Y_{lm}(\Omega_r) \end{aligned} \quad (\text{A.3})$$

$$= \sum_m \langle rlm/klm \rangle Y_{lm}^*(\Omega_k) Y_{lm}(\Omega_r)$$

and

$$\langle \mathbf{r}/\mathbf{r}' \rangle = \delta^3(\mathbf{r} - \mathbf{r}') = \frac{\delta(r - r')}{r^2 \sin^2 \theta} \delta(\theta - \theta') \delta(\phi - \phi').$$

Secondly, Spin S and orbital angular momentum l are coupled to the total angular momentum J , which together with its z-projection J_z is conserved by the nucleon-nucleon interaction. The basis states transform according to

$$c.s.c.o. \quad \{K, k, l^2, l_z, S^2, S_z\} \Leftrightarrow \{K, k, J^2, l^2, S^2, J_z\}$$

$$|Kklm\rangle \otimes |Sm_s\rangle = \sum_{mm_s} C_{mm_s M}^{lSJ} |KkJlSM\rangle, \quad (A.4)$$

where the $C_{mm_s M}^{lSJ}$ are the usual Clebsch-Gordan coupling coefficients with $M=m+m_s$. (A.2) and (A.4) have been utilized in the partial wave expansion for T^R in ch. 2.

Appendix B Hartree-Fock Approximation

In this appendix the Hartree-Fock approximation of the mean field is presented to formally supplement the reasoning in ch. 2.1 concerning its failure. Further the T -matrix might be understood as an effective interaction and one can again derive a mean field which is analogous to, but different from the Hartree-Fock potential. While the former also accounts for correlations in lowest order, the latter is the mean field for uncorrelated, independent particles. The material here follows mainly [23].

A system of n interacting fermions is characterized by its Hamiltonian. Written in the language of second quantization and assuming only 2-body interactions V it is given by

$$H = \sum_{ij} \langle i|T|j \rangle a_i^\dagger a_j + \frac{1}{2} \sum_{ijkl} \langle ij|V|kl \rangle a_i^\dagger a_j^\dagger a_k a_l, \quad (\text{B.1})$$

where the matrix elements of the kinetic energy operator T and V are taken between single-particle states $|i\rangle$, yet to be specified, and product states $|ij\rangle$. The fermion creation and annihilation operators satisfy the usual anticommutation relations

$$\{a_i^\dagger, a_j^\dagger\} = \{a_i, a_j\} = 0, \quad \{a_i, a_j^\dagger\} = \delta_{ij}, \quad (\text{B.2})$$

which take care of the Pauli principle. The Hartree-Fock approximation consists in the form of the many-body state $|\psi\rangle$ which is chosen as an antisymmetrized product of the n occupied single-particle states

$$|\psi\rangle = \prod_{i=1}^n a_i^\dagger |0\rangle. \quad (\text{B.3})$$

In configuration space the wave function is given as the Slater determinant

$$\langle r_1 \dots r_n | \psi \rangle = (n!)^{-1/2} \text{Det } \phi_i(r_j), \quad (\text{B.4})$$

The groundstate configuration is obtained by a variational principle requiring that its energy be a minimum with respect to variations of the groundstate $|\psi_0\rangle$

$$\delta \langle \psi_0 | H | \psi_0 \rangle = 0 \quad \leftrightarrow \quad E_0 = \langle \psi_0 | H | \psi_0 \rangle. \quad (\text{B.5})$$

where the variation is over the set of trial single-particle states under the constraint that their normalization remains unchanged. First order variations observe this condition and may be written as

$$\delta |\psi_0\rangle = \eta a_i^\dagger a_j |\psi_0\rangle \quad j \leq n, i > n.. \quad (\text{B.6})$$

The variation (B.6) can then be viewed as a particle-hole excitation where a particle is shifted from an occupied level i into an unoccupied level j . Carrying out the variation in (B.5) asserts that

$$\left(\langle i|T|j\rangle + \sum_k^n \langle ik|V|jk\rangle - \langle ik|V|kj\rangle \right) a_i^\dagger a_j = 0, \quad (\text{B.7})$$

for $i > n, j \leq n$. This condition is evidently also fulfilled by the self-consistent Hartree-Fock Hamiltonian

$$H_{HF} = \sum_{ij} \left(\langle i|T|j\rangle + \sum_k^n \langle ik|V|jk\rangle - \langle ik|V|kj\rangle \right) a_i^\dagger a_j, \quad (\text{B.8})$$

which is a true one-body operator; i, j are not restricted here. From condition (B.7) it follows that H_{HF} does not connect occupied and unoccupied states, hence it may be diagonalized in the subspace of the occupied states alone. Thus one has to solve the eigenvalue problem

$$\langle i|T|j\rangle + \sum_k^n \langle ik|V|jk\rangle - \langle ik|V|kj\rangle = \delta_{ij} \epsilon_i, \quad (\text{B.9})$$

whose eigenvalues are the single-particle energies ϵ_i corresponding to the single-particle states $|i\rangle$. If one takes the n lowest eigenstates as the basis for the many-body groundstate in (B.3) the groundstate expectation value of the full Hamiltonian (B.1) satisfies the minimization condition (B.5) already by construction and the groundstate energy is given by

$$E_o = \sum_i^n \epsilon_i - \frac{1}{2} \sum_i^n \langle i|U|i\rangle, \quad (\text{B.10})$$

where the self-consistent mean field is defined as

$$\langle i|U|j\rangle = \sum_k^n \langle ik|V|jk\rangle - \langle ik|V|kj\rangle. \quad (\text{B.11})$$

It enters (B.9) as the single-particle potential in a self-consistent calculation: Starting with a trial potential $\langle i|U|i\rangle$ one obtains the eigenstates which in turn yield a new potential (B.11). New wave functions are calculated from the new potential, and the procedure is iterated until there is acceptably little change in the wave functions and the potential in two consecutive iterations. The groundstate energy obtained in this manner places an upper bound on the true groundstate energy by Ritz' variational theorem. The quality of the approximation is determined by the set of trial wave functions used and is intrinsically limited by the ansatz that they be Slater determinants (B.4). They were not suitable in

treating the bare nucleon-nucleon interaction and the development of the effective nucleon-nucleon interaction in ch. 2 provided a means to overcome this difficulty.

A more general approach to many-body systems with two-body interactions involves density matrices. There the mean field approximation in general replaces the two-body density operator, the product of creation and annihilation operators associated with interaction in (B.1), by a product of one-body density operators. In the case of the Hartree-Fock ansatz (B.3) the mean field approximation is formally exact. To explore this a little further one can consider the pair-correlation function $C(\mathbf{r}_1, \mathbf{r}_2)$ defined in terms of the diagonal elements of the two-body density matrix $\rho(\mathbf{r}_1, \mathbf{r}_2)$

$$\rho(\mathbf{r}_1, \mathbf{r}_2) = \rho(\mathbf{r}_1) \rho(\mathbf{r}_2) (1 - C(\mathbf{r}_1, \mathbf{r}_2)). \quad (\text{B.12})$$

The density $\rho(\mathbf{r}_1, \mathbf{r}_2)$ is the expectation value for finding a particle at \mathbf{r}_1 if another is at \mathbf{r}_2 . Spin variables are suppressed here. If there are no correlations $C(\mathbf{r}_1, \mathbf{r}_2)$ vanishes identically. The right hand side is then just the product of the single-particle densities and nothing prevents two particles from being at the same site, $\mathbf{r}_1 = \mathbf{r}_2$. The Pauli principle however prohibits identical particles to occupy the same state, i.e. site, and the correlation function for the independent particle approximation in uniform matter

$$C(\mathbf{r}_1, \mathbf{r}_2) = \frac{1}{2} \left(3 \frac{j_1(k_{fm}|\mathbf{r}_1 - \mathbf{r}_2|)}{k_{fm}|\mathbf{r}_1 - \mathbf{r}_2|} \right)^2 \quad (\text{B.13})$$

reduces $\rho(\mathbf{r}_1, \mathbf{r}_2)$ on a scale where $|\mathbf{r}_1 - \mathbf{r}_2| < 1/k_{fm}$ giving indeed $\rho(\mathbf{r}_1, \mathbf{r}_1) = 1/2$. For nuclear matter at equilibrium density $1/k_{fm} \cong 0.75 fm$, and for low lying momenta the contributions to the long range correlations is reduced.

Appendix C Converting to the Reaction Matrix

By considering the conversion of a bubble insertion in the bare interaction V of a 3-rd order graph to the corresponding reaction matrix T_E , this appendix supplements the discussion of the ladder-approximation in Section 2.2. In the sequence of ladder graphs below, the focus is on the bubble insertion. In (a) an excited fermion interacts with one in the Fermi sea without however exciting it. From (b) on the hole-fermion is also excited and the two fermions interact repeatedly in the particle states before the second excitation is destroyed. Only the bubble conversion affects the diagram while the rest enters just via the starting energy, leaving the vertices unaffected. The contribution of the passive part will be called α . Momentum conservation is enforced.

$$\begin{aligned}
 & \text{(a)} \quad \begin{array}{c} \text{Diagram (a): Two vertical ovals. The left oval has incoming line 'b' at the bottom and outgoing line 'k' at the top. The right oval has incoming line 'a' at the bottom and outgoing line 'i' at the top. A dashed line connects the top of the right oval to a small circle with incoming line 'j' and outgoing line 'i'. } \end{array} \quad + \quad \alpha \langle ij/V/ij \rangle \\
 & \text{(b)} \quad \begin{array}{c} \text{Diagram (b): Similar to (a), but the right oval has an additional incoming line 'm' and outgoing line 'n' in the middle. A dashed line connects 'm' to a small circle with incoming line 'j' and outgoing line 'n'. } \end{array} \quad + \quad \alpha \frac{1}{2} \sum_{mn} \frac{\langle ij/V/mn \rangle \langle mn/V/ij \rangle}{E - \epsilon_m - \epsilon_n} \\
 & \text{(c)} \quad \begin{array}{c} \text{Diagram (c): Similar to (b), but the small circle has an additional incoming line 'p' and outgoing line 'q' in the middle. A dashed line connects 'p' to the right oval's middle line 'm'. } \end{array} \quad + \quad \alpha \frac{1}{4} \sum_{mn,pq} \frac{\langle ij/V/mn \rangle \langle mn/V/pq \rangle \langle pq/V/ij \rangle}{(E - \epsilon_m - \epsilon_n)(E - \epsilon_p - \epsilon_q)} \\
 & \quad \quad \quad + \quad \vdots \\
 & \quad \quad \quad = \\
 & \text{(d)} \quad \begin{array}{c} \text{Diagram (d): Similar to (a), but the line connecting the right oval to the circle is a wavy line. } \end{array} \quad \alpha \langle ij/T_E/ij \rangle
 \end{aligned}$$

with the starting energy $E = \epsilon_a + \epsilon_b - \epsilon_i - \epsilon_k$. This expression also demonstrates that in order

to avoid ambiguity for the self-consistent single-particle potential $\langle i/U/i \rangle$, E must not depend on either $\varepsilon_k, \varepsilon_a$ or ε_b but only on ε_i . Then the diagrams above depend at most on ε_i and ε_j . Diagrams where i and j appear both in E are consequently evaluated on-shell.

Appendix D Numerical Data - Samples

Numerical results of a sample calculation are reported on the following pages. The parameters were

$k_{fm} = 1.3 fm^{-1}$	$\gamma^2 = 1.4 fm^{-2}$
$K = 0.7 fm^{-1}$	$m^* = 1.0$
Starting energy	$E = -162.3 MeV$
Subspace cutoff	$k_{max} = 2.8 fm^{-1}$
Maximum Polynomial	$n = 5$
Nuclear Matter Spectrum	$\varepsilon = (100 + 41.47 \frac{1}{2} k^2) MeV$
400 radial points in TREF, with $0.05 fm \leq r \leq 10 fm$.	
40 \times 40 points for TNM (Legendgaard method).	

The matrix elements in the various channels are assigned as

"JLS000"	for $J=0, l=0$ and $S=0$ in $\langle KkJJSM/TR/Kk'JJSM \rangle$
"JLS10C"	for $J=1, l=0$ and $S=1$ in $\langle KkJ-1SM/TR/Kk'JJ+1SM \rangle$
etc.	

as

"T : JLS000"	for $\langle KkJJSM/T/Kk'JJSM \rangle$, analogous to above,
etc.	

and as

"PNM000"	for $\langle KnJJSM/TR/Kn'JJSM \rangle$.
etc.	

The last printout shows the polynomial representation of the propagator difference up to $n=10$.

TR(kf,ki) Effective Mass EFM : 1.0000 Gridsize : 40
 Healing Parameter GAMSQ : 1.4000 Cutoff PKMX : 2.8000

JLS000

kf \ ki	0.070	0.350	0.630	0.910	1.190	1.470	1.750	2.030	2.310	2.590
0.070	-26.3613	-23.6753	-19.1420	-14.3300	-9.6290	-5.2376	-1.3177	2.0011	4.6492	6.6242
0.350	-23.6753	-21.7482	-18.0315	-13.6228	-9.1723	-4.9671	-1.1955	2.0109	4.5815	6.5051
0.630	-19.1420	-18.0315	-15.5141	-12.0035	-8.1300	-4.3511	-0.9122	2.0421	4.4341	6.2419
0.910	-14.3300	-13.6228	-12.0035	-9.5560	-6.5541	-3.4182	-0.4718	2.1091	4.2330	5.8644
1.190	-9.6291	-9.1724	-8.1300	-6.5541	-4.5187	-2.2020	0.1204	2.2305	4.0127	5.4138
1.470	-5.2377	-4.9673	-4.3512	-3.4182	-2.2021	-0.7411	0.8605	2.4259	3.8099	4.9373
1.750	-1.3179	-1.1957	-0.9124	-0.4720	0.1203	0.8604	1.7432	2.7145	3.6603	4.4808
2.030	2.0008	2.0107	2.0418	2.1089	2.2303	2.4257	2.7144	3.1127	3.5956	4.0861
2.310	4.6488	4.5812	4.4337	4.2327	4.0124	3.8097	3.6601	3.5955	3.6416	3.7883
2.590	6.6238	6.5047	6.2415	5.8640	5.4135	4.9370	4.4806	4.0860	3.7883	3.6145

JLS011

kf \ ki	0.070	0.350	0.630	0.910	1.190	1.470	1.750	2.030	2.310	2.590
0.070	-0.1458	-0.5481	-0.5531	-0.3949	-0.2278	-0.0801	0.0358	0.1248	0.1854	0.2228
0.350	-0.5481	-2.1816	-2.4265	-1.8376	-1.0779	-0.3830	0.1818	0.6124	0.9119	1.0954
0.630	-0.5531	-2.4265	-3.1719	-2.7207	-1.6882	-0.6022	0.3346	1.0623	1.5789	1.8989
0.910	-0.3949	-1.8376	-2.7207	-2.6986	-1.8520	-0.6496	0.5093	1.4580	2.1494	2.5898
1.190	-0.2278	-1.0779	-1.6882	-1.8520	-1.3989	-0.4168	0.7488	1.7991	2.6059	3.1398
1.470	-0.0801	-0.3830	-0.6022	-0.6496	-0.4168	0.1963	1.1233	2.1149	2.9516	3.5412
1.750	0.0358	0.1818	0.3346	0.5093	0.7488	1.1233	1.7081	2.4647	3.2169	3.8055
2.030	0.1248	0.6124	1.0623	1.4580	1.7991	2.1149	2.4647	2.9176	3.4599	3.9677
2.310	0.1854	0.9119	1.5789	2.1494	2.6059	2.9516	3.2169	3.4599	3.7481	4.0849
2.590	0.2228	1.0954	1.8989	2.5898	3.1398	3.5412	3.8055	3.9677	4.0849	4.2224

JLS110

kf \ ki	0.070	0.350	0.630	0.910	1.190	1.470	1.750	2.030	2.310	2.590
0.070	0.0777	0.2309	0.1405	0.1291	0.2156	0.2918	0.3283	0.3193	0.2862	0.2402
0.350	0.2309	0.7808	0.6859	0.7221	1.0798	1.4303	1.5972	1.5660	1.4084	1.1904
0.630	0.1405	0.6859	1.1226	1.4874	1.9692	2.4573	2.7145	2.6882	2.4464	2.0946
0.910	0.1291	0.7221	1.4874	2.2520	2.8619	3.3355	3.6138	3.6056	3.3401	2.9128
1.190	0.2156	1.0798	1.9692	2.8619	3.5956	4.0580	4.2855	4.2851	4.0407	3.6067
1.470	0.2918	1.4303	2.4573	3.3355	4.0580	4.5468	4.7552	4.7389	4.5314	4.1427
1.750	0.3283	1.5972	2.7145	3.6138	4.2855	4.7552	4.9993	5.0053	4.8293	4.5079
2.030	0.3193	1.5660	2.6882	3.6056	4.2851	4.7389	5.0053	5.0827	4.9701	4.7154
2.310	0.2862	1.4084	2.4464	3.3401	4.0407	4.5314	4.8293	4.9701	4.9576	4.7924
2.590	0.2402	1.1904	2.0946	2.9128	3.6067	4.1427	4.5079	4.7154	4.7924	4.7418

JLS111										
kf \ ki	0.070	0.350	0.630	0.910	1.190	1.470	1.750	2.030	2.310	2.590
0.070	0.0904	0.3377	0.3530	0.3052	0.2695	0.2378	0.2086	0.1778	0.1492	0.1227
0.350	0.3377	1.3565	1.6018	1.4745	1.3166	1.1706	1.0275	0.8811	0.7408	0.6122
0.630	0.3530	1.6018	2.2967	2.4058	2.2433	2.0246	1.7900	1.5493	1.3124	1.0931
0.910	0.3052	1.4745	2.4058	2.8941	2.9342	2.7339	2.4560	2.1525	1.8467	1.5554
1.190	0.2695	1.3166	2.2433	2.9342	3.2611	3.2262	2.9832	2.6641	2.3227	1.9861
1.470	0.2378	1.1706	2.0246	2.7339	3.2262	3.4207	3.3243	3.0550	2.7199	2.3684
1.750	0.2086	1.0275	1.7900	2.4560	2.9832	3.3243	3.4246	3.2912	3.0157	2.6848
2.030	0.1778	0.8811	1.5493	2.1525	2.6641	3.0550	3.2912	3.3322	3.1832	2.9161
2.310	0.1492	0.7408	1.3124	1.8467	2.3227	2.7199	3.0157	3.1832	3.1902	3.0396
2.590	0.1227	0.6122	1.0931	1.5554	1.9861	2.3684	2.6848	2.9161	3.0396	3.0285
JLS101 (direct)										
kf \ ki	0.070	0.350	0.630	0.910	1.190	1.470	1.750	2.030	2.310	2.590
0.070	-34.9503	-32.1061	-27.0159	-21.0620	-14.6965	-8.3794	-2.5701	2.3780	6.2748	9.0862
0.350	-32.1061	-29.9227	-25.5268	-19.9417	-13.8891	-7.8692	-2.3223	2.4195	6.1713	8.8883
0.630	-27.0159	-25.5268	-22.1721	-17.4511	-12.1043	-6.7364	-1.7622	2.5242	5.9488	8.4543
0.910	-21.0620	-19.9417	-17.4511	-13.8416	-9.5461	-5.1035	-0.9333	2.7035	5.6505	7.8409
1.190	-14.6965	-13.8891	-12.1044	-9.5461	-6.4528	-3.1241	0.0994	2.9644	5.3291	7.1233
1.470	-8.3795	-7.8693	-6.7365	-5.1036	-3.1241	-0.9455	1.2623	3.3029	5.0328	6.3802
1.750	-2.5702	-2.3224	-1.7623	-0.9334	0.0993	1.2623	2.4916	3.7059	4.7959	5.6793
2.030	2.3778	2.4193	2.5240	2.7033	2.9642	3.3028	3.7058	4.1617	4.6377	5.0696
2.310	6.2745	6.1710	5.9485	5.6502	5.3289	5.0326	4.7958	4.6376	4.5699	4.5801
2.590	9.0858	8.8879	8.4539	7.8406	7.1230	6.3799	5.6791	5.0695	4.5800	4.2267
JLS10C (tensor coupled)										
kf \ ki	0.070	0.350	0.630	0.910	1.190	1.470	1.750	2.030	2.310	2.590
0.070	-0.2366	-0.1532	-0.0677	-0.0319	-0.0155	-0.0077	-0.0028	0.0006	0.0029	0.0048
0.350	-4.9257	-3.4294	-1.6939	-0.8034	-0.3964	-0.1935	-0.0708	0.0139	0.0726	0.1158
0.630	-11.1337	-8.7691	-5.2335	-2.6652	-1.3284	-0.6388	-0.2347	0.0339	0.2226	0.3531
0.910	-15.3692	-13.3463	-9.4868	-5.5790	-2.9007	-1.3917	-0.5186	0.0386	0.4188	0.6780
1.190	-17.7996	-16.2433	-12.9822	-8.8756	-5.1354	-2.5458	-0.9821	-0.0154	0.6168	1.0376
1.470	-18.9435	-17.7725	-15.1856	-11.5794	-7.6202	-4.1606	-1.7284	-0.2024	0.7596	1.3757
1.750	-19.2595	-18.3400	-16.2763	-13.2690	-9.6645	-5.9792	-2.8419	-0.6293	0.7689	1.6342
2.030	-18.9825	-18.2329	-16.5419	-14.0388	-10.9263	-7.4990	-4.1613	-1.3887	0.5445	1.7419
2.310	-18.2552	-17.6306	-16.2132	-14.1051	-11.4518	-8.4384	-5.3076	-2.3744	-0.0010	1.6127
2.590	-17.1917	-16.6574	-15.4543	-13.6648	-11.4048	-8.8120	-6.0426	-3.2883	-0.7916	1.1715

JLS121 (direct)										
kf \ ki	0.070	0.350	0.630	0.910	1.190	1.470	1.750	2.030	2.310	2.590
0.070	0.0009	0.0158	0.0222	0.0144	0.0058	-0.0012	-0.0056	-0.0078	-0.0085	-0.0082
0.350	0.0158	0.2859	0.4461	0.3245	0.1357	-0.0263	-0.1315	-0.1863	-0.2049	-0.1989
0.630	0.0222	0.4461	0.8631	0.7830	0.3665	-0.0634	-0.3732	-0.5460	-0.6096	-0.5998
0.910	0.0144	0.3245	0.7830	0.9053	0.5125	-0.1075	-0.6407	-0.9742	-1.1159	-1.1162
1.190	0.0058	0.1357	0.3665	0.5125	0.3233	-0.2302	-0.8741	-1.3554	-1.5992	-1.6357
1.470	-0.0012	-0.0263	-0.0634	-0.1075	-0.2302	-0.5633	-1.0997	-1.6266	-1.9585	-2.0542
1.750	-0.0056	-0.1315	-0.3732	-0.6407	-0.8741	-1.0997	-1.4117	-1.8128	-2.1528	-2.3015
2.030	-0.0078	-0.1863	-0.5460	-0.9742	-1.3554	-1.6266	-1.8128	-2.0033	-2.2201	-2.3628
2.310	-0.0085	-0.2049	-0.6096	-1.1159	-1.5992	-1.9585	-2.1528	-2.2201	-2.2529	-2.2886
2.590	-0.0082	-0.1989	-0.5998	-1.1162	-1.6357	-2.0542	-2.3015	-2.3628	-2.2886	-2.1727
JLS220										
kf \ ki	0.070	0.350	0.630	0.910	1.190	1.470	1.750	2.030	2.310	2.590
0.070	-0.0004	-0.0060	-0.0081	-0.0060	-0.0048	-0.0038	-0.0032	-0.0026	-0.0021	-0.0016
0.350	-0.0060	-0.1064	-0.1657	-0.1411	-0.1137	-0.0929	-0.0780	-0.0648	-0.0516	-0.0395
0.630	-0.0081	-0.1657	-0.3413	-0.3792	-0.3340	-0.2839	-0.2406	-0.2008	-0.1618	-0.1238
0.910	-0.0060	-0.1411	-0.3792	-0.5550	-0.5851	-0.5327	-0.4632	-0.3913	-0.3184	-0.2460
1.190	-0.0048	-0.1137	-0.3340	-0.5851	-0.7480	-0.7694	-0.7036	-0.6080	-0.5019	-0.3930
1.470	-0.0038	-0.0929	-0.2839	-0.5327	-0.7694	-0.9052	-0.9044	-0.8145	-0.6879	-0.5479
1.750	-0.0032	-0.0780	-0.2406	-0.4632	-0.7036	-0.9044	-0.9999	-0.9667	-0.8478	-0.6916
2.030	-0.0026	-0.0648	-0.2008	-0.3913	-0.6080	-0.8145	-0.9667	-1.0159	-0.9482	-0.8025
2.310	-0.0021	-0.0516	-0.1618	-0.3184	-0.5019	-0.6879	-0.8478	-0.9482	-0.9534	-0.8558
2.590	-0.0016	-0.0395	-0.1238	-0.2460	-0.3930	-0.5479	-0.6916	-0.8025	-0.8558	-0.8247
JLS221										
kf \ ki	0.070	0.350	0.630	0.910	1.190	1.470	1.750	2.030	2.310	2.590
0.070	-0.0017	-0.0301	-0.0442	-0.0348	-0.0252	-0.0166	-0.0109	-0.0070	-0.0044	-0.0028
0.350	-0.0301	-0.5507	-0.9091	-0.8037	-0.5968	-0.4060	-0.2677	-0.1731	-0.1094	-0.0698
0.630	-0.0442	-0.9091	-1.8940	-2.0895	-1.7088	-1.2315	-0.8345	-0.5478	-0.3525	-0.2231
0.910	-0.0348	-0.8037	-2.0895	-2.9272	-2.8603	-2.2706	-1.6250	-1.1005	-0.7220	-0.4632
1.190	-0.0252	-0.5968	-1.7088	-2.8603	-3.4155	-3.1604	-2.4756	-1.7685	-1.1980	-0.7850
1.470	-0.0166	-0.4060	-1.2315	-2.2706	-3.1604	-3.4817	-3.1299	-2.4351	-1.7384	-1.1767
1.750	-0.0109	-0.2677	-0.8345	-1.6250	-2.4756	-3.1299	-3.2949	-2.9133	-2.2578	-1.6103
2.030	-0.0070	-0.1731	-0.5478	-1.1005	-1.7685	-2.4351	-2.9133	-2.9853	-2.6137	-2.0205
2.310	-0.0044	-0.1094	-0.3525	-0.7220	-1.1980	-1.7384	-2.2578	-2.6137	-2.6355	-2.2941
2.590	-0.0028	-0.0698	-0.2231	-0.4632	-0.7850	-1.1767	-1.6103	-2.0205	-2.2941	-2.2918

JLS211 (direct)										
kf \ ki	0.070	0.350	0.630	0.910	1.190	1.470	1.750	2.030	2.310	2.590
0.070	-0.0139	-0.0726	-0.1283	-0.1620	-0.1721	-0.1653	-0.1475	-0.1240	-0.0985	-0.0738
0.350	-0.0726	-0.3617	-0.6173	-0.7791	-0.8336	-0.8052	-0.7219	-0.6092	-0.4858	-0.3651
0.630	-0.1283	-0.6173	-1.0187	-1.2846	-1.3930	-1.3627	-1.2355	-1.0523	-0.8462	-0.6407
0.910	-0.1620	-0.7791	-1.2846	-1.6275	-1.7909	-1.7847	-1.6455	-1.4224	-1.1587	-0.8878
1.190	-0.1721	-0.8336	-1.3930	-1.7909	-2.0039	-2.0383	-1.9204	-1.6930	-1.4039	-1.0934
1.470	-0.1653	-0.8052	-1.3627	-1.7847	-2.0383	-2.1188	-2.0441	-1.8459	-1.5652	-1.2447
1.750	-0.1475	-0.7219	-1.2355	-1.6455	-1.9204	-2.0441	-2.0216	-1.8739	-1.6313	-1.3303
2.030	-0.1240	-0.6092	-1.0523	-1.4224	-1.6930	-1.8459	-1.8739	-1.7848	-1.5987	-1.3419
2.310	-0.0985	-0.4858	-0.8462	-1.1587	-1.4039	-1.5652	-1.6313	-1.5987	-1.4750	-1.2772
2.590	-0.0738	-0.3651	-0.6407	-0.8878	-1.0934	-1.2447	-1.3303	-1.3419	-1.2772	-1.1424
JLS21C (tensor coupled)										
kf \ ki	0.070	0.350	0.630	0.910	1.190	1.470	1.750	2.030	2.310	2.590
0.070	0.0004	0.0013	0.0007	0.0002	0.0001	0.0000	0.0000	0.0000	0.0000	0.0000
0.350	0.0414	0.1293	0.0802	0.0317	0.0138	0.0052	0.0031	0.0011	0.0009	0.0003
0.630	0.1300	0.4606	0.3827	0.1899	0.0812	0.0349	0.0165	0.0081	0.0042	0.0020
0.910	0.1753	0.7197	0.7991	0.5294	0.2582	0.1158	0.0529	0.0257	0.0126	0.0059
1.190	0.1817	0.8089	1.0849	0.9369	0.5779	0.2853	0.1324	0.0620	0.0295	0.0130
1.470	0.1717	0.7929	1.1780	1.2202	0.9503	0.5692	0.2837	0.1328	0.0607	0.0259
1.750	0.1530	0.7268	1.1486	1.3238	1.2204	0.8996	0.5289	0.2625	0.1198	0.0499
2.030	0.1347	0.6468	1.0583	1.3025	1.3333	1.1499	0.8171	0.4709	0.2280	0.0967
2.310	0.1162	0.5647	0.9468	1.2132	1.3268	1.2666	1.0445	0.7202	0.4038	0.1854
2.590	0.1001	0.4884	0.8312	1.0949	1.2495	1.2740	1.1602	0.9242	0.6188	0.3336
JLS231 (direct)										
kf \ ki	0.070	0.350	0.630	0.910	1.190	1.470	1.750	2.030	2.310	2.590
0.070	0.0000	-0.0001	-0.0002	-0.0002	-0.0001	-0.0001	0.0000	0.0000	0.0000	0.0000
0.350	-0.0001	-0.0073	-0.0191	-0.0184	-0.0134	-0.0094	-0.0059	-0.0037	-0.0017	-0.0004
0.630	-0.0002	-0.0191	-0.0613	-0.0786	-0.0670	-0.0491	-0.0329	-0.0202	-0.0100	-0.0019
0.910	-0.0002	-0.0184	-0.0786	-0.1393	-0.1507	-0.1239	-0.0883	-0.0554	-0.0277	-0.0053
1.190	-0.0001	-0.0134	-0.0670	-0.1507	-0.2105	-0.2087	-0.1638	-0.1079	-0.0551	-0.0103
1.470	-0.0001	-0.0094	-0.0491	-0.1239	-0.2087	-0.2534	-0.2315	-0.1655	-0.0880	-0.0156
1.750	0.0000	-0.0059	-0.0329	-0.0883	-0.1638	-0.2315	-0.2504	-0.2036	-0.1152	-0.0180
2.030	0.0000	-0.0037	-0.0202	-0.0554	-0.1079	-0.1655	-0.2036	-0.1908	-0.1179	-0.0098
2.310	0.0000	-0.0017	-0.0100	-0.0277	-0.0551	-0.0880	-0.1152	-0.1179	-0.0733	0.0225
2.590	0.0000	-0.0004	-0.0019	-0.0053	-0.0103	-0.0156	-0.0180	-0.0098	0.0225	0.0945

T(kf,ki) Effective Mass EFM : 1.0000 Gridsize : 40
 Healing Parameter GAMSQ : 1.4000 Cutoff PKMX : 2.8000

T: JLS000

kf \ ki	0.070	0.350	0.630	0.910	1.190	1.470	1.750	2.030	2.310	2.590
0.070	-23.3113	-20.7675	-16.6277	-12.3674	-8.2972	-4.5510	-1.2400	1.5426	3.7495	5.3863
0.350	-20.7675	-18.9675	-15.6227	-11.7405	-7.8947	-4.3097	-1.1246	1.5647	3.7092	5.3060
0.630	-16.6277	-15.6227	-13.4251	-10.3701	-7.0213	-3.7814	-0.8528	1.6510	3.6717	5.1946
0.910	-12.3674	-11.7405	-10.3702	-8.2784	-5.6869	-2.9727	-0.4259	1.8023	3.6353	5.0435
1.190	-8.2973	-7.8948	-7.0214	-5.6869	-3.9297	-1.8989	0.1530	2.0246	3.6104	4.8610
1.470	-4.5511	-4.3099	-3.7815	-2.9728	-1.8990	-0.5834	0.8815	2.3272	3.6133	4.6660
1.750	-1.2402	-1.1248	-0.8530	-0.4261	0.1529	0.8814	1.7553	2.7207	3.6630	4.4819
2.030	1.5423	1.5644	1.6508	1.8020	2.0244	2.3270	2.7206	3.2144	3.7787	4.3329
2.310	3.7491	3.7088	3.6713	3.6350	3.6101	3.6131	3.6629	3.7786	3.9768	4.2420
2.590	5.3858	5.3055	5.1942	5.0432	4.8606	4.6657	4.4817	4.3328	4.2419	4.2292

T: JLS011

kf \ ki	0.070	0.350	0.630	0.910	1.190	1.470	1.750	2.030	2.310	2.590
0.070	-0.1267	-0.5583	-0.5761	-0.4187	-0.2445	-0.0852	0.0440	0.1453	0.2158	0.2593
0.350	-0.5583	-2.1346	-2.3599	-1.7765	-1.0372	-0.3691	0.1686	0.5762	0.8589	1.0321
0.630	-0.5761	-2.3599	-3.0732	-2.6288	-1.6267	-0.5819	0.3124	1.0034	1.4926	1.7958
0.910	-0.4187	-1.7765	-2.6288	-2.6128	-1.7946	-0.6309	0.4880	1.4018	2.0671	2.4916
1.190	-0.2445	-1.0372	-1.6267	-1.7946	-1.3603	-0.4039	0.7355	1.7631	2.5534	3.0773
1.470	-0.0852	-0.3691	-0.5819	-0.6309	-0.4039	0.2022	1.1228	2.1099	2.9441	3.5327
1.750	0.0440	0.1686	0.3124	0.4880	0.7355	1.1228	1.7228	2.4949	3.2606	3.8586
2.030	0.1453	0.5762	1.0034	1.4018	1.7631	2.1099	2.4949	2.9821	3.5531	4.0804
2.310	0.2158	0.8589	1.4926	2.0671	2.5534	2.9441	3.2606	3.5531	3.8828	4.2474
2.590	0.2593	1.0321	1.7958	2.4916	3.0773	3.5327	3.8586	4.0804	4.2474	4.4187

T: JLS110

kf \ ki	0.070	0.350	0.630	0.910	1.190	1.470	1.750	2.030	2.310	2.590
0.070	0.0848	0.2407	0.1557	0.1506	0.2430	0.3235	0.3622	0.3531	0.3179	0.2682
0.350	0.2407	0.8105	0.7374	0.7942	1.1690	1.5314	1.7043	1.6728	1.5094	1.2813
0.630	0.1557	0.7374	1.2130	1.6142	2.1259	2.6349	2.9024	2.8757	2.6237	2.2542
0.910	0.1506	0.7942	1.6142	2.4301	3.0823	3.5856	3.8785	3.8697	3.5898	3.1374
1.190	0.2430	1.1690	2.1259	3.0823	3.8689	4.3682	4.6140	4.6129	4.3505	3.8850
1.470	0.3235	1.5314	2.6349	3.5856	4.3682	4.8992	5.1285	5.1114	4.8832	4.4586
1.750	0.3622	1.7043	2.9024	3.8785	4.6140	5.1285	5.3949	5.3999	5.2020	4.8425
2.030	0.3531	1.6728	2.8757	3.8697	4.6129	5.1114	5.3999	5.4764	5.3419	5.0492
2.310	0.3179	1.5094	2.6237	3.5898	4.3505	4.8832	5.2020	5.3419	5.3087	5.1077
2.590	0.2682	1.2813	2.2542	3.1374	3.8850	4.4586	4.8425	5.0492	5.1077	5.0251

T: JLS111

kf \ ki	0.070	0.350	0.630	0.910	1.190	1.470	1.750	2.030	2.310	2.590
0.070	0.0943	0.3374	0.3502	0.3011	0.2650	0.2334	0.2048	0.1746	0.1466	0.1205
0.350	0.3374	1.3993	1.6721	1.5601	1.4078	1.2606	1.1116	0.9566	0.8065	0.6684
0.630	0.3502	1.6721	2.4144	2.5503	2.3983	2.1782	1.9339	1.6786	1.4251	1.1896
0.910	0.3011	1.5601	2.5503	3.0724	3.1265	2.9252	2.6360	2.3146	1.9882	1.6766
1.190	0.2650	1.4078	2.3983	3.1265	3.4695	3.4344	3.1796	2.8415	2.4777	2.1190
1.470	0.2334	1.2606	2.1782	2.9252	3.4344	3.6295	3.5218	3.2337	2.8762	2.5025
1.750	0.2048	1.1116	1.9339	2.6360	3.1796	3.5218	3.6120	3.4610	3.1643	2.8123
2.030	0.1746	0.9566	1.6786	2.3146	2.8414	3.2337	3.4610	3.4862	3.3180	3.0318
2.310	0.1466	0.8065	1.4251	1.9882	2.4777	2.8762	3.1643	3.3180	3.3082	3.1409
2.590	0.1205	0.6684	1.1896	1.6766	2.1190	2.5025	2.8123	3.0318	3.1409	3.1155

T: JLS101 (direct)

kf \ ki	0.070	0.350	0.630	0.910	1.190	1.470	1.750	2.030	2.310	2.590
0.070	-23.1299	-21.7762	-18.6600	-14.8711	-10.6315	-6.2337	-2.0320	1.6627	4.6403	6.7842
0.350	-21.7762	-20.6934	-17.9405	-14.2512	-10.1169	-5.8663	-1.8274	1.7214	4.5896	6.6680
0.630	-18.6600	-17.9405	-15.8647	-12.6785	-8.9196	-5.0392	-1.3488	1.9108	4.5689	6.5219
0.910	-14.8711	-14.2512	-12.6786	-10.2064	-7.1076	-3.7996	-0.6180	2.2215	4.5699	6.3297
1.190	-10.6316	-10.1170	-8.9196	-7.1077	-4.8096	-2.2408	0.3167	2.6421	4.6008	6.1038
1.470	-6.2338	-5.8664	-5.0393	-3.7997	-2.2408	-0.4638	1.3936	3.1522	4.6722	5.8706
1.750	-2.0321	-1.8275	-1.3489	-0.6182	0.3166	1.3935	2.5559	3.7247	4.7879	5.6556
2.030	1.6625	1.7212	1.9106	2.2214	2.6420	3.1521	3.7246	4.3359	4.9436	5.4761
2.310	4.6400	4.5893	4.5686	4.5697	4.6006	4.6720	4.7878	4.9435	5.1346	5.3392
2.590	6.7839	6.6676	6.5215	6.3293	6.1035	5.8703	5.6554	5.4759	5.3391	5.2499

T: JLS10C (tensor coupled)

kf \ ki	0.070	0.350	0.630	0.910	1.190	1.470	1.750	2.030	2.310	2.590
0.070	0.0636	0.0592	0.0704	0.0462	0.0172	-0.0069	-0.0223	-0.0306	-0.0354	-0.0411
0.350	-4.6962	-3.1919	-1.4773	-0.6275	-0.2725	-0.1262	-0.0589	-0.0240	-0.0063	0.0068
0.630	-10.4605	-8.0601	-4.5783	-2.1260	-0.9434	-0.4252	-0.1919	-0.0791	-0.0198	0.0157
0.910	-13.9759	-11.9330	-8.2102	-4.5459	-2.1740	-0.9968	-0.4495	-0.1864	-0.0498	0.0296
1.190	-15.6027	-14.0654	-11.0444	-7.3259	-4.0580	-1.9704	-0.8938	-0.3639	-0.0918	0.0617
1.470	-16.0067	-14.9009	-12.6550	-9.5718	-6.2361	-3.4316	-1.6299	-0.6657	-0.1659	0.1065
1.750	-15.7489	-14.9358	-13.2951	-10.9172	-8.0534	-5.1403	-2.7418	-1.1849	-0.3247	0.1396
2.030	-15.1208	-14.5064	-13.2913	-11.4845	-9.1851	-6.6012	-4.0672	-2.0057	-0.6549	0.1081
2.310	-14.2767	-13.7999	-12.8789	-11.4917	-9.6768	-7.5307	-5.2245	-3.0194	-1.2415	-0.0723
2.590	-13.2967	-12.9074	-12.1920	-11.1104	-9.6736	-7.9319	-5.9713	-3.9310	-2.0181	-0.4909

T: JLS121 (direct)

kf \ ki	0.070	0.350	0.630	0.910	1.190	1.470	1.750	2.030	2.310	2.590
0.070	0.1179	-0.0096	-0.0715	-0.0958	-0.0881	-0.0619	-0.0284	0.0028	0.0252	0.0360
0.350	-0.0096	0.3073	0.5152	0.4374	0.2849	0.1498	0.0611	0.0128	-0.0077	-0.0089
0.630	-0.0715	0.5152	1.0947	1.1608	0.8626	0.5168	0.2543	0.0951	0.0185	0.0005
0.910	-0.0958	0.4374	1.1608	1.5466	1.3836	0.9379	0.5130	0.2216	0.0667	0.0195
1.190	-0.0881	0.2849	0.8626	1.3836	1.5390	1.2596	0.7961	0.3964	0.1475	0.0496
1.470	-0.0619	0.1498	0.5168	0.9379	1.2596	1.2912	1.0045	0.6008	0.2778	0.1119
1.750	-0.0284	0.0611	0.2543	0.5130	0.7961	1.0045	0.9985	0.7581	0.4433	0.2225
2.030	0.0028	0.0128	0.0951	0.2216	0.3964	0.6008	0.7581	0.7564	0.5813	0.3701
2.310	0.0252	-0.0077	0.0185	0.0667	0.1475	0.2778	0.4433	0.5813	0.6034	0.5063
2.590	0.0360	-0.0089	0.0005	0.0195	0.0496	0.1119	0.2225	0.3701	0.5063	0.5682

T: JLS220

kf \ ki	0.070	0.350	0.630	0.910	1.190	1.470	1.750	2.030	2.310	2.590
0.070	0.0015	-0.0064	-0.0099	-0.0085	-0.0074	-0.0063	-0.0054	-0.0045	-0.0036	-0.0028
0.350	-0.0064	-0.1061	-0.1650	-0.1400	-0.1124	-0.0916	-0.0768	-0.0637	-0.0507	-0.0388
0.630	-0.0099	-0.1650	-0.3386	-0.3752	-0.3293	-0.2790	-0.2359	-0.1967	-0.1584	-0.1211
0.910	-0.0085	-0.1400	-0.3752	-0.5489	-0.5777	-0.5249	-0.4557	-0.3846	-0.3129	-0.2417
1.190	-0.0074	-0.1124	-0.3293	-0.5777	-0.7390	-0.7596	-0.6941	-0.5995	-0.4949	-0.3875
1.470	-0.0063	-0.0916	-0.2790	-0.5249	-0.7596	-0.8946	-0.8940	-0.8051	-0.6801	-0.5418
1.750	-0.0054	-0.0768	-0.2359	-0.4557	-0.6941	-0.8940	-0.9895	-0.9573	-0.8400	-0.6856
2.030	-0.0045	-0.0637	-0.1967	-0.3846	-0.5995	-0.8051	-0.9573	-1.0074	-0.9411	-0.7971
2.310	-0.0036	-0.0507	-0.1584	-0.3129	-0.4949	-0.6801	-0.8400	-0.9411	-0.9476	-0.8512
2.590	-0.0028	-0.0388	-0.1211	-0.2417	-0.3875	-0.5418	-0.6856	-0.7971	-0.8512	-0.8211

T: JLS221

kf \ ki	0.070	0.350	0.630	0.910	1.190	1.470	1.750	2.030	2.310	2.590
0.070	0.0790	-0.0462	-0.1135	-0.1254	-0.1155	-0.0937	-0.0690	-0.0460	-0.0283	-0.0184
0.350	-0.0462	-0.5443	-0.8897	-0.7786	-0.5711	-0.3831	-0.2494	-0.1598	-0.1006	-0.0640
0.630	-0.1135	-0.8897	-1.8209	-1.9902	-1.6042	-1.1361	-0.7569	-0.4912	-0.3153	-0.1990
0.910	-0.1254	-0.7786	-1.9902	-2.7885	-2.7102	-2.1301	-1.5079	-1.0133	-0.6639	-0.4256
1.190	-0.1155	-0.5711	-1.6042	-2.7102	-3.2489	-3.0006	-2.3395	-1.6653	-1.1283	-0.7400
1.470	-0.0937	-0.3831	-1.1361	-2.1301	-3.0006	-3.3251	-2.9939	-2.3303	-1.6669	-1.1307
1.750	-0.0690	-0.2494	-0.7569	-1.5079	-2.3395	-2.9939	-3.1748	-2.8195	-2.1933	-1.5688
2.030	-0.0460	-0.1598	-0.4912	-1.0133	-1.6653	-2.3303	-2.8195	-2.9113	-2.5625	-1.9877
2.310	-0.0283	-0.1006	-0.3153	-0.6639	-1.1283	-1.6669	-2.1933	-2.5625	-2.6000	-2.2713
2.590	-0.0184	-0.0640	-0.1990	-0.4256	-0.7400	-1.1307	-1.5688	-1.9877	-2.2713	-2.2773

T: JLS211 (direct)										
kf \ ki	0.070	0.350	0.630	0.910	1.190	1.470	1.750	2.030	2.310	2.590
0.070	-0.0070	-0.0686	-0.1264	-0.1614	-0.1721	-0.1654	-0.1472	-0.1233	-0.0975	-0.0729
0.350	-0.0686	-0.3366	-0.5812	-0.7392	-0.7946	-0.7696	-0.6909	-0.5830	-0.4643	-0.3483
0.630	-0.1264	-0.5812	-0.9635	-1.2212	-1.3290	-1.3029	-1.1826	-1.0073	-0.8094	-0.6120
0.910	-0.1614	-0.7392	-1.2212	-1.5527	-1.7134	-1.7106	-1.5788	-1.3650	-1.1116	-0.8512
1.190	-0.1721	-0.7946	-1.3290	-1.7134	-1.9217	-1.9582	-1.8470	-1.6293	-1.3514	-1.0525
1.470	-0.1654	-0.7696	-1.3029	-1.7106	-1.9582	-2.0393	-1.9703	-1.7812	-1.5117	-1.2030
1.750	-0.1472	-0.6909	-1.1826	-1.5788	-1.8470	-1.9703	-1.9522	-1.8127	-1.5805	-1.2906
2.030	-0.1233	-0.5830	-1.0073	-1.3650	-1.6293	-1.7812	-1.8127	-1.7306	-1.5536	-1.3067
2.310	-0.0975	-0.4643	-0.8094	-1.1116	-1.3514	-1.5117	-1.5805	-1.5536	-1.4374	-1.2478
2.590	-0.0729	-0.3483	-0.6120	-0.8512	-1.0525	-1.2030	-1.2906	-1.3067	-1.2478	-1.1193
T: JLS21C (tensor coupled)										
kf \ ki	0.070	0.350	0.630	0.910	1.190	1.470	1.750	2.030	2.310	2.590
0.070	0.0017	-0.0005	-0.0038	-0.0062	-0.0077	-0.0082	-0.0080	-0.0071	-0.0059	-0.0046
0.350	0.0414	0.1289	0.0795	0.0307	0.0126	0.0040	0.0019	0.0001	0.0000	-0.0004
0.630	0.1295	0.4575	0.3782	0.1847	0.0760	0.0302	0.0123	0.0045	0.0014	-0.0002
0.910	0.1747	0.7119	0.7870	0.5151	0.2434	0.1017	0.0402	0.0149	0.0037	-0.0009
1.190	0.1812	0.7961	1.0642	0.9120	0.5515	0.2597	0.1090	0.0418	0.0130	0.0003
1.470	0.1713	0.7758	1.1499	1.1857	0.9134	0.5329	0.2503	0.1039	0.0370	0.0076
1.750	0.1527	0.7070	1.1155	1.2827	1.1759	0.8554	0.4879	0.2267	0.0904	0.0271
2.030	0.1343	0.6260	1.0232	1.2585	1.2850	1.1015	0.7719	0.4312	0.1951	0.0712
2.310	0.1155	0.5446	0.9125	1.1697	1.2787	1.2179	0.9985	0.6795	0.3701	0.1591
2.590	0.0993	0.4701	0.7996	1.0544	1.2043	1.2278	1.1163	0.8853	0.5863	0.3082
T: JLS231 (direct)										
kf \ ki	0.070	0.350	0.630	0.910	1.190	1.470	1.750	2.030	2.310	2.590
0.070	0.0035	0.0000	-0.0011	-0.0005	0.0009	0.0025	0.0039	0.0048	0.0051	0.0050
0.350	0.0000	-0.0072	-0.0190	-0.0182	-0.0130	-0.0089	-0.0053	-0.0030	-0.0010	0.0003
0.630	-0.0011	-0.0190	-0.0602	-0.0764	-0.0640	-0.0455	-0.0293	-0.0167	-0.0069	0.0007
0.910	-0.0005	-0.0182	-0.0764	-0.1345	-0.1435	-0.1149	-0.0784	-0.0455	-0.0187	0.0028
1.190	0.0009	-0.0130	-0.0640	-0.1435	-0.1989	-0.1936	-0.1468	-0.0905	-0.0388	0.0045
1.470	0.0025	-0.0089	-0.0455	-0.1149	-0.1936	-0.2333	-0.2084	-0.1414	-0.0649	0.0055
1.750	0.0039	-0.0053	-0.0293	-0.0784	-0.1468	-0.2084	-0.2232	-0.1747	-0.0871	0.0080
2.030	0.0048	-0.0030	-0.0167	-0.0455	-0.0905	-0.1414	-0.1747	-0.1599	-0.0872	0.0190
2.310	0.0051	-0.0010	-0.0069	-0.0187	-0.0388	-0.0649	-0.0871	-0.0872	-0.0424	0.0518
2.590	0.0050	0.0003	0.0007	0.0028	0.0045	0.0055	0.0080	0.0190	0.0518	0.1225

POLYNOMIAL REPRESENTATION OF : PNM000

PFM : 1.4000 PKMX : 2.8000
 ESTART : -162.3000 GMASQ : 1.4000
 ETAB : -100.0000 EFM : 1.0000

mf mi	1	2	3	4	5	6	7	8	9	10
1	1.28868	0.26633	0.01803	-0.01213	-0.00166	0.00027	0.00079	0.00159	0.00339	0.00612
2	0.26628	-0.60538	0.05889	0.04217	-0.00572	-0.00161	0.00001	-0.00065	-0.00064	-0.00208
3	0.01802	0.05889	-0.04775	-0.00107	0.00719	-0.00044	-0.00051	0.00004	-0.00002	0.00015
4	-0.01213	0.04217	-0.00107	-0.01078	0.00063	0.00220	-0.00017	-0.00019	0.00005	0.00012
5	-0.00166	-0.00572	0.00719	0.00063	-0.00349	0.00011	0.00099	-0.00007	-0.00013	-0.00001
6	0.00027	-0.00161	-0.00044	0.00220	0.00011	-0.00140	0.00002	0.00048	-0.00003	-0.00008
7	0.00079	0.00001	-0.00051	-0.00017	0.00099	0.00002	-0.00066	0.00001	0.00025	-0.00001
8	0.00159	-0.00065	0.00004	-0.00019	-0.00007	0.00048	0.00001	-0.00033	0.00001	0.00013
9	0.00339	-0.00064	-0.00002	0.00005	-0.00013	-0.00003	0.00025	0.00001	-0.00016	0.00001
10	0.00612	-0.00208	0.00015	0.00012	-0.00001	-0.00008	-0.00001	0.00013	0.00001	-0.00008

POLYNOMIAL REPRESENTATION OF : PNM011

mf mi	1	2	3	4	5	6	7	8	9	10
1	1.17949	0.30139	-0.01671	-0.01061	-0.00148	0.00002	0.00053	0.00151	0.00304	0.00572
2	0.30139	-0.13148	-0.02542	0.04084	-0.00060	-0.00325	0.00013	0.00015	0.00029	0.00057
3	-0.01671	-0.02542	-0.03820	-0.00065	0.01210	0.00000	-0.00151	-0.00008	-0.00018	-0.00038
4	-0.01061	0.04084	-0.00065	-0.01900	0.00009	0.00494	0.00002	-0.00072	0.00003	0.00007
5	-0.00148	-0.00060	0.01210	0.00009	-0.00711	0.00003	0.00213	0.00001	-0.00036	0.00002
6	0.00002	-0.00325	0.00000	0.00494	0.00003	-0.00302	0.00002	0.00100	0.00000	-0.00019
7	0.00053	0.00013	-0.00151	0.00002	0.00213	0.00002	-0.00136	0.00000	0.00049	0.00000
8	0.00151	0.00015	-0.00008	-0.00072	0.00001	0.00100	0.00000	-0.00064	0.00000	0.00025
9	0.00304	0.00029	-0.00018	0.00003	-0.00036	0.00000	0.00049	0.00000	-0.00031	0.00001
10	0.00572	0.00057	-0.00038	0.00007	0.00002	-0.00019	0.00000	0.00025	0.00001	-0.00014

POLYNOMIAL REPRESENTATION OF : PNM101

mf mi	1	2	3	4	5	6	7	8	9	10
1	1.61836	0.31589	-0.00872	-0.02032	0.00020	0.00073	0.00087	0.00185	0.00398	0.00726
2	0.31584	-0.85815	0.10083	0.05698	-0.01091	-0.00154	0.00029	-0.00099	-0.00098	-0.00309
3	-0.00873	0.10083	-0.04566	-0.00513	0.00605	-0.00024	-0.00031	0.00009	0.00000	0.00027
4	-0.02032	0.05698	-0.00513	-0.00768	0.00092	0.00108	-0.00011	-0.00002	0.00005	0.00017
5	0.00020	-0.01091	0.00605	0.00092	-0.00232	0.00014	0.00062	-0.00008	-0.00008	-0.00003
6	0.00073	-0.00154	-0.00024	0.00108	0.00014	-0.00092	0.00001	0.00036	-0.00003	-0.00007
7	0.00087	0.00029	-0.00031	-0.00011	0.00062	0.00001	-0.00050	0.00001	0.00020	-0.00001
8	0.00185	-0.00099	0.00009	-0.00002	-0.00008	0.00036	0.00001	-0.00028	0.00001	0.00012
9	0.00398	-0.00098	0.00000	0.00005	-0.00008	-0.00003	0.00020	0.00001	-0.00015	0.00001
10	0.00726	-0.00309	0.00027	0.00017	-0.00003	-0.00007	-0.00001	0.00012	0.00001	-0.00007

POLYNOMIAL REPRESENTATION OF : PNM10C

mf mi	1	2	3	4	5	6	7	8	9	10
1	0.80079	-1.57774	0.22674	0.10724	-0.02303	-0.00312	0.00004	-0.00158	-0.00104	-0.00462
2	0.32584	-0.28184	-0.13856	0.05954	0.02322	-0.00861	-0.00129	0.00001	-0.00051	-0.00073
3	0.03572	0.16806	-0.08812	-0.04004	0.02317	0.00813	-0.00394	-0.00056	0.00030	0.00035
4	-0.01326	0.04721	0.03196	-0.03326	-0.01214	0.01034	0.00291	-0.00189	-0.00025	0.00024
5	-0.00444	-0.01256	0.01878	0.01068	-0.01377	-0.00459	0.00487	0.00116	-0.00098	-0.00015
6	-0.00067	-0.00302	-0.00389	0.00874	0.00375	-0.00618	-0.00183	0.00234	0.00050	-0.00051
7	0.00050	-0.00063	-0.00182	-0.00167	0.00419	0.00151	-0.00293	-0.00075	0.00116	0.00022
8	0.00133	-0.00134	-0.00006	-0.00103	-0.00072	0.00205	0.00065	-0.00143	-0.00033	0.00059
9	0.00265	-0.00273	-0.00008	0.00017	-0.00064	-0.00032	0.00103	0.00029	-0.00072	-0.00016
10	0.00490	-0.00539	-0.00014	0.00028	0.00006	-0.00036	-0.00015	0.00053	0.00013	-0.00038

POLYNOMIAL REPRESENTATION OF : PNM110

mf mi	1	2	3	4	5	6	7	8	9	10
1	1.63923	0.10696	-0.14032	0.00485	0.00444	-0.00048	0.00043	0.00141	0.00278	0.00534
2	0.10696	0.05952	0.01873	0.00052	-0.00289	-0.00085	0.00036	0.00036	0.00047	0.00087
3	-0.14032	0.01873	0.01248	-0.00498	0.00241	0.00042	-0.00085	-0.00002	0.00001	-0.00031
4	0.00485	0.00052	-0.00498	-0.00062	0.00053	-0.00033	0.00011	-0.00008	-0.00004	0.00004
5	0.00444	-0.00289	0.00241	0.00053	-0.00001	0.00018	-0.00063	-0.00002	0.00014	0.00001
6	-0.00048	-0.00085	0.00042	-0.00033	0.00018	0.00110	-0.00003	-0.00060	-0.00001	0.00014
7	0.00043	0.00036	-0.00085	0.00011	-0.00063	-0.00003	0.00097	-0.00001	-0.00044	0.00000
8	0.00141	0.00036	-0.00002	-0.00008	-0.00002	-0.00060	-0.00001	0.00063	0.00000	-0.00028
9	0.00278	0.00047	0.00001	-0.00004	0.00014	-0.00001	-0.00044	0.00000	0.00038	0.00001
10	0.00534	0.00087	-0.00031	0.00004	0.00001	0.00014	0.00000	-0.00028	0.00001	0.00024

POLYNOMIAL REPRESENTATION OF : PNM111

mf mi	1	2	3	4	5	6	7	8	9	10
1	1.02989	0.05178	-0.09635	0.00254	0.00350	0.00018	0.00033	0.00079	0.00164	0.00321
2	0.05178	0.10152	0.00953	-0.01847	-0.00035	0.00131	0.00012	0.00019	0.00034	0.00065
3	-0.09635	0.00953	0.02740	-0.00039	-0.00550	0.00005	0.00054	-0.00002	-0.00004	-0.00013
4	0.00254	-0.01847	-0.00039	0.00861	0.00009	-0.00238	0.00000	0.00033	-0.00002	-0.00003
5	0.00350	-0.00035	-0.00550	0.00009	0.00337	0.00002	-0.00113	-0.00001	0.00020	0.00000
6	0.00018	0.00131	0.00005	-0.00238	0.00002	0.00163	-0.00001	-0.00058	0.00000	0.00012
7	0.00033	0.00012	0.00054	0.00000	-0.00113	-0.00001	0.00082	0.00000	-0.00031	0.00000
8	0.00079	0.00019	-0.00002	0.00033	-0.00001	-0.00058	0.00000	0.00042	0.00000	-0.00016
9	0.00164	0.00034	-0.00004	-0.00002	0.00020	0.00000	-0.00031	0.00000	0.00022	0.00001
10	0.00321	0.00065	-0.00013	-0.00003	0.00000	0.00012	0.00000	-0.00016	0.00001	0.00013

POLYNOMIAL REPRESENTATION OF : PNM121

mf mi	1	2	3	4	5	6	7	8	9	10
1	-0.69934	-0.13520	0.05962	0.01219	-0.00614	0.00051	0.00039	-0.00072	-0.00142	-0.00267
2	-0.13520	0.04623	0.02455	-0.02004	-0.00510	0.00332	0.00033	-0.00015	-0.00013	-0.00029
3	0.05962	0.02455	0.01968	0.00246	-0.00938	-0.00207	0.00184	0.00036	0.00009	0.00040
4	0.01219	-0.02004	0.00246	0.01566	0.00108	-0.00515	-0.00065	0.00095	0.00015	-0.00001
5	-0.00614	-0.00510	-0.00938	0.00108	0.00709	0.00045	-0.00245	-0.00025	0.00046	0.00000
6	0.00051	0.00332	-0.00207	-0.00515	0.00045	0.00325	0.00015	-0.00115	-0.00010	0.00024
7	0.00039	0.00033	0.00184	-0.00065	-0.00245	0.00015	0.00151	0.00005	-0.00056	-0.00004
8	-0.00072	-0.00015	0.00036	0.00095	-0.00025	-0.00115	0.00005	0.00071	0.00002	-0.00028
9	-0.00142	-0.00013	0.00009	0.00015	0.00046	-0.00010	-0.00056	0.00002	0.00035	0.00001
10	-0.00267	-0.00029	0.00040	-0.00001	0.00000	0.00024	-0.00004	-0.00028	0.00001	0.00016

POLYNOMIAL REPRESENTATION OF : PNM211

mf mi	1	2	3	4	5	6	7	8	9	10
1	-0.51172	0.03313	0.07023	-0.00512	-0.00298	0.00023	-0.00002	-0.00024	-0.00053	-0.00109
2	0.03313	-0.04133	-0.00954	0.00855	0.00046	-0.00071	0.00000	0.00001	-0.00006	-0.00010
3	0.07023	-0.00954	-0.01283	0.00097	0.00115	0.00000	-0.00010	0.00002	0.00006	0.00011
4	-0.00512	0.00855	0.00097	-0.00209	0.00004	0.00019	0.00000	-0.00001	0.00001	0.00002
5	-0.00298	0.00046	0.00115	0.00004	-0.00020	0.00000	0.00000	0.00000	0.00000	0.00000
6	0.00023	-0.00071	0.00000	0.00019	0.00000	0.00001	0.00000	-0.00002	0.00000	0.00000
7	-0.00002	0.00000	-0.00010	0.00000	0.00000	0.00000	0.00003	0.00000	-0.00002	0.00000
8	-0.00024	0.00001	0.00002	-0.00001	0.00000	-0.00002	0.00000	0.00002	0.00000	-0.00001
9	-0.00053	-0.00006	0.00006	0.00001	0.00000	0.00000	-0.00002	0.00000	0.00001	0.00000
10	-0.00109	-0.00010	0.00011	0.00002	0.00000	0.00000	0.00000	-0.00001	0.00000	0.00001

POLYNOMIAL REPRESENTATION OF : PNM21C

mf mi	1	2	3	4	5	6	7	8	9	10
1	-0.19140	0.12062	0.02942	-0.02818	-0.00018	0.00204	-0.00004	0.00003	-0.00001	-0.00005
2	-0.08149	0.01260	0.03631	-0.00122	-0.00948	0.00062	0.00109	-0.00011	-0.00001	-0.00004
3	-0.00843	-0.02505	0.00946	0.01332	-0.00308	-0.00355	0.00059	0.00050	-0.00009	-0.00003
4	0.00455	-0.00808	-0.00839	0.00535	0.00500	-0.00195	-0.00145	0.00040	0.00022	-0.00006
5	0.00115	0.00207	-0.00409	-0.00321	0.00278	0.00197	-0.00106	-0.00062	0.00024	0.00010
6	0.00008	0.00093	0.00094	-0.00203	-0.00134	0.00143	0.00082	-0.00057	-0.00028	0.00014
7	-0.00008	0.00002	0.00060	0.00043	-0.00102	-0.00059	0.00073	0.00036	-0.00030	-0.00013
8	-0.00032	0.00005	0.00004	0.00034	0.00020	-0.00053	-0.00026	0.00037	0.00016	-0.00016
9	-0.00063	0.00009	0.00012	-0.00002	0.00018	0.00010	-0.00028	-0.00012	0.00020	0.00007
10	-0.00117	0.00021	0.00025	-0.00001	-0.00003	0.00010	0.00005	-0.00015	-0.00006	0.00010

POLYNOMIAL REPRESENTATION OF : PNM220

mf mi	1	2	3	4	5	6	7	8	9	10
1	-0.26903	-0.02574	0.04142	0.00791	-0.00327	-0.00039	0.00000	-0.00015	-0.00033	-0.00068
2	-0.02574	-0.03178	-0.00369	0.00832	0.00165	-0.00099	-0.00014	-0.00003	-0.00010	-0.00019
3	0.04142	-0.00369	-0.01463	-0.00132	0.00348	0.00047	-0.00049	-0.00004	0.00003	0.00003
4	0.00791	0.00832	-0.00132	-0.00473	-0.00034	0.00145	0.00018	-0.00025	-0.00001	0.00004
5	-0.00327	0.00165	0.00348	-0.00034	-0.00207	-0.00011	0.00071	0.00007	-0.00014	-0.00001
6	-0.00039	-0.00099	0.00047	0.00145	-0.00011	-0.00098	-0.00005	0.00037	0.00003	-0.00008
7	0.00000	-0.00014	-0.00049	0.00018	0.00071	-0.00005	-0.00049	-0.00002	0.00019	0.00001
8	-0.00015	-0.00003	-0.00004	-0.00025	0.00007	0.00037	-0.00002	-0.00025	-0.00001	0.00011
9	-0.00033	-0.00010	0.00003	-0.00001	-0.00014	0.00003	0.00019	-0.00001	-0.00014	-0.00001
10	-0.00068	-0.00019	0.00003	0.00004	-0.00001	-0.00008	0.00001	0.00011	-0.00001	-0.00007

POLYNOMIAL REPRESENTATION OF : PNM221

mf mi	1	2	3	4	5	6	7	8	9	10
1	-0.73424	-0.03606	0.12461	0.01509	-0.01115	-0.00069	-0.00023	-0.00044	-0.00077	-0.00168
2	-0.03606	-0.16105	-0.02848	0.04648	0.00888	-0.00655	-0.00066	0.00003	-0.00040	-0.00067
3	0.12461	-0.02848	-0.06718	-0.00571	0.01940	0.00303	-0.00314	-0.00037	0.00013	-0.00008
4	0.01509	0.04648	-0.00571	-0.02854	-0.00184	0.00882	0.00103	-0.00155	-0.00014	0.00016
5	-0.01115	0.00888	0.01940	-0.00184	-0.01220	-0.00067	0.00411	0.00040	-0.00079	-0.00004
6	-0.00069	-0.00655	0.00303	0.00882	-0.00067	-0.00550	-0.00024	0.00197	0.00016	-0.00041
7	-0.00023	-0.00066	-0.00314	0.00103	0.00411	-0.00024	-0.00258	-0.00009	0.00097	0.00007
8	-0.00044	0.00003	-0.00037	-0.00155	0.00040	0.00197	-0.00009	-0.00126	-0.00004	0.00050
9	-0.00077	-0.00040	0.00013	-0.00014	-0.00079	0.00016	0.00097	-0.00004	-0.00063	-0.00002
10	-0.00168	-0.00067	-0.00008	0.00016	-0.00004	-0.00041	0.00007	0.00050	-0.00002	-0.00033

POLYNOMIAL REPRESENTATION OF : PNM231

mf mi	1	2	3	4	5	6	7	8	9	10
1	-0.01316	0.01817	0.01803	0.00352	-0.00152	-0.00044	0.00009	0.00008	0.00015	0.00025
2	0.01817	-0.00068	-0.00083	0.00353	0.00147	-0.00050	-0.00021	0.00007	0.00007	0.00012
3	0.01803	-0.00083	-0.00672	-0.00111	0.00191	0.00058	-0.00030	-0.00009	0.00004	0.00003
4	0.00352	0.00353	-0.00111	-0.00274	-0.00034	0.00086	0.00021	-0.00016	-0.00004	0.00002
5	-0.00152	0.00147	0.00191	-0.00034	-0.00121	-0.00013	0.00041	0.00009	-0.00008	-0.00002
6	-0.00044	-0.00050	0.00058	0.00086	-0.00013	-0.00055	-0.00005	0.00020	0.00004	-0.00004
7	0.00009	-0.00021	-0.00030	0.00021	0.00041	-0.00005	-0.00026	-0.00002	0.00010	0.00002
8	0.00008	0.00007	-0.00009	-0.00016	0.00009	0.00020	-0.00002	-0.00013	-0.00001	0.00005
9	0.00015	0.00007	0.00004	-0.00004	-0.00008	0.00004	0.00010	-0.00001	-0.00006	0.00000
10	0.00025	0.00012	0.00003	0.00002	-0.00002	-0.00004	0.00002	0.00005	0.00000	-0.00003

POLYNOMIAL REPRESENTATION OF THE PROPAGATOR DIFFERENCE

PFM : 1.3000 PKMX : 2.8000
 ESTART : -162.3000 GMASQ : 1.4000
 ETAB(1): 100.0000 EFM : 1.0000

mf mi	1	2	3	4	5	6	7	8	9	10
1	0.06100	-0.11210	0.06406	0.00736	-0.01636	-0.00283	0.00502	0.00049	-0.00180	0.00151
2	-0.11210	0.23203	-0.19040	0.04921	0.02532	-0.01076	-0.00922	0.00348	0.00483	-0.00362
3	0.06406	-0.19040	0.26377	-0.19153	0.04759	0.02320	-0.00919	-0.00639	-0.00028	0.00363
4	0.00736	0.04921	-0.19153	0.27893	-0.20081	0.04693	0.02751	-0.01226	-0.00745	0.00246
5	-0.01636	0.02532	0.04759	-0.20081	0.28671	-0.20031	0.04240	0.02766	-0.00917	-0.00731
6	-0.00283	-0.01076	0.02320	0.04693	-0.20031	0.28690	-0.20223	0.04459	0.02840	-0.01140
7	0.00502	-0.00922	-0.00919	0.02751	0.04240	-0.20223	0.29200	-0.20288	0.04178	0.02926
8	0.00049	0.00348	-0.00639	-0.01226	0.02766	0.04459	-0.20288	0.29114	-0.20291	0.04256
9	-0.00180	0.00483	-0.00028	-0.00745	-0.00917	0.02840	0.04178	-0.20291	0.29327	-0.20399
10	0.00151	-0.00362	0.00363	0.00246	-0.00731	-0.01140	0.02926	0.04256	-0.20399	0.29367